AFOSR TN 60-442

THE UNIVERSITY OF MICHIGAN
COLLEGE OF ENGINEERING
Department of Aeronautical and Astronautical Engineering
Aircraft Propulsion Laboratory

Technical Note

STABILIZATION OF GASEOUS DETONATION WAVES WITH EMPHASIS ON THE IGNITION TIME DELAY ZONE

J. A. Nicholls

UMRI Project 2874

under contract with:

PROPULSION RESEARCH DIVISION
AIR FORCE OFFICE OF SCIENTIFIC RESEARCH
AIR RESEARCH AND DEVELOPMENT COMMAND
CONTRACT NO. 49(638)-562
WASHINGTON, D. C.

administered by:

THE UNIVERSITY OF MICHIGAN RESEARCH INSTITUTE ANN ARBOR

June 1960

ACKNOWLEDGMENT

This research was partially supported by the United States Air Force under Contract No. 49(638)-562, monitored by the Air Force Office of Scientific Research, Propulsion Research Division, Air Research and Development Command. The support of the agency is gratefully acknowledged.

The work reported herein served as my doctoral dissertation and I am especially indebted to Professors R. B. Morrison and T. C. Adamson, Jr., who served as co-chairmen of the doctoral committee and provided much inspiration and assistance. I am also very appreciative of the support and assistance of Mr. Eliahou K. Dabora who has worked closely with me on the experimental portions of the study.

TABLE OF CONTENTS

TABLE OF CONTENTS (CONT'D)

LIST OF TABLES

LIST OF FIGURES

LIST OF FIGURES (CONT'D)

LIST OF FIGURES (CONT'D)

NOMENCLATURE

a	speed of sound
a	$[c]k_1$, sec^{-1}
A	area
A	frequency factor or pre-exponential factor
b	$2\eta_{H_2}[C]k_2$, sec^{-1}
B	a non-reacting gas
c	$2\eta_{O_2}[C]k_3$, sec^{-1}
C_1, C_2	constants of integration
[C]	total concentration, moles/cc
C_p	specific heat at constant pressure
E	activation energy, k cal/mole
f	$\eta_{O_2}[C]k_6$
F	defined by Equation (2.10)
g	gas
g	$\eta_{H_2}[C]k_7$
G	mass flow per unit area per unit time
h	$\eta_{H_2}[C]k_8$
h	enthalpy
[H]	concentration of hydrogen atoms, moles/cc
$[H_2O]$	concentration of water vapor, moles/cc
$[H_2]$	concentration of hydrogen, moles/cc
i	$[C]k_9$
k_i	reaction rate constant for reaction "i"

K_{RAD}*	radiation correction coefficient
K	constant
m	temperature exponent in reaction rate constant (Equation 6.2)
m	molecular weight
M	Mach number
M	a third body
N	number of moles of reactants
n	mole fraction
$[O_2]$	concentration of oxygen, moles/cc
[OH]	cencentration of hydroxl radical, moles/cc
[O]	concentration of oxygen atoms, moles/cc
P	pressure
Q	heat release
R	gas constant = 1.986 $\frac{\text{cal}}{\text{mole} - ^\circ\text{K}}$
t	time, secs
t'	dimensionless time = $\frac{t}{tc}$
T_d	equivalent duct temperature, °R
T	temperature
T_w	indicated junction temperature, °R
T_g	temperature of gas surrounding junction, °R
u	component of velocity
v	specific volume or component of velocity
V	velocity

w	mass
$\dot{w}$	mass flow per second
x,y,z	number of moles
β	wave angle
ϵ	$2\eta_{O_2}\eta_{H_2}[C]k_5$
γ	ratio of specific heats
δ	wedge half angle
ρ	density
$\varphi(M)$	function of Mach number, defined by Equation (2.16)
$\psi(M_2)$	function of Mach number, defined by Equation (4.17)
λ	ratio of stagnation temperatures across a detonation, or the value of η_H defining the ignition delay time
Δx	distance between shock wave and flame front
Δ	recovery correction factor
τ	ignition time delay

Subscripts

o	time zero, immediately behind shock
1	station no. 1
2	station no. 2
a	air
b	base of dividing plate between two streams
c	value at the characteristic time
C-J	Chapman-Jouguet

Subscripts (Con't)

eff	effective
f	fuel
n	normal
N	nozzle exit
s	stagnation condition
t	tangential
t	stagnation temperature at the Mach disc
τ	value at $t = \tau$

ABSTRACT

The characteristics of gaseous detonation waves are considered insofar as they influence the dynamic conditions that must be met in order to generate a standing gaseous detonation wave. In view of these requirements, a few possible methods of stabilization are presented and discussed. The method adopted for the experimental study consists of mixing unheated hydrogen with the heated air in the supersonic portion of an axisymmetric convergent-divergent nozzle. The nozzle is operated underexpanded so that acceleration of the mixture to the required high Mach number is realized in the open jet. Combustion occurs downstream of the normal shock wave that exists in such underexpanded jets. The experimental facility which evolved for these studies is described.

Experiments are described wherein stationary shock wave-combustion configurations were realized. These experiments covered the mixture stagnation temperature range of about 1800°R-2430°R and a wide fuel-air range. In all cases of interest the shock wave and flame were separated by a distance corresponding to the mixture ignition delay time. This delay time varied from 10-50 μ secs, the shorter times occurring with higher temperatures. At lower temperatures, where the separation between shock and flame is greater, there was no apparent interaction between the shock wave and flame. At higher temperatures the onset of combustion was observed to drive the shock wave upstream to a new stable position wherein the Mach number into the shock was lower. This latter type is considered to be a standing detonation wave.

A theoretical analysis of the ignition delay zone of hydrogen-oxygen combustion is presented. Nine reactions are considered but the order of magnitude of many of the terms allows the reaction scheme to be considerably simplified. As a result it is possible to predict the rate of growth of all radical and water vapor concentrations behind the shock. Particular attention is given to the time variation of the hydrogen atom concentration. In order to arrive at an explicit analytical expression for the ignition delay time, a value for the mole fraction of hydrogen atoms, characteristic of this delay time, is introduced. It is found that the delay time is dependent on the temperature, pressure, and composition of the mixture behind the shock as well as the pertinent reaction rate constants. The rate controlling reaction is that of $O_2 + H \rightarrow OH + O$. These theoretical predictions are compared with the experimental results obtained and very good agreement shown. The results, both theoretical and experimental, are in contrast to the findings of Gross who observed no ignition delay zone in similar experiments with hydrogen and air.

The main results of this study are:

1) standing detonation waves have been successfully generated. Such waves offer many advantages to the study of combustion processes and represent a possible mode of combustion in hypersonic ramjets.

2) a new experimental technique for the study of ignition time delays of gaseous mixtures at high temperatures has evolved. Other applications to chemical kinetic problems are possible.

3) a theoretical prediction of ignition time delay of hydrogen-oxygen mixtures is presented which is consistent with the experimental results of this investigation as well as those of other investigations.

I INTRODUCTION

Combustion processes have been subject to study for many years by chemists, physical chemists, physicists, and engineers. Accordingly, the problem has been attacked from many different viewpoints dependent on the information desired and the individual researcher's area of interest. For instance, the early work in the field concentrated solely on the chemistry and completely excluded the fluid dynamic aspect. Under certain restrictive environmental conditions, this attack is plausible and suffices for the goal at hand. On the other hand, there are many cases wherein the hydrodynamic aspects are just as important or more so, and a suitable description may be obtained by treating the combustion process as a discontinuity with some suitable energy release. Today, considerable effort is being spent on merging these two extreme approaches into a general theory. This merging has imposed a burden on the researcher (but an exciting and rewarding burden) in that it has forced the appreciable broadening of his field of knowledge. The chemist, on the one hand, has been obliged to learn hydrodynamics and the hydrodynamicist, on the other hand, has been obliged to learn chemistry. It is undoubtedly a fair statement to say that the engineer, in his constant search for more efficient conversion of chemical energy to useful mechanical energy, has been the main motivating force behind this marriage of disciplines.

Early combustion studies centered around the relatively leisurely combustion process known as deflagration. In these processes the flame propagation rate is mainly controlled by diffusion and/or heat conduction.

With the advent of jet propulsion it became imperative to increase the space heating rates (energy release per unit volume per unit time) and flame stabilization by means of bluff bodies, or flameholders, became a necessity. In these cases all of the transport phenomena become of importance in limiting the propagation rates. The other mode of combustion, detonation, is in direct contrast to deflagration in that it represents an exceedingly rapid combustion rate and, in fact, propagates supersonically. This wave can often be considered as a shock wave followed by combustion wherein the combustion is initiated by the elevated temperature behind the shock wave. Such waves may often be profitably treated as a discontinuity although much attention is currently being given to the structure of the wave. It is interesting to note that simple hydrodynamic principles predict the two modes of combustion. First a wave can exist across which the pressure and density decrease and the rate of propagation is subsonic. Such a wave corresponds to the deflagration wave. The second case, detonation, is characterized by increased pressure and density and propagates supersonically. These facts will be discussed in some detail in section II.

Experimentalists, in their study of deflagration, have had the advantage of stabilized flames through the use of Bunsen type flames, flat low pressure flames, diffusion flames, and the flameholder anchored flames. Heretofore, the experimentalist in detonation has been seriously handicapped by the necessity of effecting measurements on a very thin reaction zone propagating at high velocities (5000-13000 ft/sec). Such experiments always resulted in a stable detonation wave corresponding to the Chapman-Jouguet state; that is, the case in which the Mach number of the burned

gases relative to the wave front is unity. There appears to be no real reason why other forms of detonation, i.e. strong detonation waves, should not exist. It would appear, then, that many advantages could accrue from the generation of stable gaseous detonation waves. In particular, many more varied measurements could be effected; such as pressure, temperature, ionization, Mach number, spectral, and composition. In addition, there would be the possibility of generating detonation waves other than those of the Chapman-Jouguet type. Another advantage that could accrue is in the application of stabilized detonation waves to hypersonic ramjets. It has always been an intriguing thought to the proponents of ramjets that the necessity of diffusing the incoming air to the low velocities required for combustion, with the attendant high stagnation pressure losses, be circumvented. The achievement of stationary detonation waves would allow this aim to be realized. That is, the detonation wave would replace the conventional combustion chamber so that there would be no necessity to diffuse to subsonic velocities. The attractiveness of this idea was first mentioned by Roy[1] and first analyzed by Dunlap, Brehm, and Nicholls[2]. More recently, extensive calculations have been made by Sargent and Gross.[3]

In 1949, personnel of the University of Michigan embarked on a study of detonative combustion with the WADC which had as the ultimate goal the generation of stable detonation waves. Because of the limited information available on gaseous detonation at that time, a concentrated study was undertaken utilizing the shock tube as a means of establishing the detonation waves. The results of this study (which include the detonation velocity of many gaseous mixtures, detonation limits, reflection of waves,

pressure distribution across the wave, schlieren photographs of the waves, and overdriven waves) are reported by Morrison (4) and by Nicholls, Morrison, Reid, and Ong (5). This work terminated in 1953. During this time, no attempt was made to actually stabilize a detonation wave but the wealth of information obtained has been of inestimatable value in motivating and guiding the research program reported herein.

Subsequent to this work, a research program was initiated in 1954 under the auspices of the AFOSR which was explicitly aimed at the generation of stable gaseous detonation waves. This thesis concerns a portion of that task in addition to subsequent related problems. In the following sections an attempt is made to summarize the important characteristics of gaseous detonation as they affect this study, to set forth the required conditions for stabilizing the wave, to describe the experimental arrangement adopted, to report some experimental results which culminated in the establishment of standing detonation waves, and to verify analytically the observed ignition time delays in hydrogen-air mixtures. It should be pointed out that no attempt is made to analyze the stability of the detonation wave when subjected to disturbances.

II Characteristics of Gaseous Detonation Waves

Berthelot [6] and Mallard and Le Chatelier [7], in the course of their studies of flames, were evidently the first to recognize the supersonic mode of combustion which we know as detonation. However, it remained for Chapman [8] and Jouguet [9] to independently support this observation by hydrodynamic theory. In particular they pointed out that the phenomenon could be treated as a shock wave followed by combustion and propagating at a rate such that the Mach number of the burned gases relative to the front was exactly one. Such waves, the type always observed in flame tubes and detonation tubes in the steady state, are commonly referred to as Chapman-Jouguet, or C-J, detonation waves.

At this point it is instructive to consider the characteristics of gaseous detonation; that is, what are typical propagation rates, what pressure and temperature ratios are realized across the wave, etc.? This information can be gleaned readily if a simplified model is treated; a model which, while sacrificing the accuracy of the quantitative results, leads to good qualitative information. Comparison of these results with those of detailed calculations on a more realistic model will then be made.

2.1 Mach Number of Detonation and Changes Across the Wave.

Consider, as shown in Figure 1, an exothermic wave with free stream conditions (unburned gas) denoted by (1) and the final conditions (burned gas) denoted by (2). Assuming a perfect gas, the wave to be a discontinuity, steady flow, constant specific heats, and constant molecular weight, we can write:

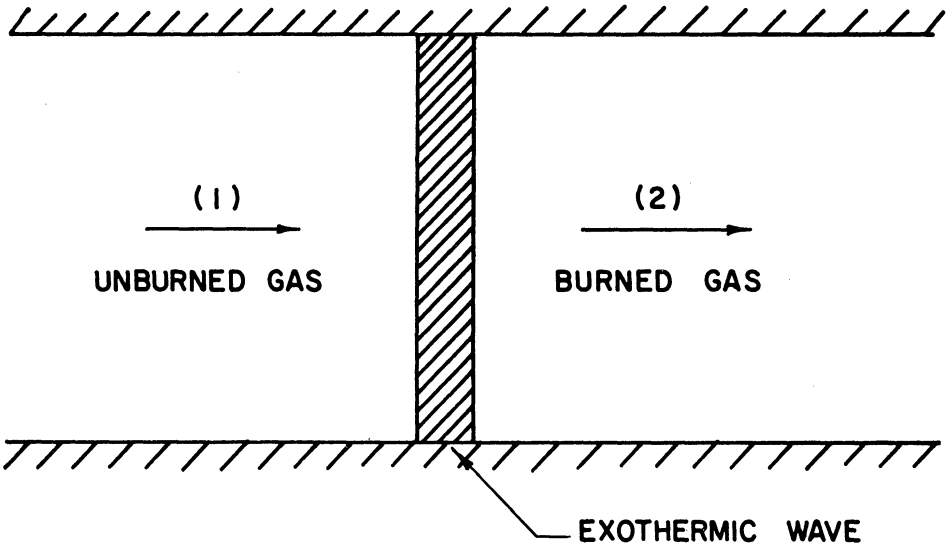

Figure 1. One Dimensional Exothermic Wave.

Conservation of mass:

$$\rho_1 V_1 = \rho_2 V_2 \tag{2.1}$$

Conservation of momentum:

$$P_1 + \rho_1 V_1^2 = P_2 + \rho_2 V_2^2 \tag{2.2}$$

Equation of State:

$$P = \rho \frac{R}{m} T \tag{2.3}$$

Introducing the Mach number, $M = \frac{V}{a}$, and restricting the analysis to C-J waves $(M_2 = 1)$ for the present, we readily determine that;

$$\frac{P_2}{P_1} = \frac{1 + \gamma M_{C-J}^2}{1 + \gamma} \tag{2.4}$$

$$\frac{T_2}{T_1} = \frac{1}{M_{C-J}^2} \left(\frac{1 + \gamma M_{C-J}^2}{1 + \gamma} \right)^2 \tag{2.5}$$

$$\frac{\rho_2}{\rho_1} = \frac{V_1}{V_2} = M_{C-J}^2 \left(\frac{1 + \gamma}{1 + \gamma M_{C-J}^2} \right) \tag{2.6}$$

$$\frac{P_{S_2}}{P_{S_1}} = \left(\frac{\gamma + 1}{2} \right)^{\frac{\gamma}{\gamma - 1}} \left(\frac{1 + \gamma M_{C-J}^2}{1 + \gamma} \right) \left(1 + \frac{\gamma - 1}{2} M_{C-J}^2 \right)^{\frac{-\gamma}{\gamma - 1}} \tag{2.7}$$

$$\frac{T_{S_2}}{T_{S_1}} = \left(\frac{\gamma + 1}{2} \right) \left[\frac{1 + \gamma M_{C-J}^2}{M_{C-J} (1 + \gamma)} \right]^2 \left(1 + \frac{\gamma - 1}{2} M_{C-J}^2 \right)^{-1} \tag{2.8}$$

These values are shown in Figure 2 as a function of the Mach number of detonation for $\gamma = 1.4$. In view of the known fact that typical detonation Mach numbers lay in the approximate range $3 < M_{C-J} < 10$ [4] we

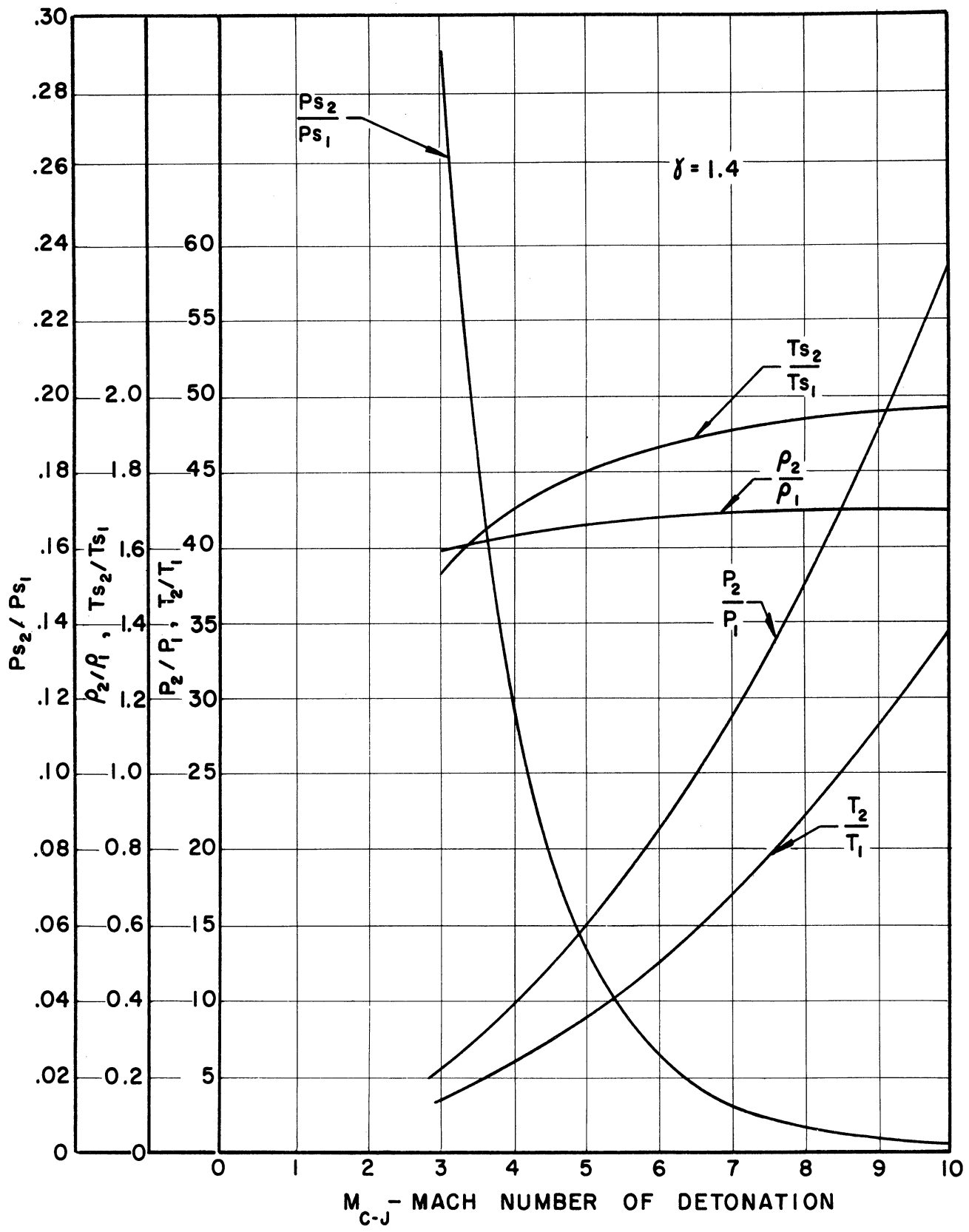

Figure 2. Characteristics of Chapman-Jouguet Detonation Waves.

see that C-J detonation waves are capable of producing high pressures and high temperatures while sustaining high stagnation pressure losses.

It is interesting to examine these same characteristics when the C-J condition is relaxed. That is, we will include strong detonations ($M_2 < 1$) but will not consider weak detonations ($M_2 > 1$) which are not known to exist. In fact, the latter are ordinarily ruled out on the basis of a violation of the Second Law of Thermodynamics [4]. More will be said on the classification of detonation waves in the next section. In order to derive the required relations, the energy equation is introduced which is,

$$C_p T_1 + \frac{V_1^2}{2} + Q = C_p T_2 + \frac{V_2^2}{2} \tag{2.9}$$

Adamson and Morrison [10] have postulated a convenient parameter for classifying such waves which will be used here. They define;

$$F = 1 + \sqrt{1 - \frac{2(1+\gamma) M_1^2}{(M_1^2 - 1)^2} \cdot \frac{Q}{C_p T_1}} \tag{2.10}$$

so that the changes across the wave may be written in terms of F as follows;

$$\frac{P_2}{P_1} = 1 + \frac{\gamma F}{1+\gamma}(M_1^2 - 1) \tag{2.11}$$

$$\frac{T_2}{T_1} = \left[1 + \frac{\gamma F}{1+\gamma}(M_1^2 - 1)\right]\left[1 - \frac{F}{1+\gamma}\left(\frac{M_1^2 - 1}{M_1^2}\right)\right] \tag{2.12}$$

$$M_2^2 = \frac{(1+\gamma-F)(M_1^2-1) + (1+\gamma)}{\gamma F (M_1^2 - 1) + (1+\gamma)} \tag{2.13}$$

The significance of F is;

$F = 2$ shock wave

$F = 1$ C-J detonation wave

$1<F<2$ strong detonation wave.

Equations (2.11) - (2.13) are plotted in Figure 3 for a few different values of F where $\gamma = 1.4$. As can be seen, strong detonation waves involve higher final pressures than in the case of C-J detonation but, over most of the range, lower temperatures for a given M_1. It may be inferred that for a given Q/C_pT_1, a strong detonation wave will propagate at a higher rate (greater M_1) than will the C-J wave. This, of course, is a well known characteristic, that the C-J detonation velocity is the minimim velocity consistent with the conservation laws.

It is now desired to refine the above idealized results so that useable quantitative information as to the Mach number of detonation can be presented. For this purpose, only C-J detonations in hydrogen-air mixtures will be considered. As a first refinement to the foregoing, the assumption of γ = constant and C_p = constant will be dropped and instead the assumption made that $\gamma_1 = 1.4$ and $\gamma_2 = 1.25$. It will still be assumed that the molecular weight remains unchanged and the heat release will be taken as the handbook value. Compared to this will be the extensive calculations of Eisen, Gross, and Rivlin [11] who calculated the Mach number of detonation under the assumption of chemical equilibrium at the C-J plane. Their calculations include the effects of ionization as well as dissociation and are in good agreement with experimental results. A comparison of the three

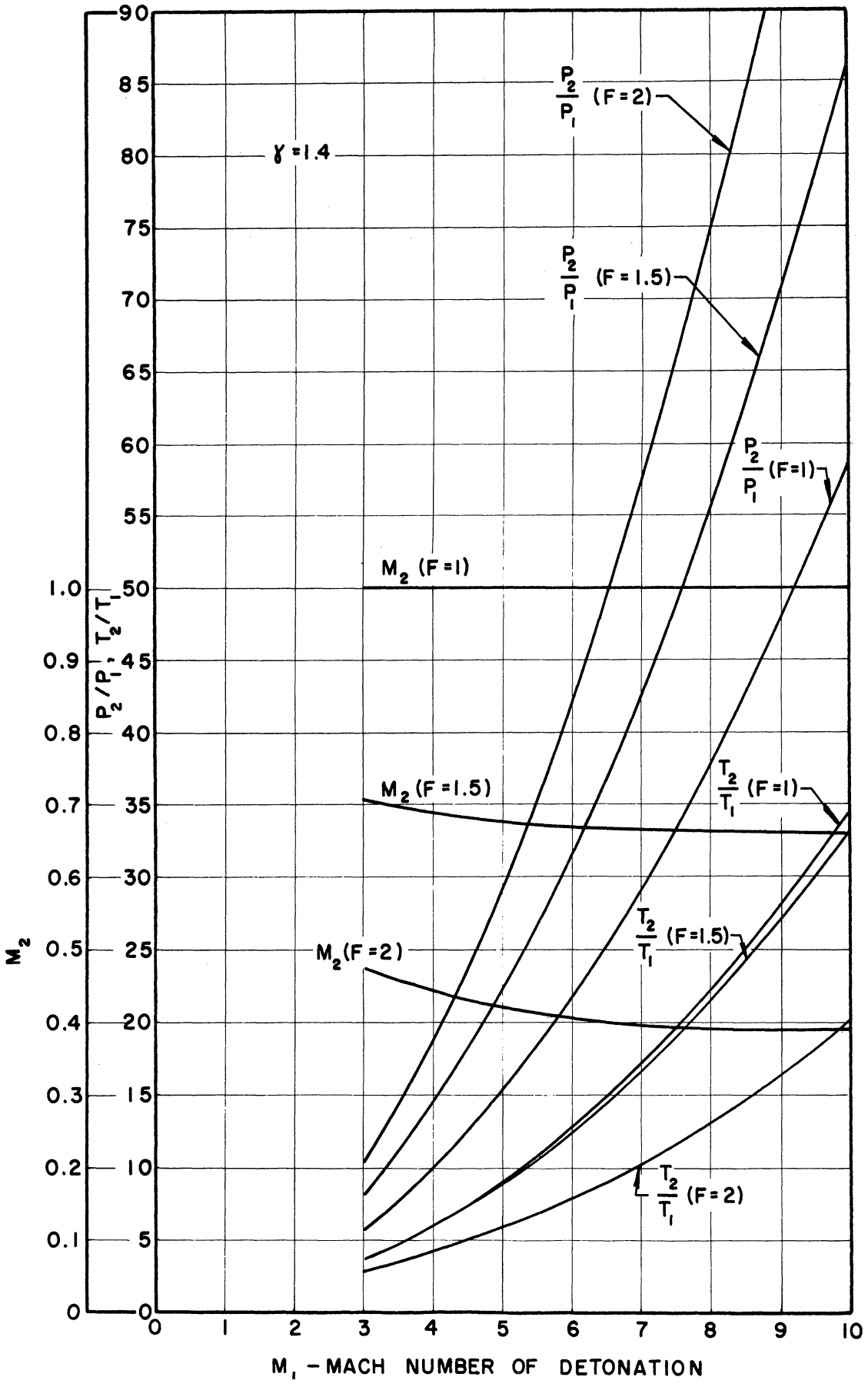

Figure 3. Characteristics of Strong Detonation Waves.

methods of calculating M_{C-J} is shown in Figure 4. There is an appreciable difference between the exact calculations and the approximations although the curve allowing for a change in γ is fairly accurate in the neighborhood of stoichiometric mixtures. The constant γ assumption, however, is subject to considerable error in this range and should only be used on a qualitative basis. The differences noted are attributable to a change in molecular weight, a change in γ, a change in specific heat, and a lower effective heat release as a result of dissociation. The assumption of a perfect gas introduces negligible error. Actually in the case of fuel - oxygen mixtures there is even much more discrepancy because of the higher Mach numbers and temperatures and hence the greater effects of dissociation.

Experimentally observed Mach numbers of detonation [4] for some common fuel - oxygen mixtures are plotted in Figure 5. It is obvious that, except for hydrogen and mixtures near the lean limit of detonation, these Mach numbers are quite high. This leads to complications in the actual stabilization of the wave as will be brought out later.

2.2 Representation of Detonation on a Hugoniot Curve.

The classical treatment of detonation has centered around a Hugoniot Curve representation of detonative combustion wherein the kinetic terms are eliminated in favor of the thermodynamic variables. Such a treatment leads to a convenient means of classifying exothermic waves. Briefly, this is seen as follows. If the velocity terms are eliminated from Equations (2.1), (2.2), (2.3), and (2.9), the locus of all possible end states can then be determined for a given Q, P_1, and v_1. This locus of end states in

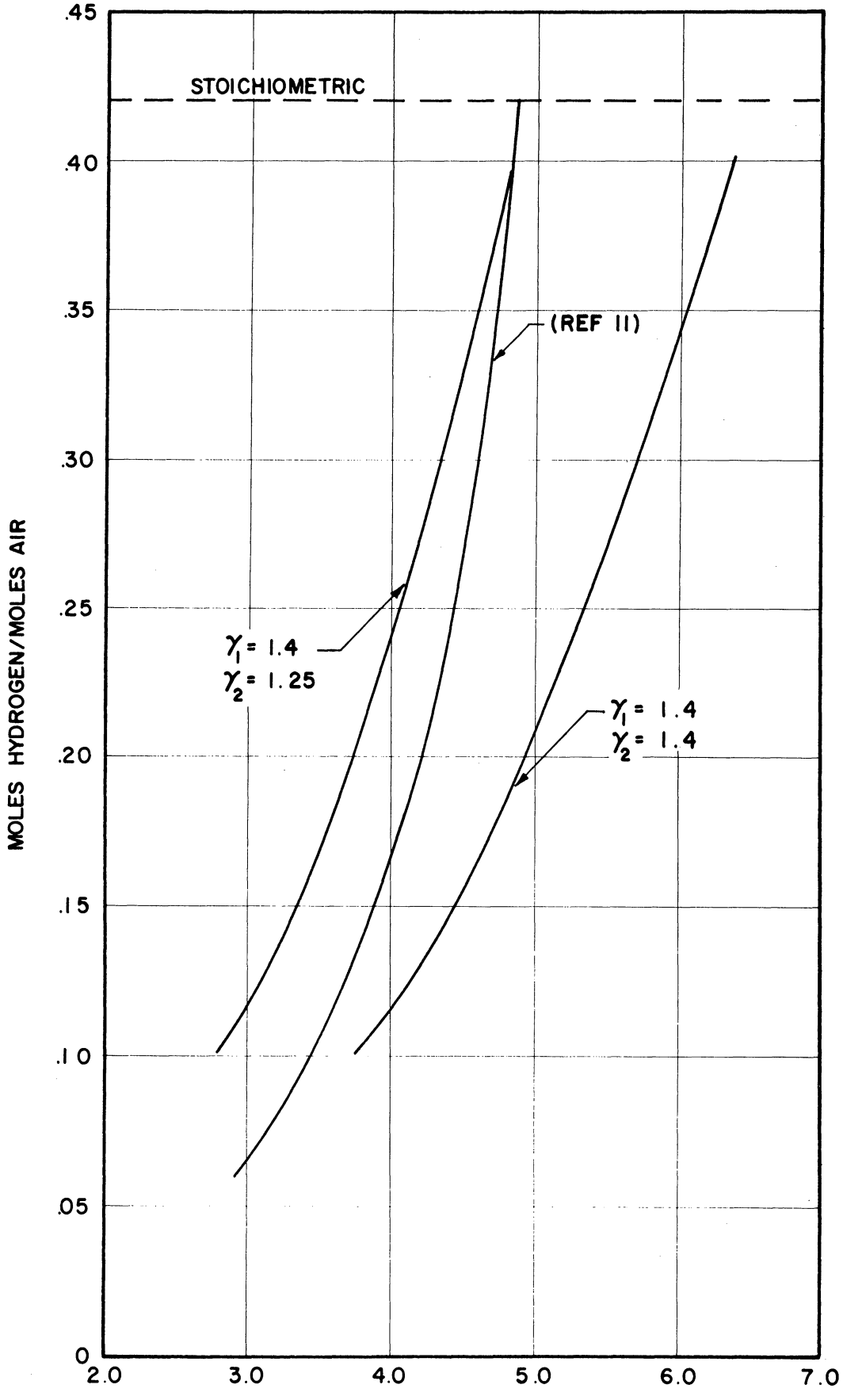

Figure 4. Mach Number of Detonation versus Fuel-Air Ratio (Hydrogen-Air)

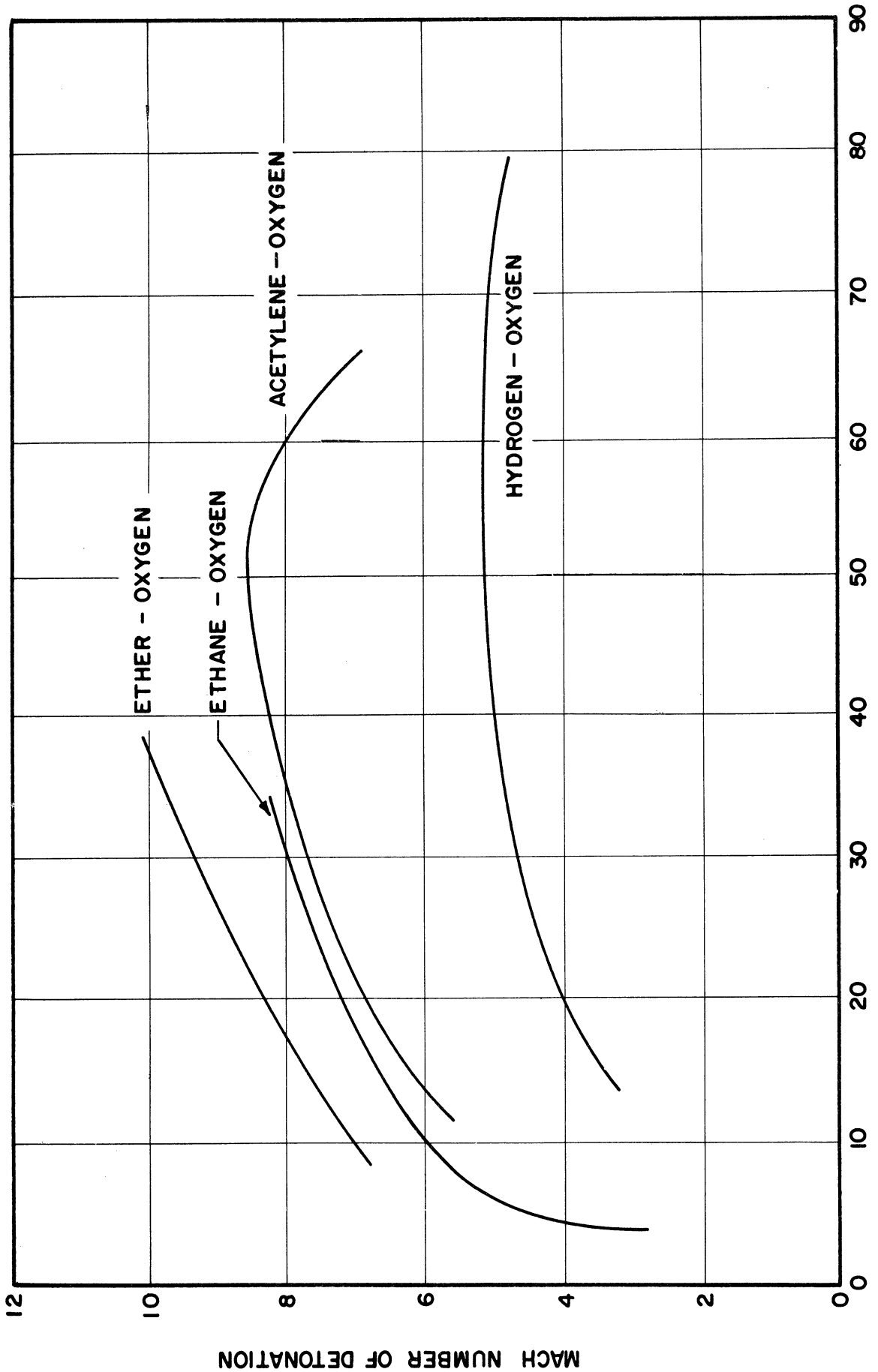

Figure 5. Mach Number of Detonation of Various Gaseous Mixtures.

p-v coordinates is known as a Hugoniot Curve and is shown in Figure 6. The upper branch represents detonative combustion and the lower deflagrative combustion. The divisions of each branch are characterized by the following:

Strong detonation	M_1 Supersonic	M_2 Subsonic
Weak detonation	M_1 Supersonic	M_2 Supersonic
C-J detonation	M_1 Supersonic	M_2 Sonic
Strong deflagration	M_1 Subsonic	M_2 Supersonic
Weak deflagration	M_1 Subsonic	M_2 Subsonic
C-J deflagration	M_1 Subsonic	M_2 Sonic

A straight line through the initial conditions intersects the detonation branch at two points in general. The slope of this line corresponds to the square of the mass flow per unit area. This is readily derived from a combination of Equations (2.1) and (2.2) to give:

$$\frac{P_2 - P_1}{v_2 - v_1} = -(\rho_1 V_1)^2 = -(\rho_2 V_2)^2 \qquad (2.14)$$

The weak detonation solution is ruled out as violating the Second Law when we consider the detonation wave to be a shock wave followed by combustion. Thus, the only possible solutions correspond to strong detonation or C-J detonation. For the C-J condition the straight line given by Equation (2.14) is tangent to the Hugoniot curve. It is interesting that this singular solution is the one always detected in flame tubes and shock tubes in the steady state.

2.3 Representation of Detonation on a φ (M) curve.

Another instructive representation of detonation combustion is

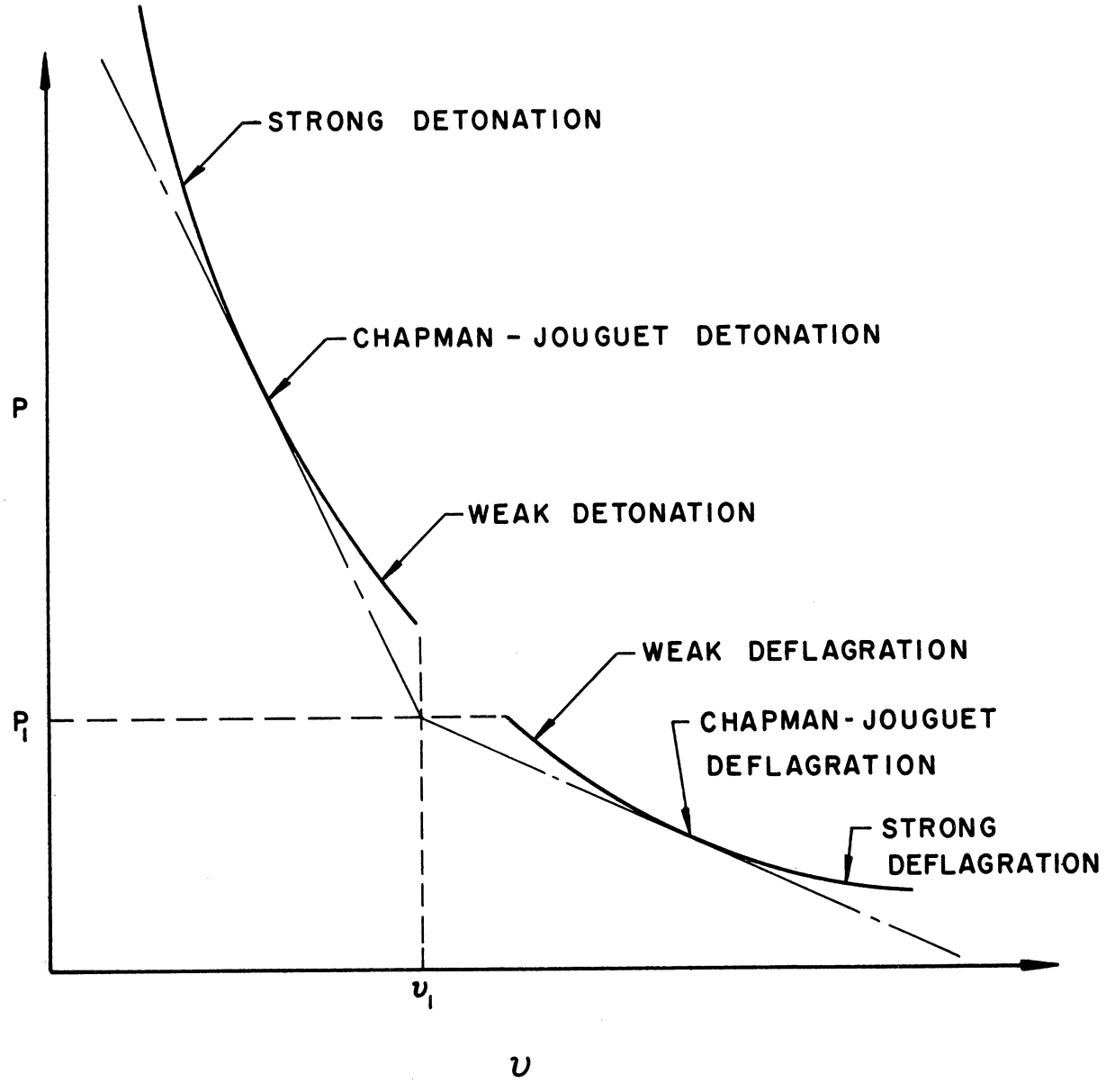

Figure 6. Hugoniot Curve.

possible by eliminating the thermodynamic variables in favor of Mach number. In this case, assuming constant specific heats and constant molecular weight, Equations (2.1), (2.2), (2.3), and (2.9) and the definition of Mach number combine to yield:

$$\frac{M_1^2\left(1+\frac{\gamma-1}{2}M_1^2+\frac{Q}{C_pT_1}\right)}{\left(1+\gamma M_1^2\right)^2}=\frac{M_2^2\left(1+\frac{\gamma-1}{2}M_2^2\right)}{\left(1+\gamma M_2^2\right)^2}=\varphi(M_2) \qquad (2.15)$$

where φ (M) is defined by:

$$\varphi(M)=\frac{M^2\left(1+\frac{\gamma-1}{2}M^2\right)}{\left(1+\gamma M^2\right)^2} \qquad (2.16)$$

A plot of φ (M) versus M is shown in Figure 7. It is to be noted that when $\varphi(M_1) = \varphi(M_2)$, $Q = 0$; that is, the process 1-a is adiabatic. Thus from Equation (2.15) with the initial conditions and Q given $\varphi(M_2)$ is readily calculated. But this value of $\varphi(M_2)$ corresponds to two different values of M_2 and other information is required in order to fix M_2. For detonation waves, where M_1 is supersonic, this is relatively easy. For example, the three types of detonation may be visualized on such a curve in the following way. A supersonic free stream at a Mach number $M_1 > 1$ (point 1) is shocked to a subsonic Mach number, M_a (point a). Subsonic heat addition then accelerates the stream. If this heat added is only sufficient to accelerate the stream to $M_{2s} < 1$, the combined process, $1\text{-}2_s$ corresponds to strong detonation. C-J detonation is realized when the final condition is at $\phi(M)_{max}$ corresponding to $M_2 = M_{2C\text{-}J} = 1$. Weak detonation would be the process $1 - a - 2_s - 2_w$ wherein $M_{2w} > 1$. But the

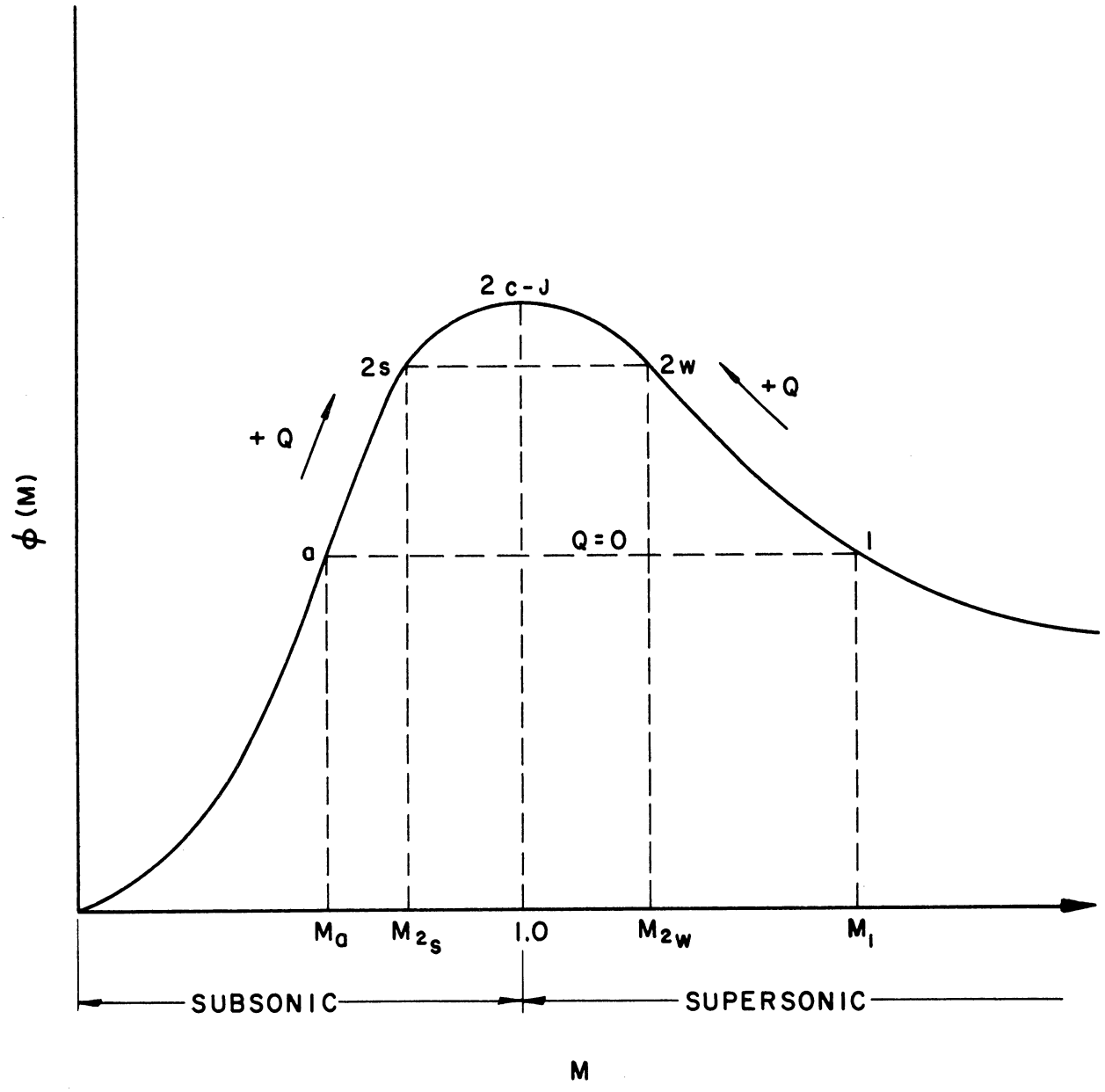

Figure 7. φ(M) Representation of Detonative Combustion.

path, 2_s - 2_w (which is the same as strong deflagration), corresponds to an increase in Mach number at constant area under adiabatic conditions for $\varphi\,(M_{2s}) = \varphi\,(M_{2w})$. This transition violates the Second Law in that the entropy at 2_w is less than that at 2_s. Hence we conclude that weak detonations and strong deflagrations are impossible, at least within the restriction that a detonation wave is a shock followed by combustion.

2.4 Effect of Initial Conditions on M_{C-J}.

The effects of mixture ratio on the Mach number of detonation is evident in Figure 5. Peak M_{C-J}'s usually occur near the stoichiometric mixture ratio with a gradual falling off on the lean and rich side. The problem of stabilizing a wave becomes simpler experimentally for lower M_{C-J} (as will be discussed later) so that there is some advantage to be gained in the use of leaner mixtures.

The simplified analytical treatment of detonation predicts no effect of the initial temperature and pressure on the velocity of detonation. Actually, however, the pressure enters in that it influences the degree of dissociation of the burned gases which in turn influences the velocity of propagation. That is, the higher the pressure the less the dissociation and hence the greater the velocity of detonation. Information in this regard, both experimental and analytical, may be gathered from References 4, 11, 12, and 13 . Inasmuch as low pressures and hydrogen-air mixtures are of interest here, it will suffice to show some results (Figure 8) obtained by the author and co-workers recently [14]. As expected for these mixtures, the effect is rather small over most of the

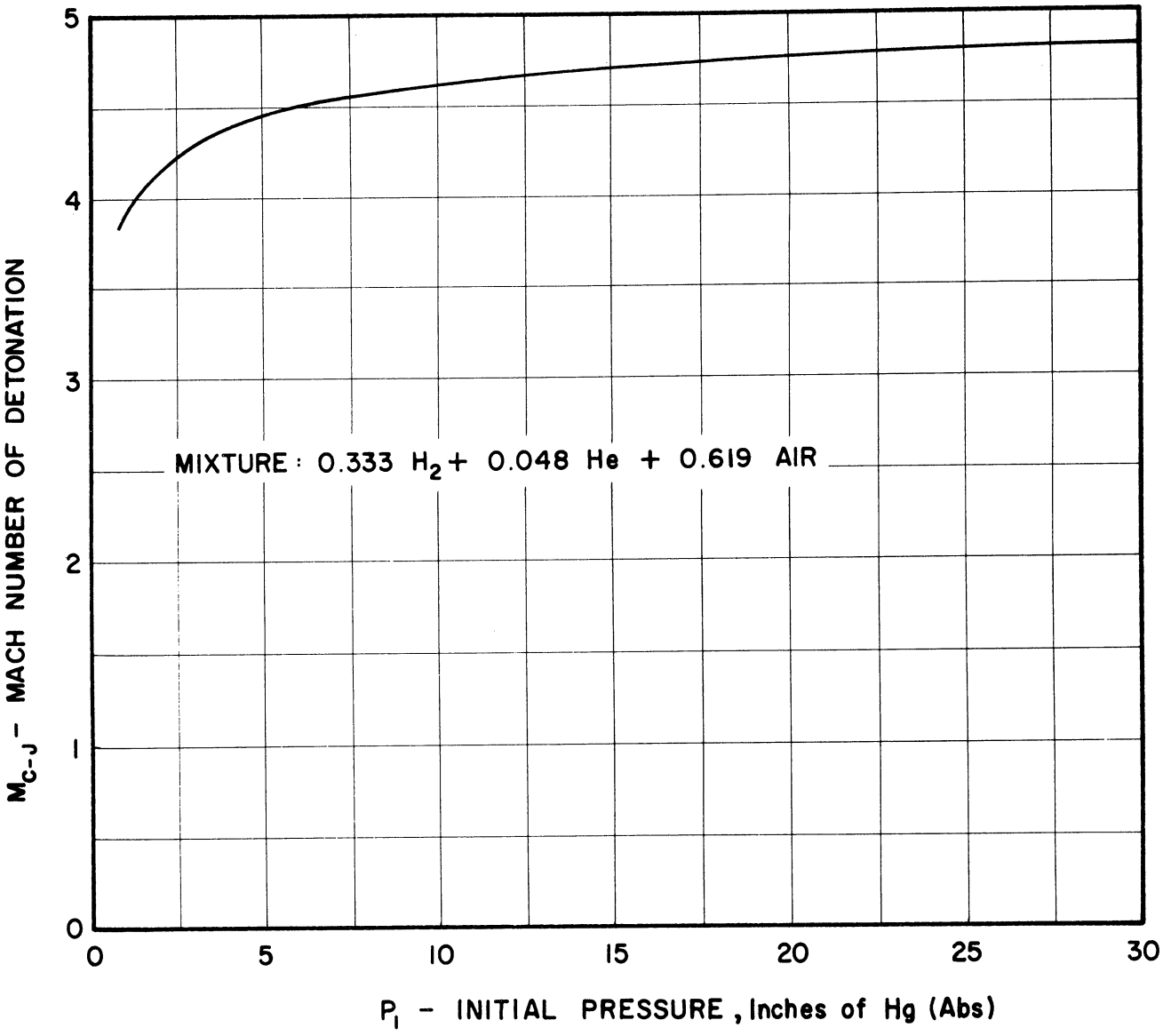

Figure 8. Mach Number of Detonation versus Initial Pressure.

pressure range. The rapid drop off in Mach number near the lean limit is probably a range of unstable detonation. Experimental points in this range suffer from considerable scatter.

The primary effect of static temperature arises from the fact that it alters the speed of sound of the unburned gas. Thus, for constant velocity of detonation, M_{C-J} will vary inversely with the square root of initial temperature. But changing M_{C-J} yields different pressure ratios and temperature ratios across the wave so that the extent of dissociation will differ. This results in rather small change in the velocity of detonation as has been reported by Lewis and von Elbe [15], Cannon and Jewell [16], and Moyle [17]. Cannon and Jewell's results for ethane-oxygen and Moyle's results for hydrogen-oxygen are each compared with the simplified prediction, $M_{C-J} \propto \frac{1}{\sqrt{T}}$, in Figure 9. The curves are made to agree at $T_1 = 300°$ K. The agreement is seen to be quite good.

2.5 Structure of the Wave.

The discussion to this point has assumed the wave to be a discontinuity. Under many conditions this is a perfectly reasonable assumption as is evident from the very good agreement between experiment and theory. However in the case of detonations in very lean mixtures or at low pressures the wave has been found to become quite extended. This was first observed by means of shadowgraph photography by Bone, Fraser, and Wheeler [18]. Schlieren photographs of the same phenomena have been published by Morrison [4] and Nicholls, Morrison, and Cullen [19]. This effect is shown in

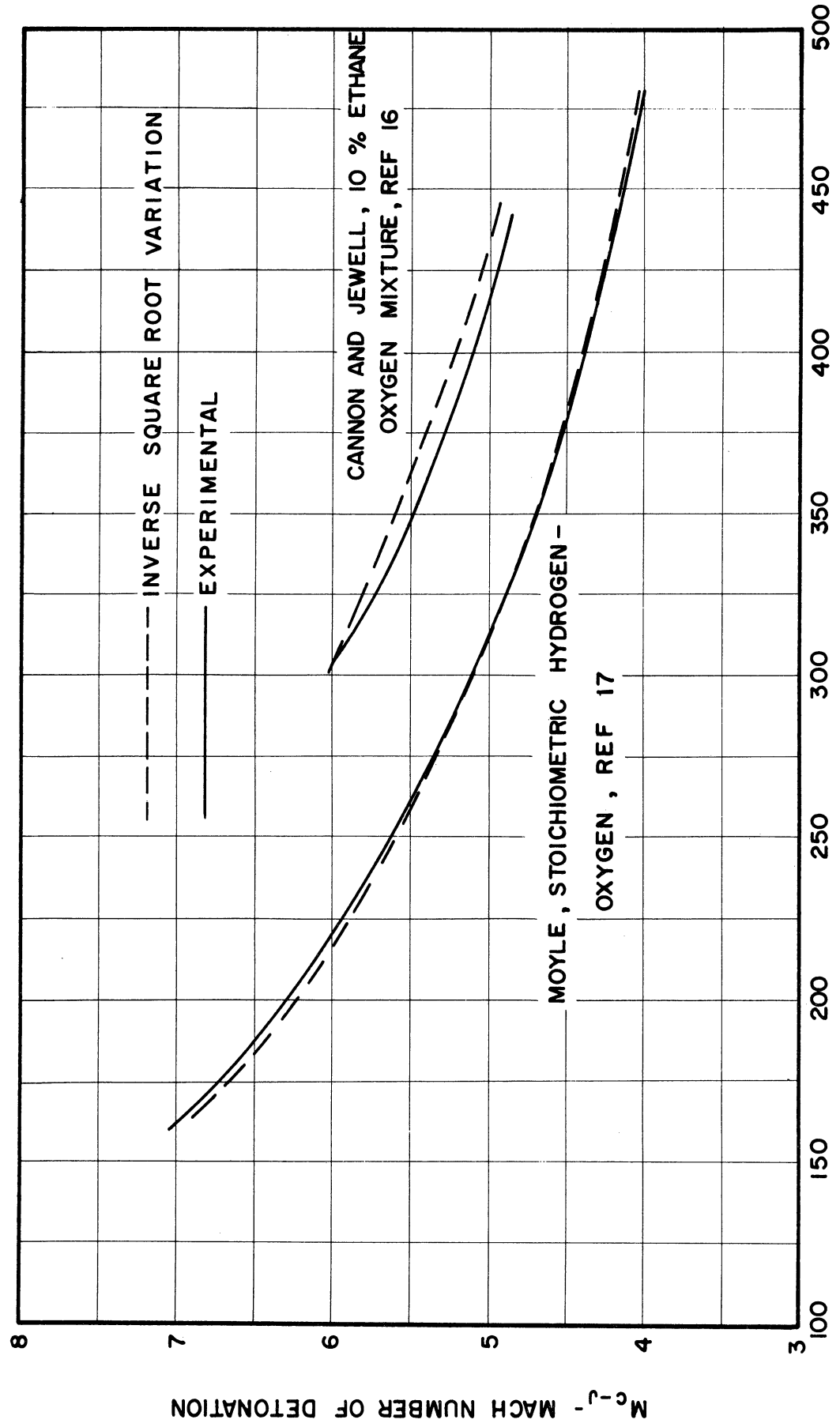

Figure 9. Mach Number of Detonation versus Initial Temperature.

Figure 10 which shows spark schlieren photographs of ethane-oxygen detonations at different mixture ratios. It is apparent that for the richer mixtures the wave appears to be a relatively clean discontinuity. For the leaner mixtures the reactions extend over a much greater time and the initial shock with some combustion is trailed by oblique shock waves as well as residual combustion. It is not entirely clear as to the correct explanation of these effects. Certainly the wall boundary layers play some role leading to two dimensional effects. Another likelihood is the existence of spinning detonation which has recently been shown to be a common occurrence in the case of hydrogen mixtures near the limits. Gordon, Mooradian, and Harpes [20] have reported on extensive work in this regard. The other possibility or contribution may arise from the importance of transport processes in the propagation of the wave. Until relatively recently, analytical attempts to describe the structure of the wave did not account for the influences of heat conduction and viscosity and thus predicted a structure characterized by the finite chemical reaction rates. Hirschfelder and Curtiss [21], Linder, Curtiss, and Hirschfelder [22], and Curtiss, Hirschfelder, and Barnett [23] have reported on their extensive calculations which take into account the transport terms. These results reveal that under certain conditions there is appreciable influence on the structure of the wave arising from these effects. Adamson *, in an analytical study of the problem, has likewise found the transport terms to be important under certain conditions.

It was felt that for purposes of stabilizing a detonation wave, the extended reaction zone type, as described above, should be avoided if

---

* Associate Professor T. C. Adamson, Jr., Department of Aeronautical and Astronautical Engineering, University of Michigan, private communication, to be published.

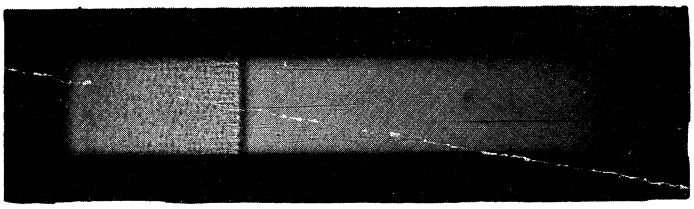

25% Ethane-Oxygen (volummetric)

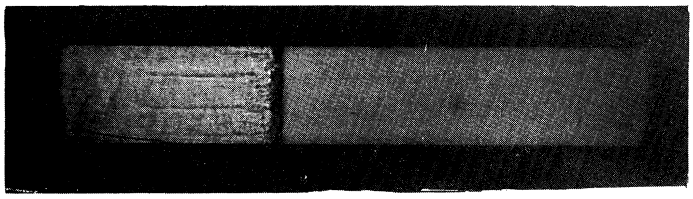

10% Ethane-Oxygen (volummetric)

6% Ethane-Oxygen (volummetric)

Figure 10. Schlieren Photographs of Detonation Waves.

possible. One of the main reasons for this is that a stabilized "smeared" wave could yield highly complicated two dimensional effects and modified combustion that would render accurate identification and description of the detonation wave nearly impossible. Recognizing this restriction, the problem of stabilizing a wave becomes somewhat more trying in that richer mixtures and higher pressures are indicated in order to get clean discontinuities. In other words, higher detonation Mach numbers, with the attendant experimental complications, are indicated.

III CONDITIONS TO BE MET IN STABILIZING THE WAVE

3.1 Dynamic Conditions.

In Section II the properties of gaseous detonation waves were reviewed in so far as they influence the problem at hand. It is now desired to relate these characteristics to the dynamic conditions that must be met in order to stabilize a wave. For this purpose it is instructive to consider the expansion of a gaseous fuel and oxidizer in a convergent-divergent nozzle. The stagnation temperature and pressure of the potentially detonatable mixture are denoted by T_s and P_s respectively. It is then hypothesized that a detonation wave is initiated at some station (1) in the nozzle where the static temperature is T_1 and the Mach number is M_1, as indicated in Figure 11. In order that any combustion be initiated behind the shock the temperature must equal or exceed the "ignition" temperature of the mixture under the given conditions. For an isentropic expansion from the stagnation conditions the variation of static temperature with Mach number may be readily obtained and is shown in Figure 12 where curves for a few different values of T_s are given and γ is taken as 1.4. Now the simplified treatment of C-J detonation (Section 2.1) indicates that the C-J Mach number of detonation varies inversely with the square root of temperature. Utilizing this relation and specifying the combustible mixture for which the C-J Mach number is known at some initial temperature, it is possible to incorporate in Figure 12 the M_{C-J} at any T_1. For this purpose, a slightly lean mixture of hydrogen-air with a M_{C-J} of about 4.5 at a temperature of 530° R, was considered. In addition a curve is superimposed for a strong detonation wave, F = 1.5,

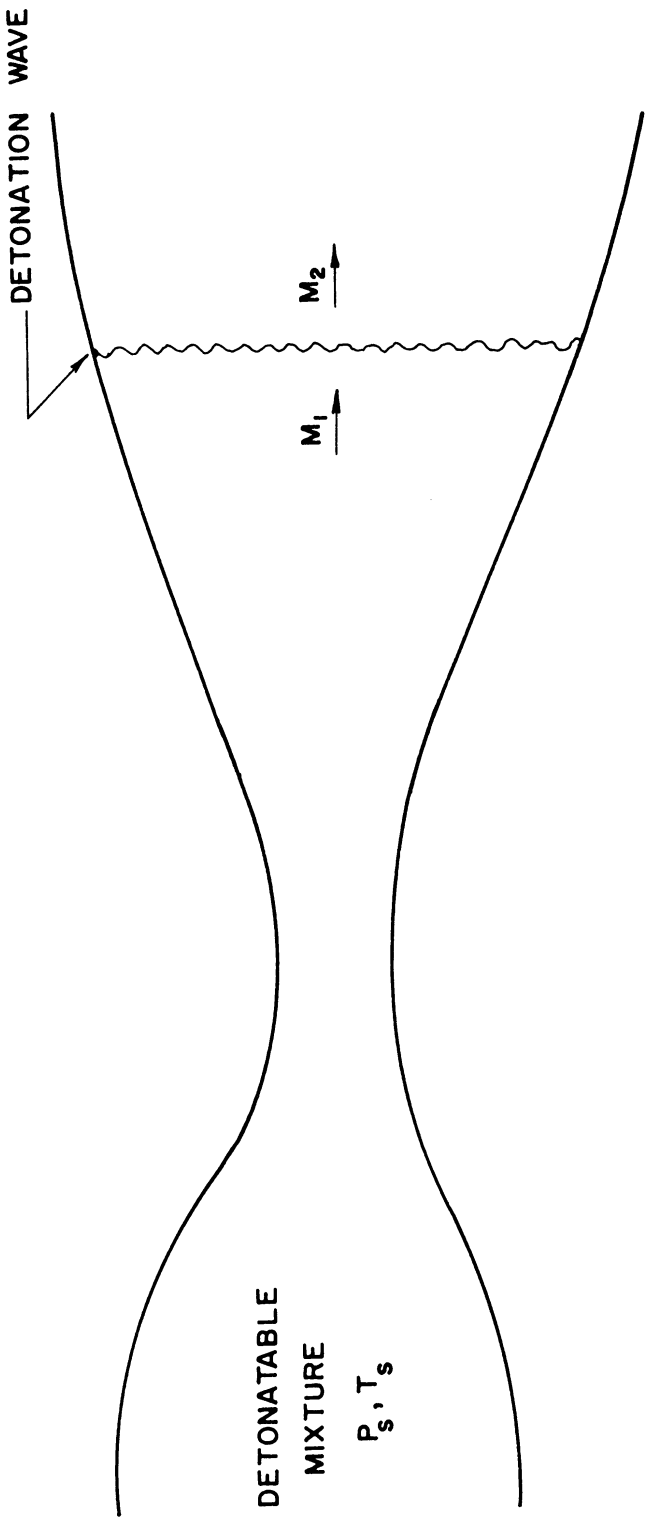

Figure 11. Detonation Wave in a Convergent-Divergent Nozzle.

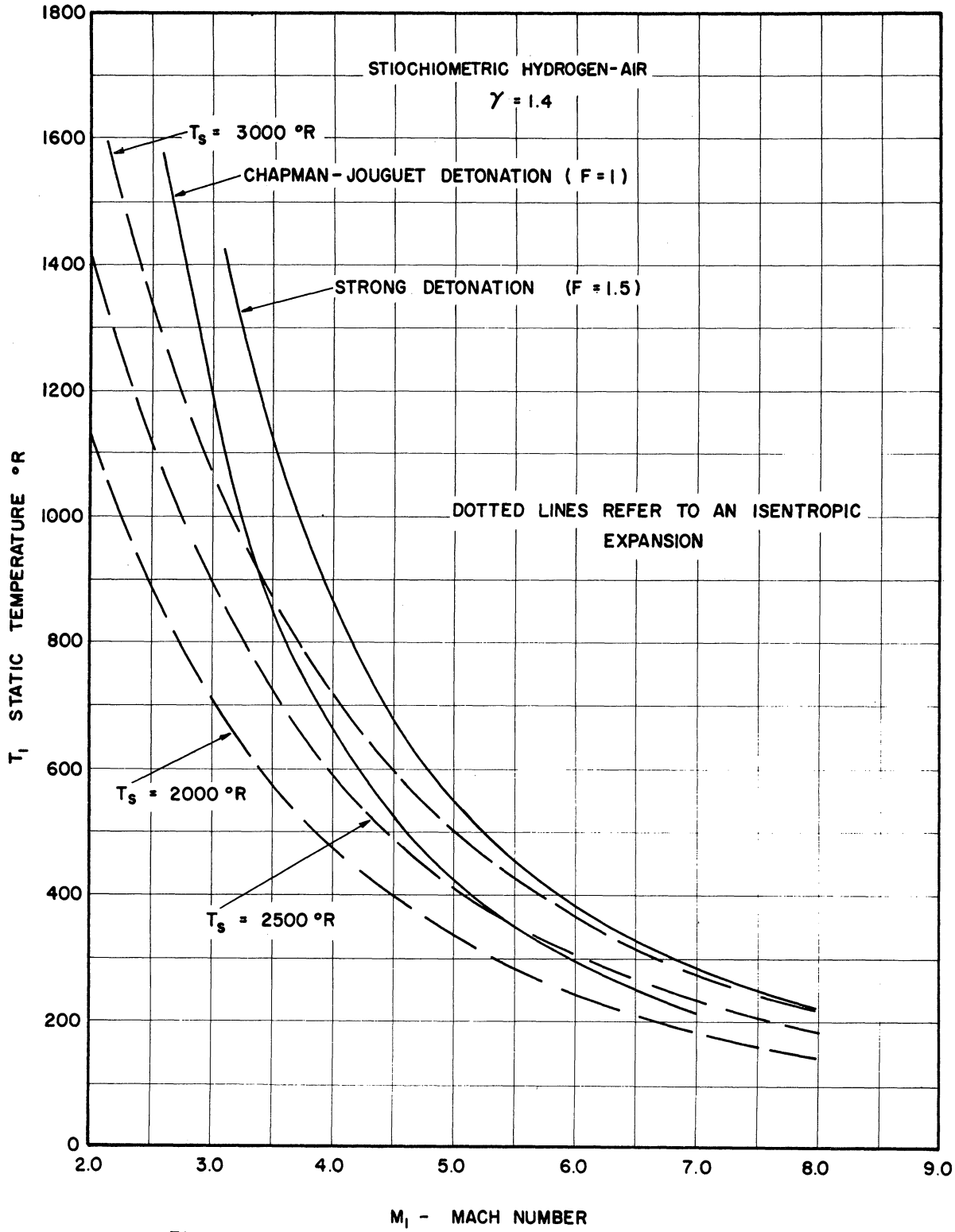

Figure 12. Isentropic Nozzle Expansion to Detonation Conditions.

for the same combustible mixture. This curve was determined through use of Equations 2.10 in the following way. The known value of M_{C-J} for any T_1 was used to evaluate Q (F=1). The same value of Q was then assumed in determining M_1 for any T_1 and F = 1.5 from Equation 2.10. The results shown in Figure 12 reveal the importance of stagnation temperature and bring out some interesting points. For example, let us consider the case of a stagnation temperature of 2500° R. Then in view of the fact that C-J detonation represents the minimum Mach number, no stable C-J detonation wave can exist in the nozzle at a Mach number less than 5.2, the intersection point between the two curves. If a detonation wave were generated in this zone, it would propagate upstream as the detonation Mach number is greater than the local Mach number corresponding to the local static temperature. On the other hand if a detonation wave were initiated at a point in the nozzle corresponding to higher Mach numbers than the intersection Mach number, one of the three things could happen. There is the possibility that the wave would move upstream and stabilize at the C-J point just described. There is also the possibility that the wave would stabilize as a strong detonation wave corresponding to some value F such that the position would be that of the intersection of the F = constant curve and the T_s = 2500° R curve. Finally there is the possibility of no stable solution in the nozzle and the wave could conceivably stabilize external to the nozzle or set up an oscillating flow. It would seem that the actual wave realized would be determined by the pressure ratio across the nozzle, just as the position of a shock wave in a nozzle is determined.

These curves serve to point out the significance of stagnation

temperature. Operation at high stagnation temperature indicates that the Mach numbers required for stabilization are minimized and thus alleviates the necessity of high pressures. But the development of high temperatures in a "steady flow" experiment presents many difficulties as well as being expensive for the flow conditions of interest here. The opposite solution is presented by operating with low stagnation temperatures but at higher Mach numbers although there is a limit to how low this temperature can be. The objection to the higher Mach numbers is, of course, the high pressures required. This arises not only from the aerodynamic consequences (separation) but also becuase of the influence of initial pressure on detonation. In view of these considerations, one is faced with the necessity of accelerating a potentially detonatable mixture to a rather high Mach number and at a high stagnation temperature.

3.2 Selection of a Particular Fuel.

As shown in Figure 5, characteristic values of M_{C-J} are very high when we exclude those mixtures near the detonation limit where the wave structure tends to become extended. These high Mach numbers infer high stagnation temperatures and pressures which, in many cases, appear unattainable. Accordingly it behooves one to select a mixture with a low M_{C-J}. In this respect hydrogen is one of the best although a stoichiometric mixture of hydrogen-oxygen under standard conditions detonates at $M_{C-J} = 5.2$. This is still quite high and hence consideration was given to the effect of diluents in hopes of lowering this Mach number. In order to evaluate this possibility, use was made of an equation presented by Morrison [4] which

was obtained from the correlation of many experimental results. The correlation equation is;

$$M_{C\text{-}J} = 2.37 \left(\frac{m_1}{m_2} \cdot \frac{Q}{C_{P_1} T_1} \right)^{0.328} \qquad (3.1)$$

First consider a low molecular weight diluent such as helium. Then the simplified chemical reaction (dissociation neglected) can be represented by;

$$H_2 + x O_2 + y\,He \longrightarrow H_2O + \left(\frac{2x-1}{2}\right) O_2 + y\,He \qquad (3.2)$$

where: x = moles of oxygen

y = moles of helium

The terms of Equation (3.1) may be written as;

$$m_1 = \frac{2 + 32x + 4y}{1 + x + y}$$

$$m_2 = \frac{18 + \left(\frac{2x-1}{2}\right)32 + 4y}{1 + \left(\frac{2x-1}{2}\right) + y} = \frac{2 + 32x + 4y}{1 + \frac{2x-1}{2} + y}$$

$$Q = (\text{Heating value of hydrogen}) \times \frac{\text{mass of hydrogen}}{\text{mass of reactants}}$$

$$= 51{,}620 \left(\frac{2}{2 + 32x + 4y} \right) \quad \frac{\text{BTU}}{\#\text{ of reactants}}$$

$$C_{P_1} = \frac{w_{H_2} C_{P_{H_2}} + w_{O_2} C_{P_{O_2}} + w_{He} C_{P_{He}}}{w_{H_2} + w_{O_2} + w_{He}}$$

where: w = mass of the particular gas

$$C_{P_{H_2}} = 3.5 \quad \frac{BTU}{\#^\circ R}$$

$$C_{P_{O_2}} = 0.22 \quad \frac{BTU}{\#^\circ R}$$

$$C_{P_{He}} = 1.25 \quad \frac{BTU}{\#^\circ R}$$

When the above relations are combined, (3.1) becomes;

$$M_{C-J} = 2.37 \left[\frac{51{,}620}{520} \left\{ \frac{2x + 2y + 1}{(x + y + 1)(7.04x + 5y + 7)} \right\} \right]^{0.328} \quad (3.3)$$

The results are shown in Figure 13 and reveal that significant reductions can be effected only by using lean mixtures (large values of x) and/or large diluent concentrations (large values of y). In either case, on the basis of Morrison's schlieren photographs of lean hydrogen-oxygen waves, it was felt that very extended reaction waves would be realized. Also there is considerable doubt that the lean mixtures with high dilution would even detonate. Meager experimental results are available in this regard.

The same approach was used in considering a high molecular weight diluent, argon. Almost identical results were obtained and the idea was abandoned. Instead it was decided to use a hydrogen-air mixture which detonates at a somewhat lower Mach number than hydrogen-oxygen (4.8 compared to 5.2 for stoichiometric ratio). It was known that the detonation front was less clean than in the case of hydrogen-oxygen but this compromise was accepted. In addition to the lower Mach number there is the great advantage of using conventional air compressors to generate the high steady flows of high pressure air. Compared to this would be the necessity of utilizing an unreasonably large number of bottles of stored oxygen for any given experiment.

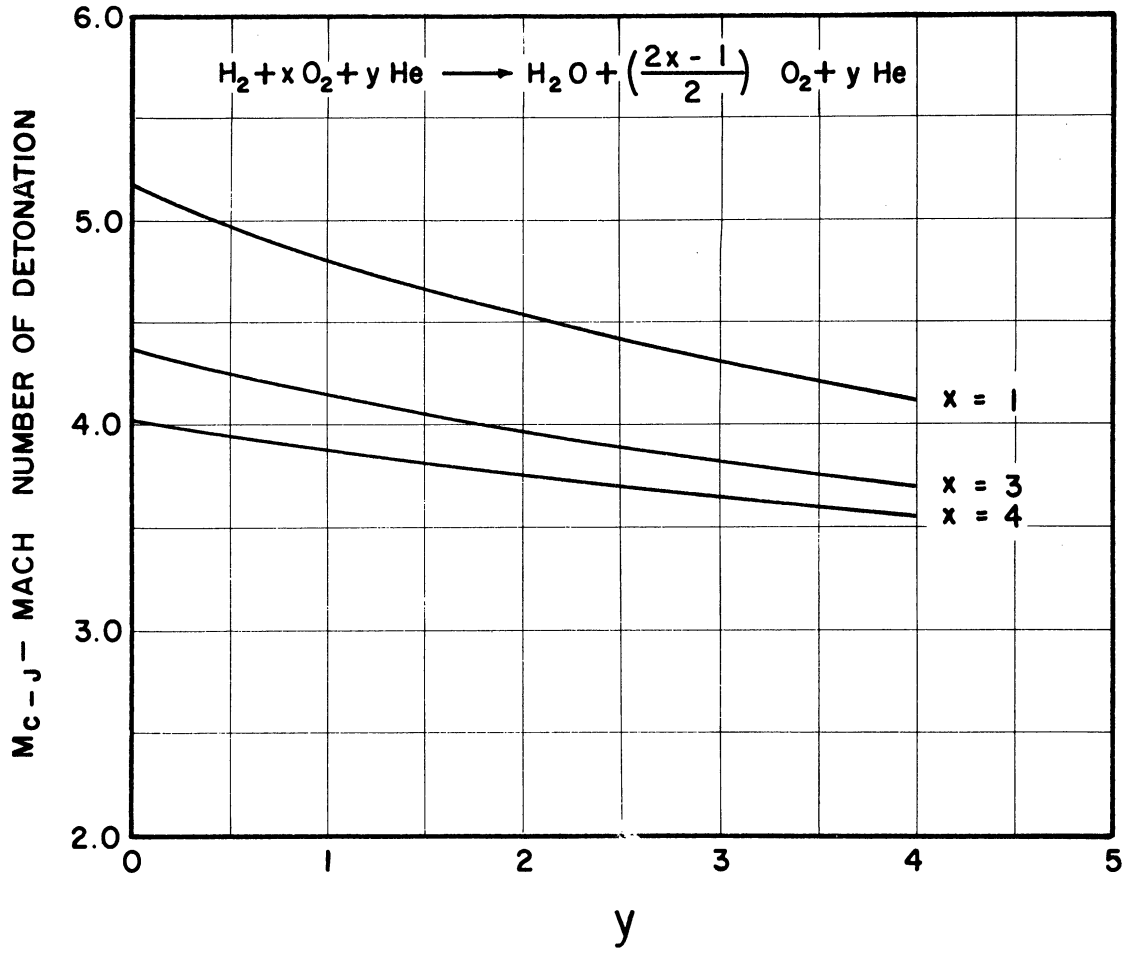

Figure 13. Effect of a Diluent on Mach Number of Detonation.

3.3 Method of Stabilization of the Wave.

Assuming now that the proper dynamic conditions can be obtained, there remains the problem of the actual means of stabilization. One of the first methods considered was stabilization in a supersonic diverging nozzle by controlling the reservior to receiver pressure ratio. In the case of shock waves the position of the shock in the nozzle (when this is possible) is determined by this pressure ratio such that the boundary condition of receiver pressure can be met. Similarly it might be supposed that if energy is released across the shock (as in a detonation wave) the attendant greater stagnation pressure loss will mean that the wave must stabilize at a lower Mach number in order to meet the same downstream boundary condition of receiver pressure.* Of course the wave can only stabilize there if the dynamic conditions into the wave are met as pointed out in section 3.1. In this discussion, as well as in subsequent discussion, attention is given to stability only in the steady flow sense. That is no account is taken of time variant flow fluctuations and their influence on wave stability. In this regard it should be pointed out that with normal strong detonation waves the downstream flow is subsonic so that pressure disturbances generated downstream can influence the wave. This could, of course, be influential in determining stability.

Again in analogy to shock waves, another means of stabilization might be on a wedge or cone in a supersonic stream. Samaras [24] first analyzed the properties of oblique detonation waves while Siestrunck and Fabri [25] and Rutkowski and Nicholls [14] made use of the concept of detonation polars in connection with wedge stabilization. More recently

---

* In general this wave would be a strong detonation with the C-J case a singular solution as pointed out in section 3.1.

Chinitz, Bohrer, and Rivlin [26] have reported on extensive calculations of oblique detonation waves stabilized on a wedge. The results of such a treatment point out some interesting aspects which are worthy of some discussion. We consider the case of a supersonic detonatable mixture flowing over a two dimensional wedge of half angle, δ , as shown in Figure 14. An oblique detonation wave is stabilized on this wedge at a wave angle, β , and the detonation Mach number is now the normal component of M_1 into the wave. Then the problem may be treated in the same way as in the case of shock waves except that the energy equation includes a term for the chemical energy release. The details of this analysis are presented in Reference 14. The simplified analysis leads to results such as shown in Figure 15 where the parameter, λ, is the ratio of stagnation temperature behind the wave to that in front. The curve for $\lambda = 1$ represents the classical shock hodograph while $\lambda_1 > 1$ is a similar plot of the locus of possible end states for detonations with a constant $\lambda = \lambda_1$. The branch c-d along λ_1 can be shown to represent weak detonation solutions while c-a corresponds to strong detonations. The singular point c corresponds to the Chapman-Jouguet condition. That is, a wedge angle of δ_c is the only one yielding C-J detonation. The point c is a point of tangency for a straight line drawn from g tangent to the λ_1 curve. There is a maximum angle, δ_f , beyond which the detonation wave would become detached just as in the case of shock waves. A wedge angle of δ_b leads to two possible attached strong detonation waves. The solution realized, as in the case of shock waves, is probably dependent upon downstream conditions. Similarly, in the case of a wedge angle less than δ_c , two solutions would appear to be possible. One would be the

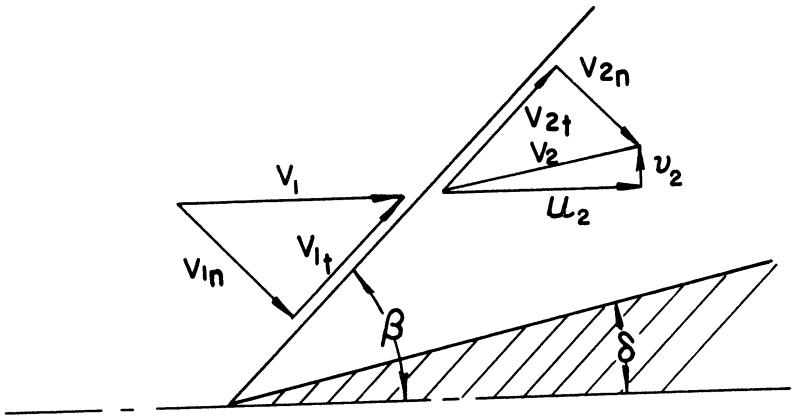

Figure 14. Oblique Detonation Wave Stabilized on a Wedge.

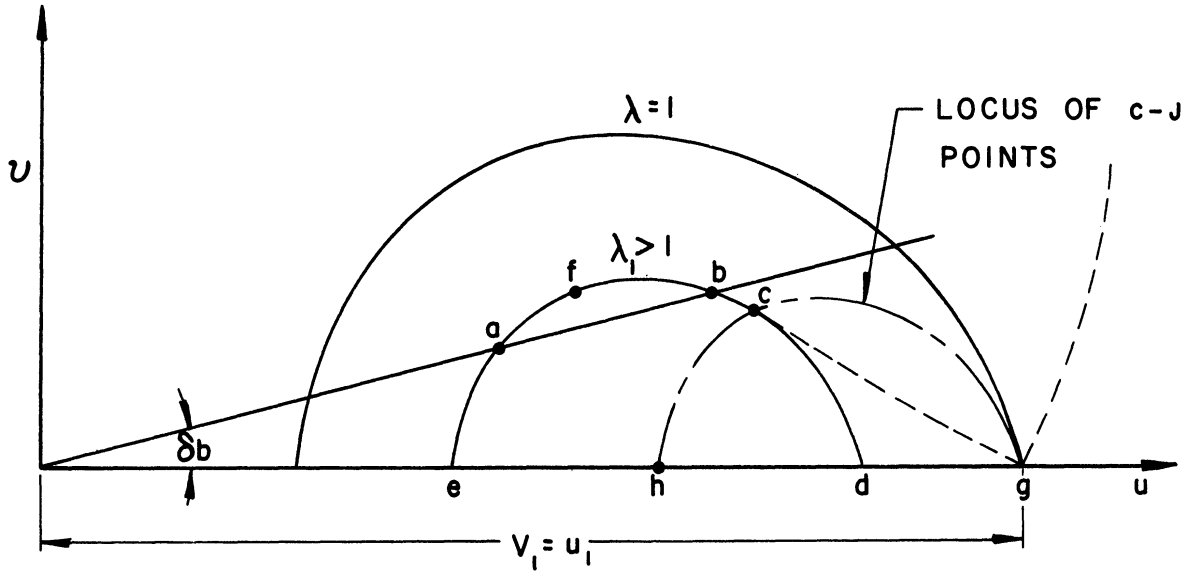

Figure 15. Detonation Polar.

strong detonation solution near point e. The other might be more complex. Inasmuch as weak detonations are impossible, the region near point d might lead to a C-J detonation immediately followed by a rarefaction fan so that the final flow could meet the required turning angle.

There are, of course, an infinite number of curves of λ = contant for any given free stream condition. The particular value would depend on the combustible mixture used. The locus of all possible C-J points is indicated. There is, however, a maximum value of heat release beyond which no steady flow solution can be realized. This is represented by the single point, h, which is the case of a normal C-J detonation. Heat addition greater than that corresponding to λ_h would imply that the wave moves upstream.

Thus the idea of stabilizing a detonation wave on a wedge is an attractive one and was seriously considered. One great advantage would appear to be that the burned gases are, in general, supersonic so that downstream distrubances should not affect the wave. Also, different strengths of detonation may be realized for the same free stream conditions by merely changing the wedge angle. In spite of these favorable characteristics the idea of stabilizing a detonation wave on a wedge was deferred for the present. It was felt that uncertain detonation wave-boundary layer interaction effects, the possibility of combustion in the boundary layer, and excessive heat transfer to the walls and wedge would all be serious problems.

In order to circumvent these difficulties, it was decided to attempt stabilization in the open jet of an axisymmetric nozzle exhausing to the atmosphere and operating under highly underexpanded conditions. The

structure of such jets has been observed and studied by many investigators for many years. Among the pertinent investigations is the work of Prandtl [27], Owen and Thornhill [28], Love and Grisby [29], Wilcox, Weir, Nicholls, and Dunlap [30], and Adamson and Nicholls [31]. A typical configuration is shown in Figure 16 wherein the major features are indicated. In these cases the exit pressure is much greater than the ambient pressure so that the flow expands upon leaving the nozzle. Because of the three dimensionality of the flow, expansion waves are generated from the leading characteristic which reflect from the jet boundary as compression waves. These compression waves coalesce to form the intercepting shock. The intercepting shock is terminated by an almost normal shock wave often referred to as the Mach disc. As indicated, Mach reflection occurs at the juncture of the intercepting shock and Mach disc and there is a reflected shock as well as a slip line. The zone between the nozzle exit plane, the intercepting shock, and the Mach disc is one of isentropic expansion which may be likened to the expansion in a supersonic nozzle. In the case at hand, the gas passing through the disc is the high stagnation temperature hydrogen-air mixture so that the shock serves to ignite the mixture as previously discussed. This, then, under the proper conditions should become a detonation wave. Contrary to the case of wedge stabilization, generation of a strong detonation in this system implies subsonic gas velocities behind the wave. Thus downstream influences could be felt and there is the possibility that the strong detonation would always degenerate to the Chapman-Jouguet state.

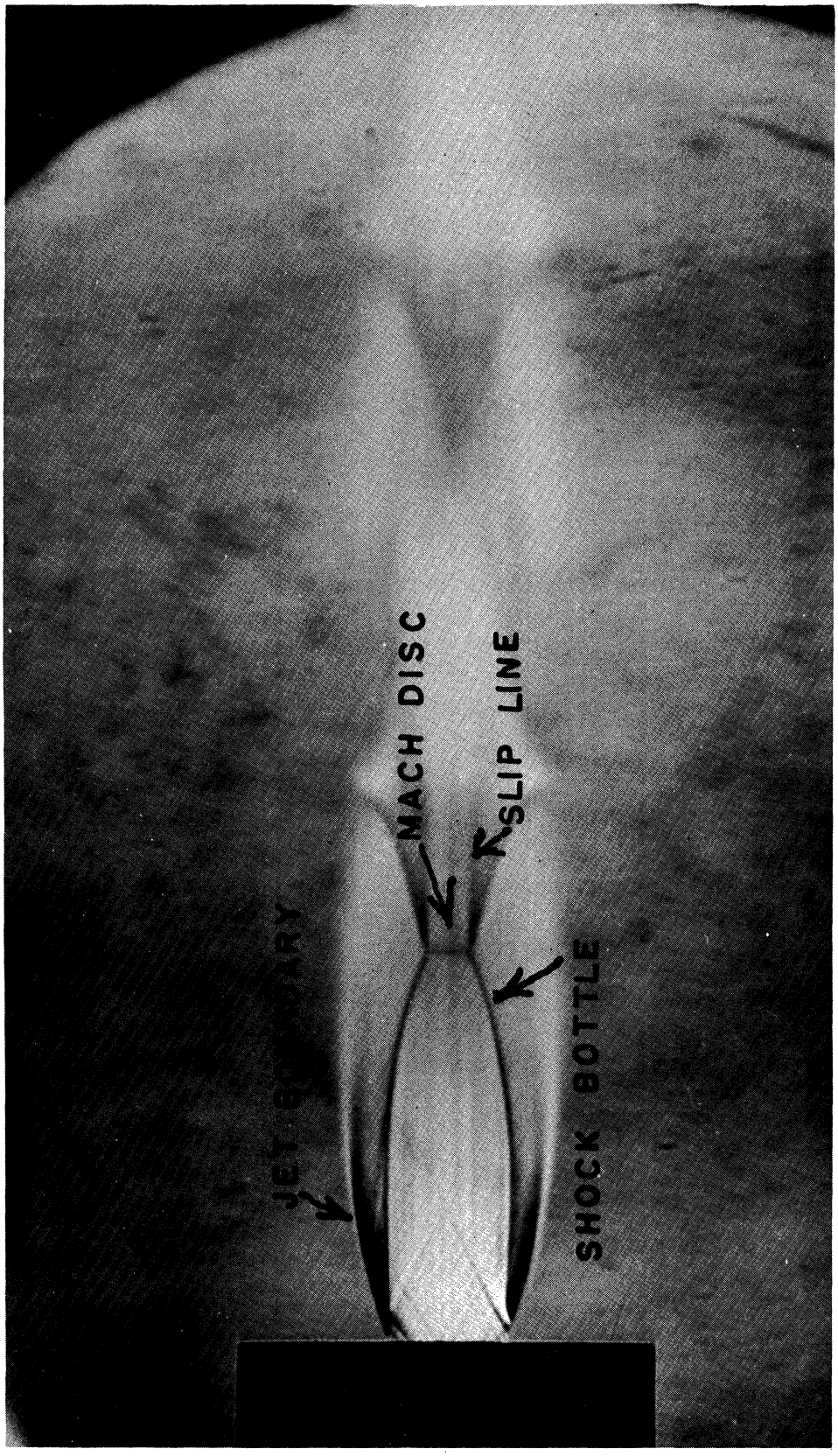

Figure 16. Structure of a Highly Underexpanded Axisymmetric Jet.

IV EXPERIMENTAL ARRANGEMENT AND PROCEDURE

Consideration of the necessary conditions for the stabilization of a hydrogen-air detonation, as brought out earlier, reveal that a stagnation temperature in the neighborhood of 2500°R is required. This temperature is well above the ignition temperature (approximately 1500°R) for hydrogen-air and thus precludes mixing the gases under stagnation conditions. One is then faced with the following problem: high pressure air must be heated to the appropriate value and expanded in a supersonic nozzle where high pressure hydrogen (not necessarily heated) is injected; the gases mix supersonically in the diverging part of the nozzle where the temperature will be below ignition temperature; the mixed gases pass through a shock wave which serves to increase the temperature above the ignition value and hence initiate combustion. The experimental arrangement adopted for effecting these functions is described in the following sections.

4.1 Expermental Facility.

The standing detonation wave facility is shown schematically in Figure 17. This facility is located at the Aircraft Propulsion Laboratory, Department of Aeronautical and Astronautical Engineering, North Campus. There are two circuits, as indicated in the figure, as the system is of the blowdown type. The first circuit, the one shown in dotted lines, represents the path for the pre-run phase of heating up the pebbles in the storage type heat exchanger. The solid lines represent the test circuit activated on blowdown.

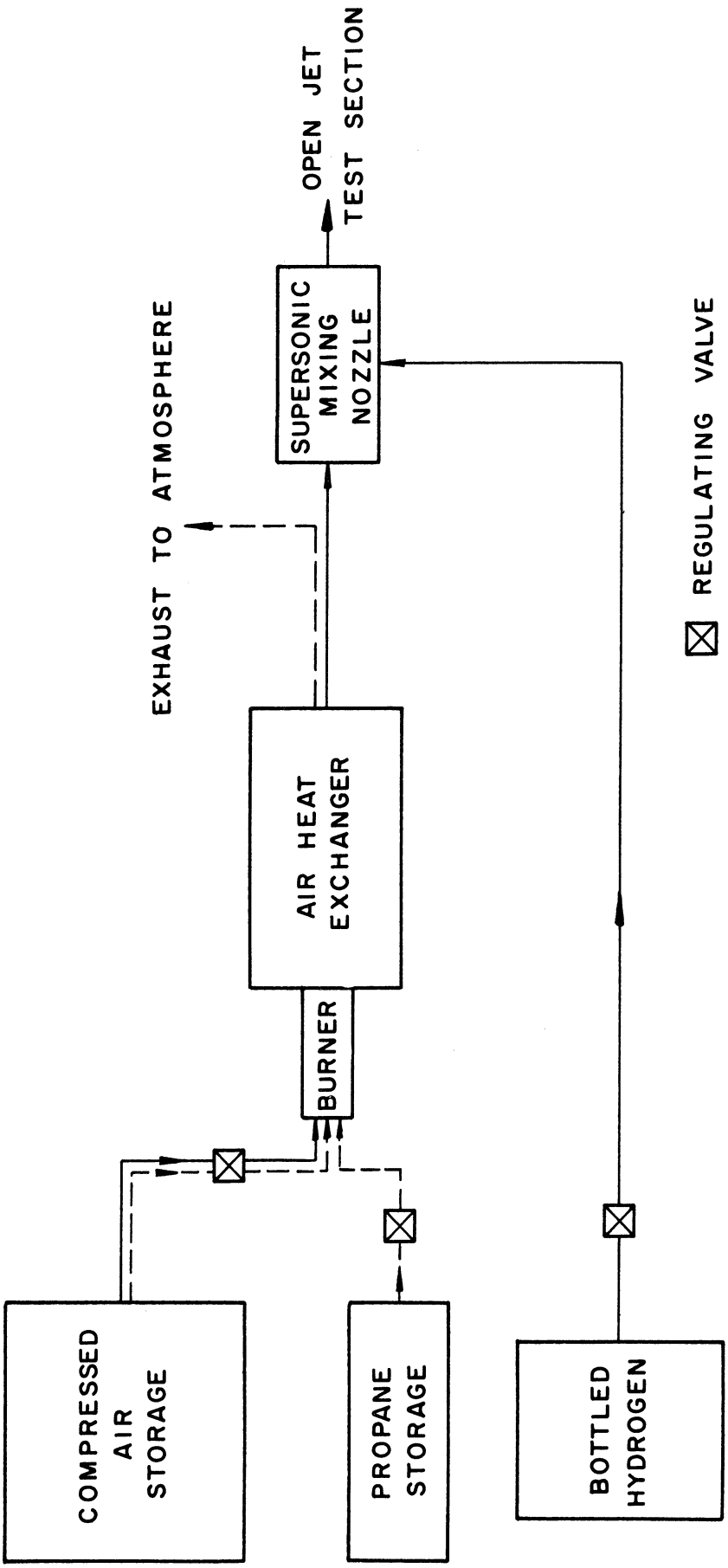

Figure 17. Schematic of Experimental Facility.

The air is compressed by a 250 HP Ingersoll-Rand Compressor which is located in the Pump House of the Aeronautical Laboratories. The air is stored at a pressure of 2500 psi in 4 storage tanks. The volume of each tank is 80 ft^3 so that (including the pipe line volume of about 55 ft^3) a total of 375 ft^3 is available for air storage. At the pressure mentioned and at a temperature of 60°F., about 4800 pounds of air are stored. At this pressure the air is quite dry provided some time is allowed after pump-up for the moisture to condense and settle out. As a matter of interest, the compressor will replenish the storage pressure at a rate of about 500 psi per half hour.

Liquid propane is stored in a 4000 gallon commercial tank which is located outside and near the Pump House. Propane vapor is used to fire a propane-air burner on the head end of the heat exchanger during the heat-up period. While the vapor pressure in the tank is highly temperature sensitive and the temperature will tend to drop as the vapor is drawn-off, no difficulty has been experienced in obtaining the desired flow rate.

High pressure hydrogen storage consists of 6 commercial bottles feeding a common manifold. The manifold is throttled to the desired pressure and flow rate for the run. The initial pressure in the bottles as received from the distributor is ordinarily about 1900 psi. Under usual operating conditions the 6 bottles are then sufficient for a run time of about 12 minutes.

The remainder of the experimental facility consists of the heat exchanger, the nozzle, the control panel, and instrumentation. These components will be described in the subsequent sections.

4.2 Regenerative Heat Exchanger.

The heat exchanger for the type of experiment of interest here is required to heat approximately 0.5 pounds/seconds of air through a temperature difference of over 2000°F. and at an elevated pressure up to 1000 psi. This corresponds to a steady state heating power level of about 300 KW. These conditions are difficult and expensive to achieve and the most logical solution appeared to be an exchanger of the pebble bed regenerative type. Accordingly such an exchanger was designed and fabricated and is being used. A cross section of the unit is shown in Figure 18. The assembly consists of a 14 foot long Navy surplus catapult steel cyclinder (1), 24 inch O.D. by 18 inch I.D., lined with lap-joined ceramic rings 12 inches long and 12.5 inches I.D. (2), and with ceramic pebble retainer (3) and plug (8) at the end. Between the ceramic rings and the shell, ceramic grog is packed to allow for any differences in radial expansion. An allowance for longitudinal expansion is made by making the total length of the liner shorter than the shell. The space inside the liner is filled with 3/8 inch alumina pebbles which make up the heat storage medium. The burner (7) is a stainless steel cylinder lined with ceramic. The propane and air are mixed in a stainless steel unlined pipe (11) prior to entering the burner. At the end of the mixing chamber a spark plug is positioned in the 1 inch stainless steel pipe shown to provide for ignition of the mixture.

The downstream end of the unit is similar to the above with the exception of the burner. The hot gases exit into a $4\frac{1}{2}$ inch stainless steel ceramic lined pipe.

The physical arrangement of the heat exchanger and controls is

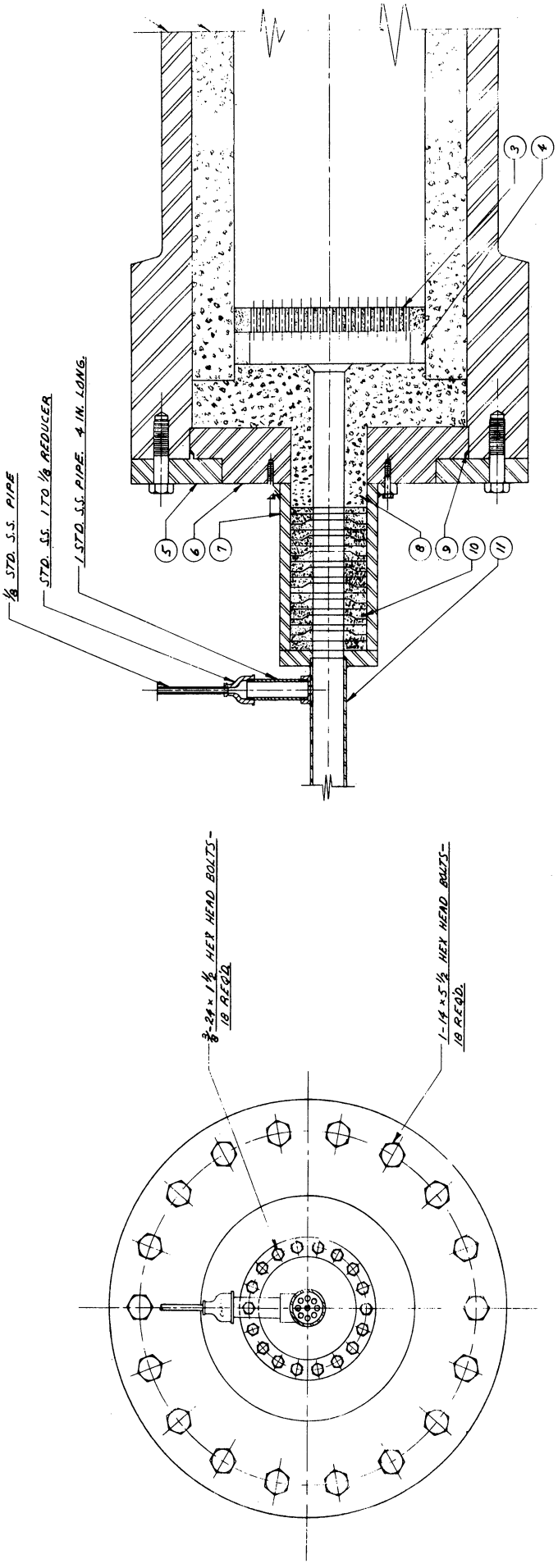

Figure 18. Cross Section of Air Heat Exchanger.

shown in Figure 19 (the hydrogen heat exchanger has not been used). The exchanger is submerged in a water filled concrete tank in order to lower the skin temperature and avoid the dangers of hot spots. This tank is located at the rear of the propulsion laboratory while all operating controls are within the laboratory.

A comprehensive theoretical analysis of regenerative heat exchangers with heat-loss consideration has been reported by Dabora [32] with special attention given to the exchanger described herein. A more complete physical description of the exchanger described here and a comparison of theory with experimental results for this exchanger is given by Dabora, Moyle, Phillips, Nicholls, and Jackson[33]. Some of the experimental results will be presented in section 5.1

4.3 Supersonic Mixing Nozzle.

As already indicated the hydrogen cannot be added to the air under stagnation conditions as the temperature is too high. Consequently, the method adopted has been to accelerate the hot air to high velocity with the associated drop in static temperature. The hydrogen is then introduced at this point in the flow direction. This aspect of the problem was beset with many doubts as practically no pertinent information was available in the literature. For one thing there is the problem of the boundary layer along the surface separating the hydrogen and air so that there is the possibility of some immediate combustion. In fact there was always the worry that the whole experimental setup might result in a "supersonic blow-torch." However, it was realized that a finite time is required to mix the gases and for any appreciable reaction to occur.

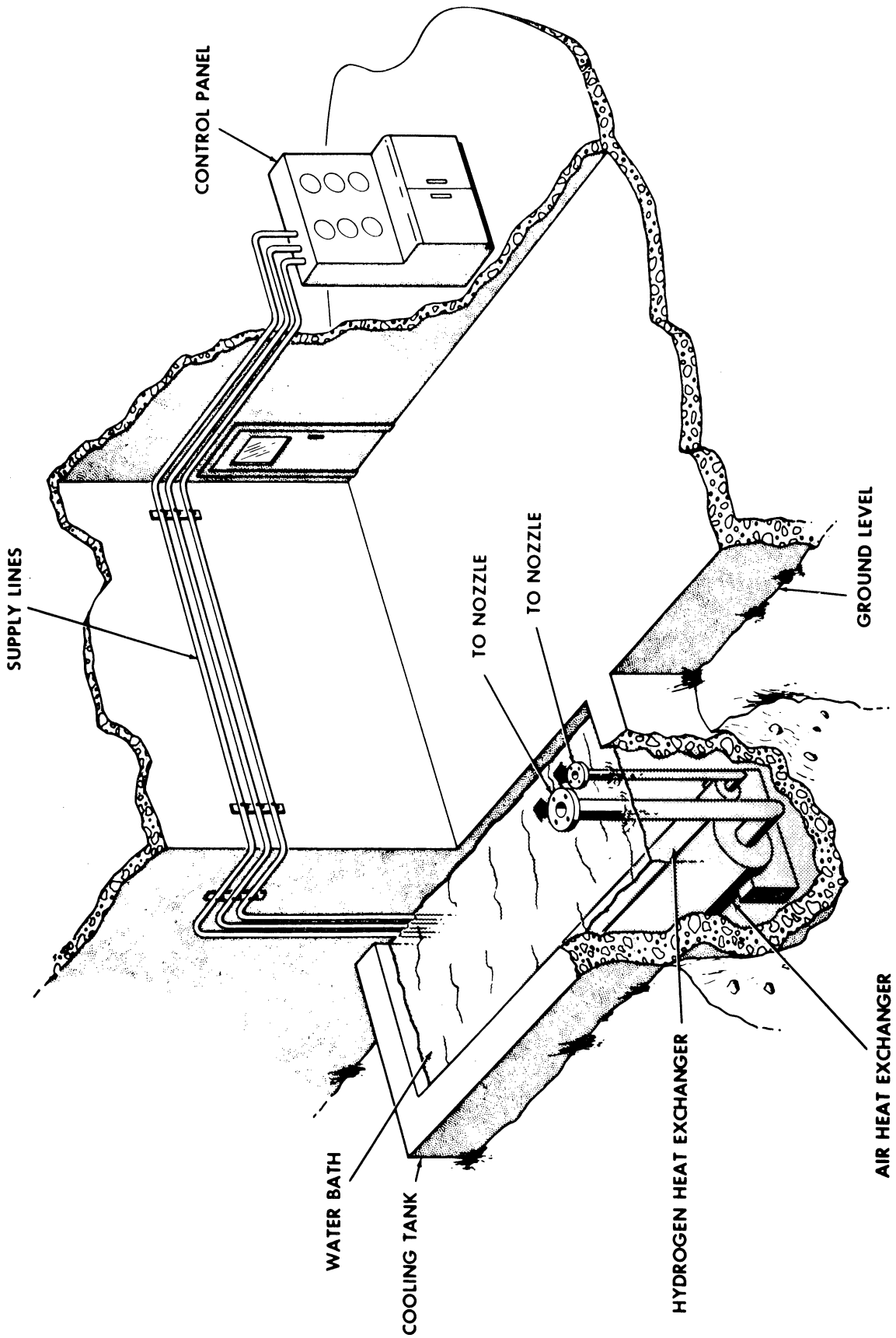

Figure 19. Physical Arrangement of Heat Exchanger and Controls.

Further it was reasoned that mixing supersonically in a divergent nozzle would lead to a rapid fall-off in pressure and temperature which could serve to avoid appreciable reactions. Another favorable condition would appear to lie in not heating the hydrogen. In that way time would be required for heat conduction to the hydrogen.

The other phase of this particular problem lies in the relatively slow rate of mixing of supersonic streams. This is advantageous as far as premature combustion is concerned but on the other hand is a disadvantage to the attainment of a uniformly mixed hydrogen-air supersonic stream. Wilder and Hindersinn [34] had reported mixing angles of fractional parts of one degree for the supersonic mixing of two air streams in two dimensional flow. In the case at hand there was reason to believe that somewhat more favorable angles could be realized because of the great difference in molecular weight of the gases and the greater degree of turbulence expected. The effect of mixing in a divergent section was unknown, however. In order to gain a little knowledge as to the rate of mixing, some experiments were run by R. Dunlap, H. R. Bulmer, and the author. These experiments were run in a divergent two dimensional nozzle with no heating of the gases and with helium substituted for hydrogen. A schlieren photograph of one of the runs is shown in Figure 20. The flow is from left to right with the helium flow at the bottom and the air at top. A wedge, part of which can be seen in the photograph, spans the width of the nozzle and serves to separate the gases. The two gases start mixing at the trailing edge of the wedge. For the case shown, the Mach number of the air is 2.0 and that of the helium is 3.2. The ratio of static pressures, air to helium, at the trailing edge is 2.1. From the figure it

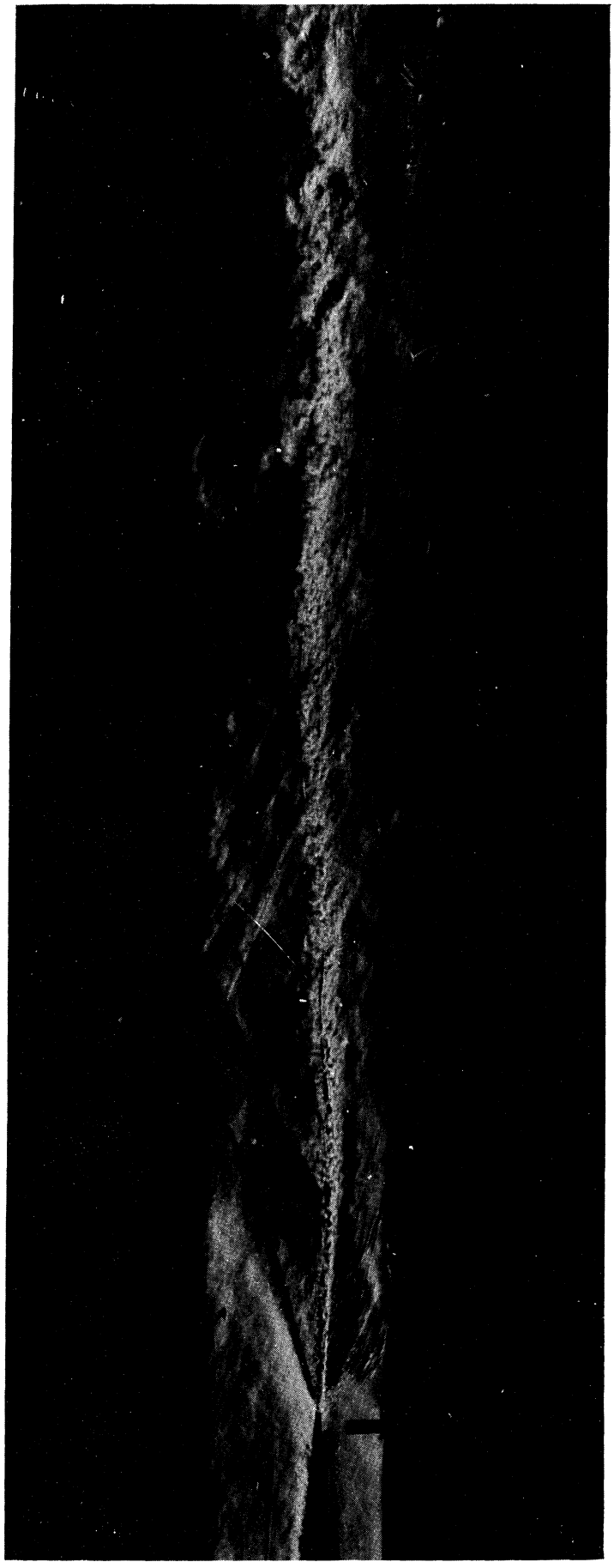

Figure 20. Schlieren Photograph of Supersonic Mixing.

can be seen that the mixing zone is apparently undulating. This seemed to hold true in almost all cases. The results of this particular run, along with the results of many similar runs over a range of conditions, indicated that effective mixing angles of at least 1-2 degrees could be realized.

With the above considerations in mind, calculations were effected to determine the scaling of the nozzle, the stagnation pressure losses due to mixing, and suitable Mach numbers for mixing. A complete mixing analysis appears almost hopeless for this problem and approximate equations based on one dimensional flow were used. The analysis proceeds as follows wherein the subscripts correspond to the stations indicated in Figure 21. For the case at hand the subscript "a" refers to the air stream, "f" to the hydrogen, and "b" to the base of the dividing plate. Cross section "2" is assumed to be a section where the gases are fully mixed. The steady flow, adiabatic, inviscid, one dimensional equations are then;

Conservation of Mass:

$$\rho_{a_1} A_{a_1} V_{a_1} + \rho_{f_1} A_{f_1} V_{f_1} = \rho_2 A_2 V_2 \tag{4.1}$$

Conservation of Momentum

$$P_b A_b + P_{a_1} A_{a_1} + \rho_{a_1} A_{a_1} V_{a_1}^2 + P_{f_1} A_{f_1} + \rho_{f_1} A_{f_1} V_{f_1}^2 + \int_{A_1}^{A_2} P \, dA = P_2 A_2 + \rho_2 A_2 V_2^2 \tag{4.2}$$

where:

$$A_1 = A_{a_1} + A_{f_1} + A_b$$

Conservation of Energy:

$$\dot{w}_a h_{s_a} + \dot{w}_f h_{s_f} = (\dot{w}_a + \dot{w}_f) h_{s_2} \tag{4.3}$$

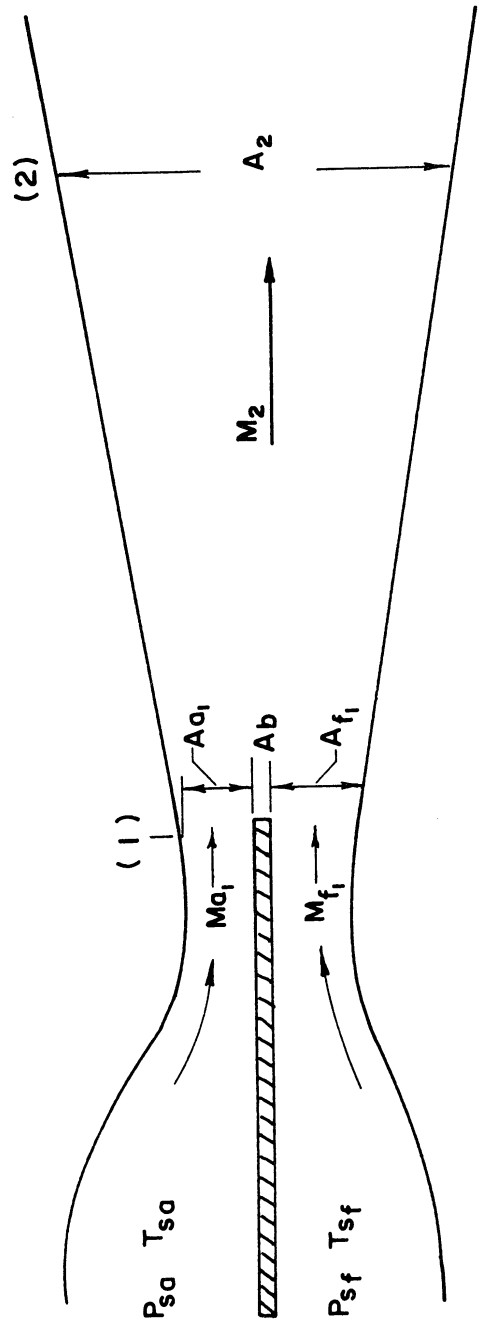

Figure 21. Supersonic Mixing Analysis.

In order to simplify these equations a few assumptions and approximations are made. First, the wall force term in (4.2) cannot be evaluated without complete knowledge of the mixing action. The approximation is made that this can be replaced by an average pressure acting over the difference in area between (1) and (2). Thus;

$$\int_{A_1}^{A_2} P\,dA = \left(\frac{P_1+P_2}{2}\right)\left(A_2-A_1\right) \tag{4.4}$$

Inasmuch as we are not considering unreasonably high temperatures in the mixing zone and all major concentrations of gas are composed of diatomic molecules, it is assumed that,

$$\gamma_a = \gamma_f = \gamma = \text{constant} \tag{4.5}$$

and

$$h = c_p T = \frac{\gamma R T}{\gamma - 1} \tag{4.6}$$

Further, it would appear wise to minimize any chances of a strong shock causing premature combustion in the mixing zone so the condition is imposed that the static pressure will be uniform across A_1.

Introducing the perfect gas law,

$$P = \rho R T \tag{4.7}$$

and making use of the above simplifications, (4.1) can be written

$$\frac{\gamma M_{a_1} A_{a_1} P_1}{\sqrt{\gamma R_a T_{a_1}}} + \frac{\gamma M_{f_1} A_{f_1} P_1}{\sqrt{\gamma R_f T_{f_1}}} = \frac{\gamma M_2 A_2 P_2}{\sqrt{\gamma R_2 T_2}} \tag{4.8}$$

which can be written as;

$$P_1 M_{f_1} \sqrt{\frac{m_f}{m_2 T_{f_1}}} \left[\frac{M_{a_1}}{M_{f_1}} \cdot \frac{A_{a_1}}{A_2} \sqrt{\frac{T_{f_1} m_a}{T_{a_1} m_f}} + \frac{A_{f_1}}{A_2}\right] = \frac{M_2 P_2}{\sqrt{T_2}} \tag{4.9}$$

Noting that;

$$\frac{\dot{w}_f}{\dot{w}_a} = \frac{\gamma M_{f_1} A_{f_1} P_1}{\sqrt{\gamma R_f T_{f_1}}} \cdot \frac{\sqrt{\gamma R_a T_{a_1}}}{\gamma M_{a_1} A_{a_1} P_1} = \frac{M_{f_1}}{M_{a_1}} \cdot \frac{A_{f_1}}{A_{a_1}} \sqrt{\frac{m_f T_{a_1}}{m_a T_{f_1}}} \tag{4.10}$$

and

$$\frac{T_s}{T} = 1 + \frac{\gamma - 1}{2} M^2 \tag{4.11}$$

(4.9) becomes;

$$P_1 M_{f_1} \sqrt{\frac{m_f}{m_2 T_{s_f}}} \left(1 + \frac{\gamma-1}{2} M_{f_1}^2\right)^{\frac{1}{2}} \left[\frac{A_{f_1}}{A_2}\left(1 + \frac{\dot{w}_a}{\dot{w}_f}\right)\right]$$

$$= \frac{M_2 P_2}{\sqrt{T_{s_2}}} \left(1 + \frac{\gamma-1}{2} M_2^2\right)^{1/2} \tag{4.12}$$

(4.2) becomes,

$$P_1\left[\frac{A_1 + A_2}{2A_2} + \gamma \frac{A_{a_1}}{A_2} M_{a_1}^2 + \gamma \frac{A_{f_1}}{A_2} M_{f_1}^2\right] = P_2\left[\frac{A_1 + A_2}{2A_2} + \gamma M_2^2\right] \tag{4.13}$$

Equation (4.3) can be written,

$$\dot{w}_a c_{p_a} T_{s_a} + \dot{w}_f c_{p_f} T_{s_f} = (\dot{w}_a + \dot{w}_f) c_{p_2} T_{s_2}$$

but

$$(\dot{w}_a + \dot{w}_f) c_{p_2} = \dot{w}_a c_{p_a} + \dot{w}_f c_{p_f}$$

so that,

$$T_{s_a} + \frac{\dot{w}_f c_{p_f}}{\dot{w}_a c_{p_a}} T_{s_f} = \frac{\dot{w}_a c_{p_a} + \dot{w}_f c_{p_f}}{\dot{w}_a c_{p_a}} T_{s_2}$$

or,

$$T_{s_a} + \frac{\dot{w}_f}{\dot{w}_a} \frac{\left(\frac{\gamma R_f}{\gamma - 1}\right)}{\left(\frac{\gamma R_a}{\gamma - 1}\right)} T_{s_f} = \left[1 + \frac{\dot{w}_f}{\dot{w}_a} \frac{\left(\frac{\gamma R_f}{\gamma - 1}\right)}{\left(\frac{\gamma R_a}{\gamma - 1}\right)}\right] T_{s_2}$$

or,

$$T_{s_a} + \frac{m_a}{m_f}\frac{\dot{w}_f}{\dot{w}_a} T_{s_f} = \left(1 + \frac{m_a}{m_f}\frac{\dot{w}_f}{\dot{w}_a}\right) T_{s_2} \tag{4.14}$$

Combining (4.12), (4.13), and (4.14) yields,

$$\frac{M_{f_1}^2 \frac{m_f}{m_2}\left(1 + \frac{\gamma-1}{2} M_{f_1}^2\right)\left[\frac{A_{f_1}}{A_2}\left(1 + \frac{\dot{w}_a}{\dot{w}_f}\right)\right]^2 \left[\frac{\frac{T_{s_a}}{T_{s_f}} + \frac{m_a}{m_f}\frac{\dot{w}_f}{\dot{w}_a}}{1 + \frac{m_a}{m_f}\frac{\dot{w}_f}{\dot{w}_a}}\right]}{\left[\frac{A_1/A_2 + 1}{2} + \gamma\frac{A_{a_1}}{A_2} M_{a_1}^2 + \gamma\frac{A_{f_1}}{A_2} M_{f_1}^2\right]^2}$$

$$= \frac{M_2^2\left(1 + \frac{\gamma-1}{2} M_2^2\right)}{\left[\frac{A_1/A_2 + 1}{2} + \gamma M_2^2\right]^2} \tag{4.15}$$

Now,

$$m_2 = \frac{\dot{w}_f + \dot{w}_a}{\frac{\dot{w}_f}{m_f} + \frac{\dot{w}_a}{m_a}} = \frac{m_a\left(1 + \frac{\dot{w}_f}{\dot{w}_a}\right)}{1 + \frac{m_a}{m_f}\cdot\frac{\dot{w}_f}{\dot{w}_a}} \tag{4.16}$$

and so (4.15) becomes

$$\frac{M_{f_1}^2\left(1 + \frac{\gamma-1}{2} M_{f_1}^2\right)\left(\frac{A_{f_1}}{A_2}\right)^2\left(1 + \frac{\dot{w}_a}{\dot{w}_f}\right)\left[\frac{m_f}{m_a}\cdot\frac{T_{s_a}}{T_{s_f}}\cdot\frac{\dot{w}_a}{\dot{w}_f} + 1\right]}{\left[\frac{A_1/A_2 + 1}{2} + \gamma\frac{A_{a_1}}{A_2} M_{a_1}^2 + \gamma\frac{A_{f_1}}{A_2} M_{f_1}^2\right]^2}$$

$$= \frac{M_2^2\left(1 + \frac{\gamma-1}{2} M_2^2\right)}{\left[\frac{A_1/A_2 + 1}{2} + \gamma M_2^2\right]^2} \equiv \psi(M_2) \qquad (4.17)$$

It can be noted that for $A_1 = A_2$ (constant area mixing), $\psi(M_2) = \phi(M_2)$ as given in Equation (2.16).

The procedure for evaluating the conditions at station 2 is to set the initial conditions $\left(\frac{\dot{w}_a}{\dot{w}_f}, \frac{T_{sa}}{T_{sf}}, M_{f_1}, M_{a_1}\right)$, choose a reasonable value of $\frac{A_b}{A_{f_1}}$, and arbitrarily select a value of A_1/A_2. Then $\frac{A_{f_1}}{A_{a_1}}$ is determined by Equation (4.10) and $\frac{A_{a_1}}{A_2}$ and $\frac{A_{f_1}}{A_2}$ follow from this and the relation $A_b + A_{a_1} + A_{f_1} = A_1 = (A_1/A_2) A_2$. Equation (4.17) is then solved for M_2. Equations (4.13) and (4.14) along with the isentropic relations can then be used to determine the remaining unknowns. A plot of $\psi(M_2)$ with A_1/A_2 a parameter is shown in Figure 22. Plots of some results in the general area of interest are shown in Figures 23, 24, 25. For these calculations the following values were used throughout;

$$\gamma = 1.4, \qquad T_{sa} = 2600°R, \qquad T_{sf} = 520°R,$$

$\frac{\dot{w}_a}{\dot{w}_f}$ = 35.2 (approximately stoichiometric mixture ratio), and $\frac{A_b}{A_{f_1}}$ = 3.0. There are, of course, two possible solutions to the equations corresponding to the two values of M_2 that will satisfy $\psi(M_2)$ = constant. One solution yields $M_2 < 1$ while the other yields $M_2 > 1$. Inasmuch as the pressure level of the nozzle is to be much greater than atmospheric pressure, the only meaningful solution here is the supersonic and consequently is the only one included in the results.

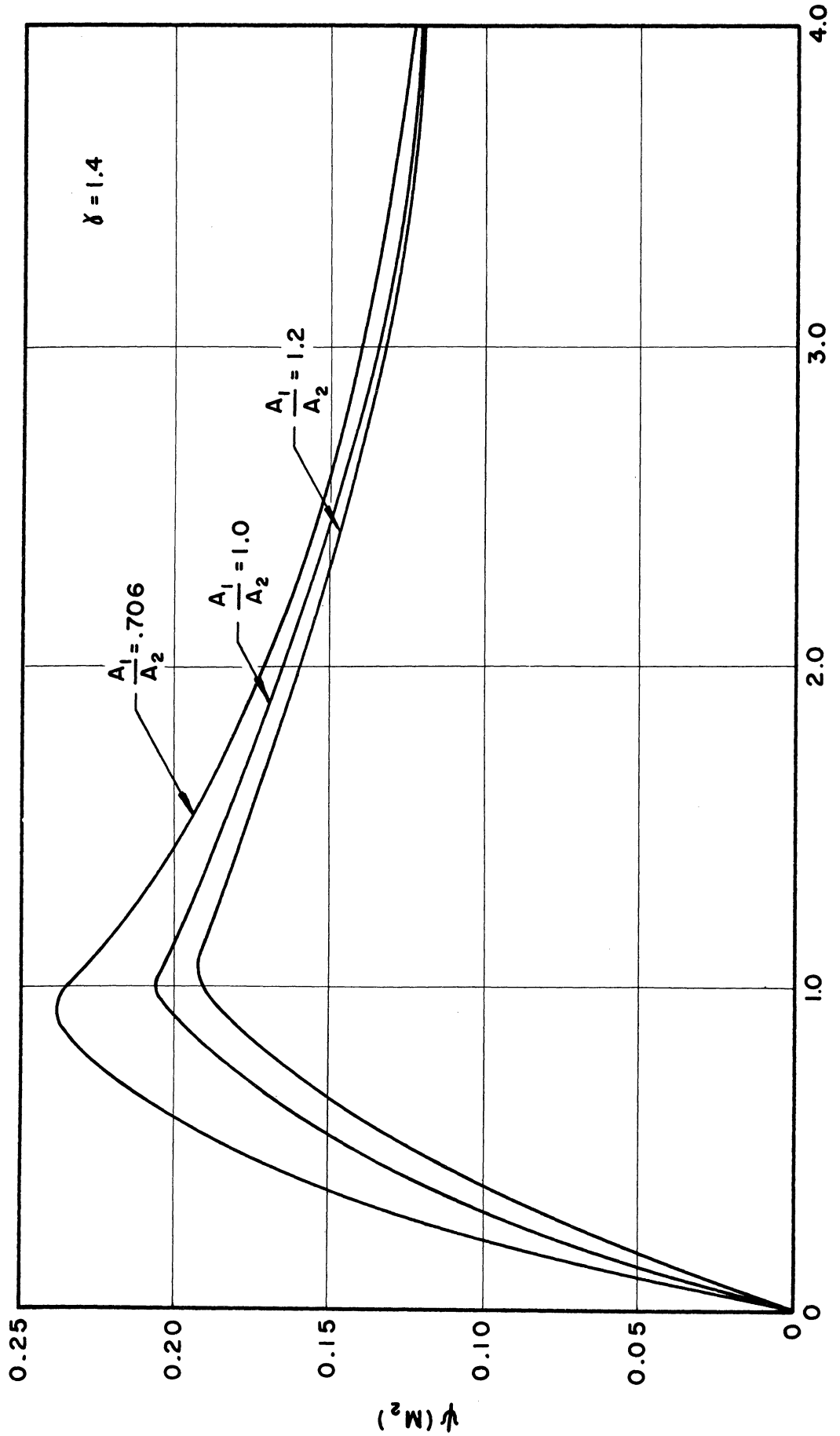

Figure 22. $\psi(M_2)$ versus M_2.

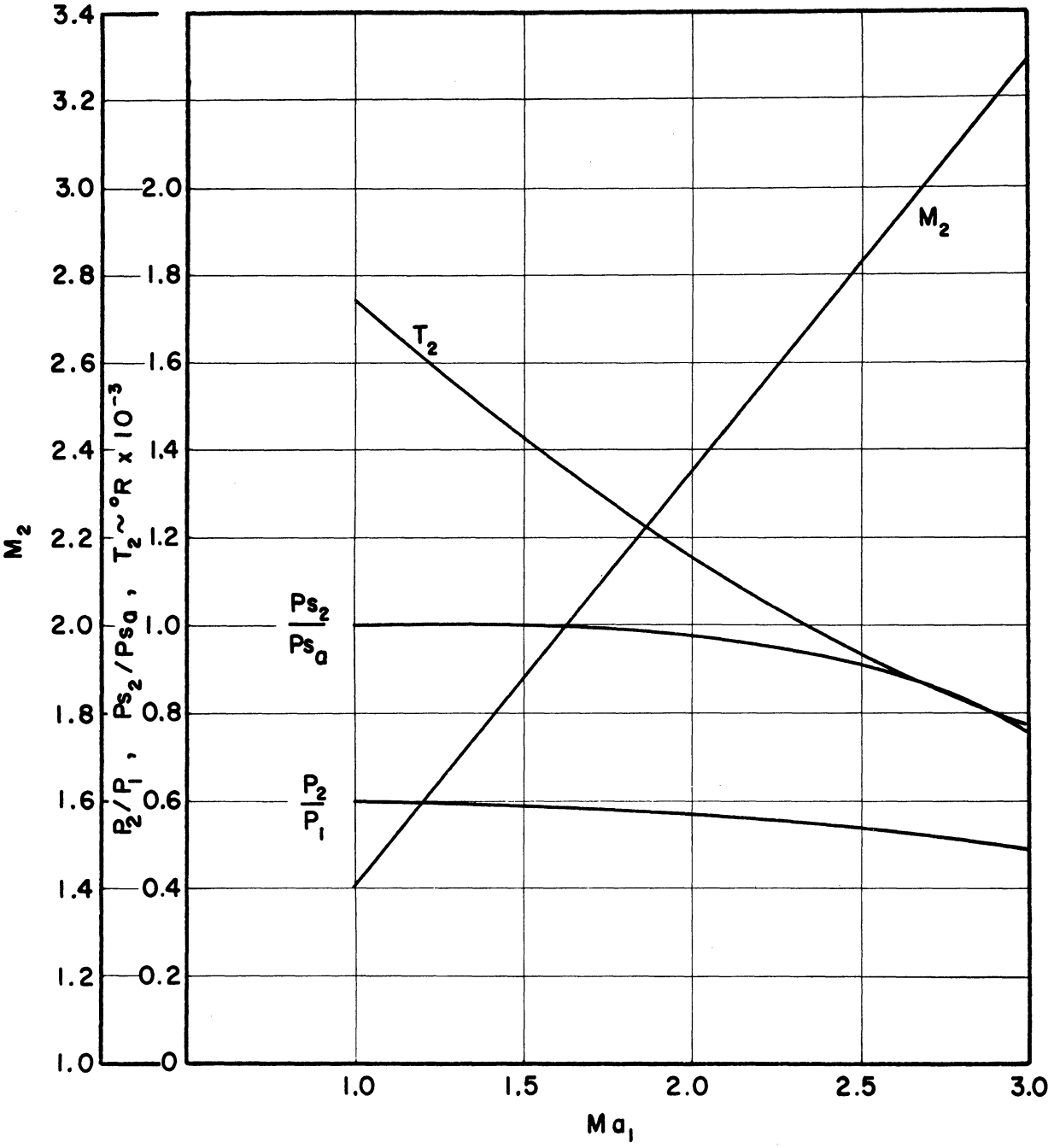

Figure 23. Supersonic Mixing of Hydrogen and Air

$\left(\frac{\dot{w}_a}{\dot{w}_f} = 35.2,\ A_1/A_2 = 1,\ M_{f_1} = 1 \right)$

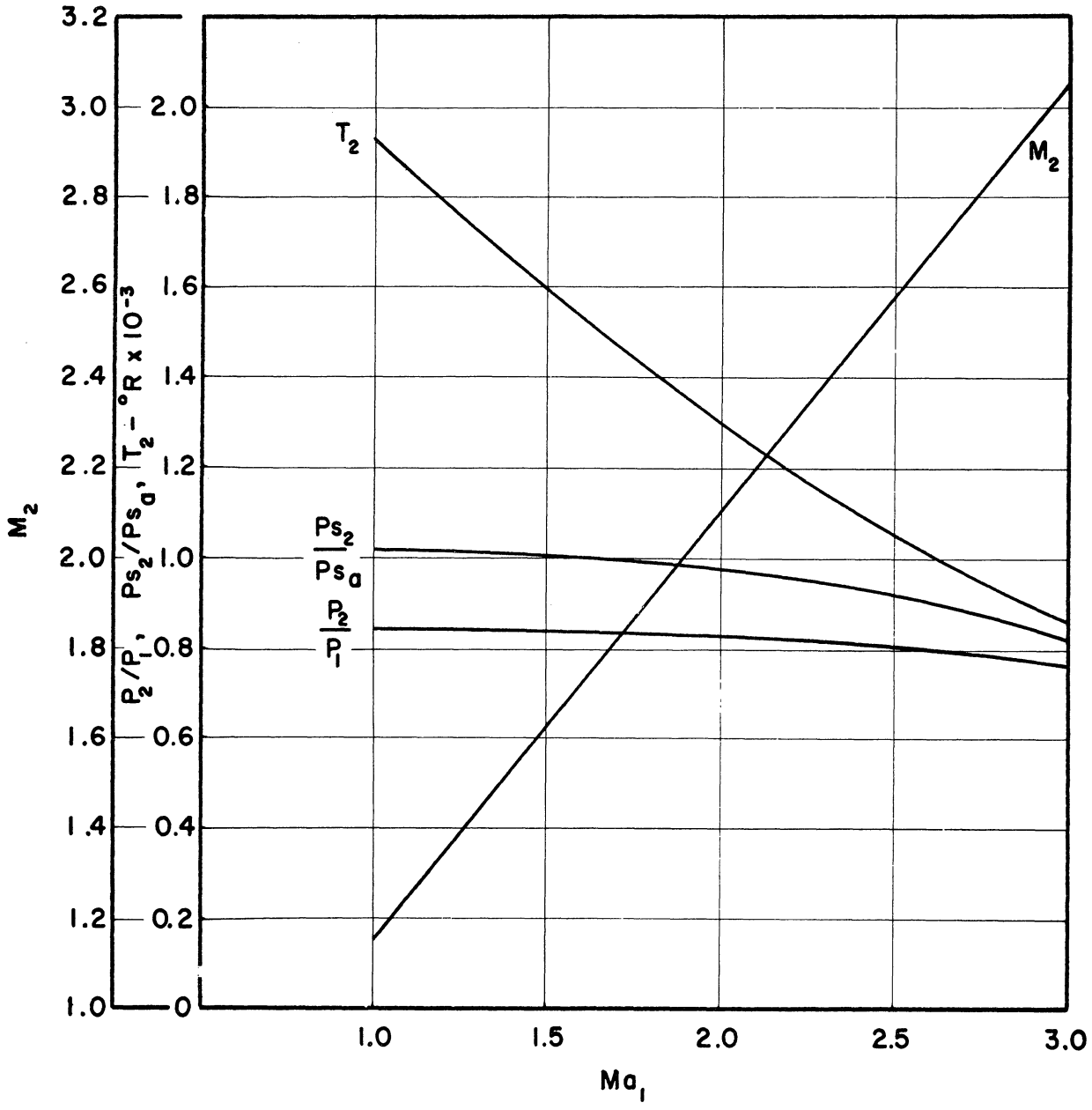

Figure 24. Supersonic Mixing of Hydrogen and Air

$$\left(\frac{\dot{w}_a}{\dot{w}_f} = 35.2,\ A_1/A_2 = 1,\ M_{f_1} = 2 \right)$$

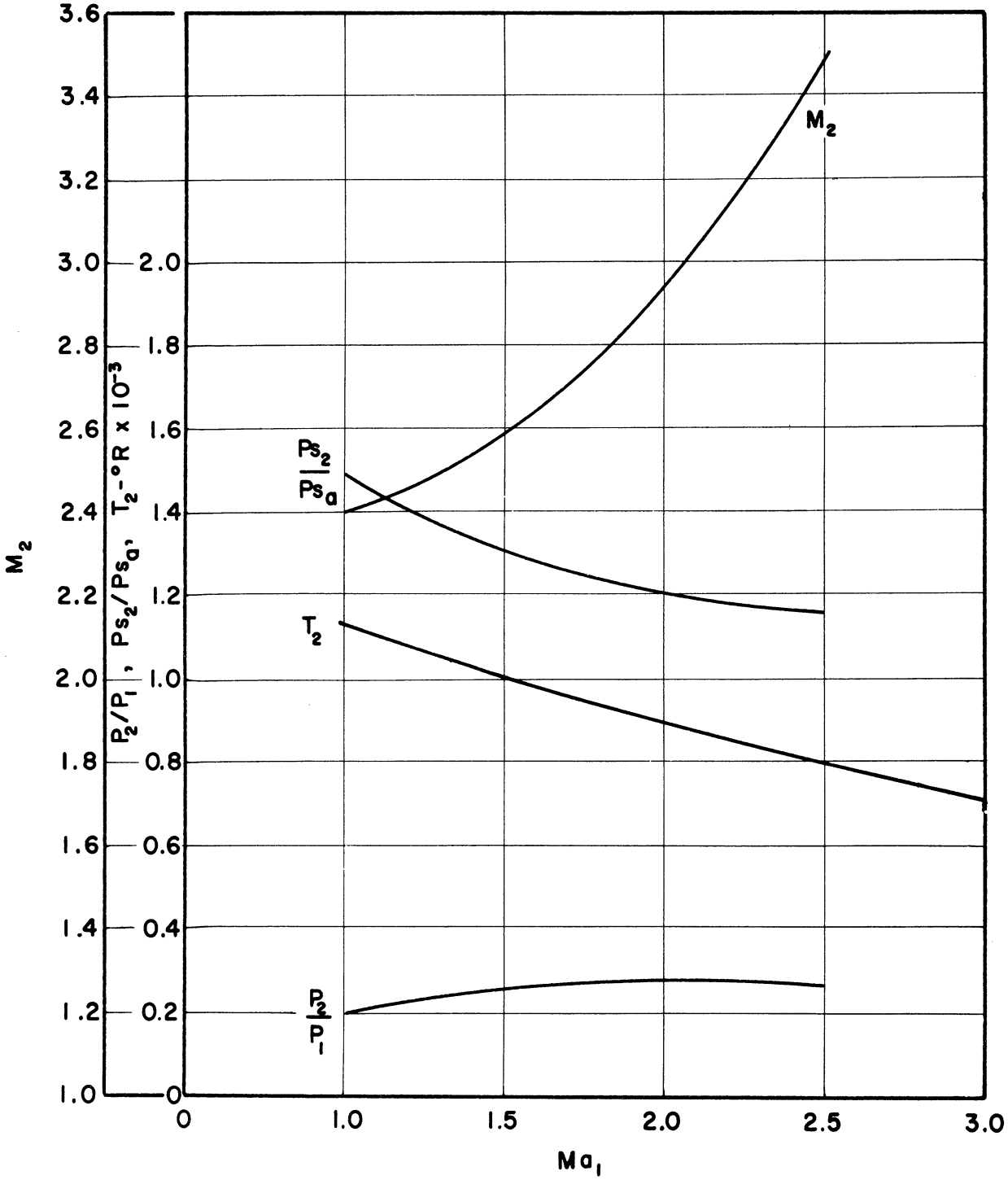

Figure 25. Supersonic Mixing of Hydrogen and Air

$$\left(\frac{\dot{w}_a}{\dot{w}_f} = 35.2,\ A_1/A_2 = 0.706,\ M_{f_1} = 1 \right)$$

Examination of the graphs reveals some interesting trends. The final temperature and stagnation pressure ratio fall off continuously with increased M_{a1} for any given value of M_{f1}. The final Mach number increases linearly with M_{a1} for the constant area case and at a greater rate for the divergent nozzle case. Now higher values of M_{a1} are desireable to the extent that lower values of T_2 are realized which would minimize the possibilities of premature combustion. However, the drop in stagnation pressure would be a disadvantage in that it necessitates unreasonably high initial stagnation pressures for the hydrogen and air. Also, the use of higher Mach numbers in the nozzle leads to the possibility of oblique shock waves sufficiently strong to initiate combustion.

The performance of the divergent nozzle appears to be much more favorable, as can be seen in Figure 25. Here, low values of M_{a1} yield final temperatures that are well below the ignition temperature of hydrogen. Furthermore, ther is a marked increase in stagnation pressure across the mixing zone which is advantageous. This effect is a consequence of the difference in stagnation temperature between the two streams and the resultant heat exchange process. The disadvantage of mixing at low Mach numbers lies in the high static temperature of the air at the initial point of contact with the hydrogen. In order to preclude combustion at this point, it is desireable to expand the gases rapidly (high nozzle divergence angle). This may result in incomplete mixing which would be advantageous to the extent that no appreciable hydrogen concentration would be realized near the walls (assuming the hydrogen to be introduced in the center of an axisymmetric stream). Thus there would be no difficulty arising from burning in the wall boundary layers.

As a result of these considerations, along with design considerations, it was decided to inject hydrogen at Mach one ($M_{fl} = 1$) into a surrounding air stream at Mach one ($M_{al} = 1$) in an axisymmetric divergent nozzle. The size of the nozzle had to be limited so as not to require unreasonable hydrogen flows. One such nozzle, with the pertinent dimensions indicated, is shown in Figure 26. The nozzle is made of stainless steel and when in operation is cooled by water circulating through copper tubing wrapped around the hub.

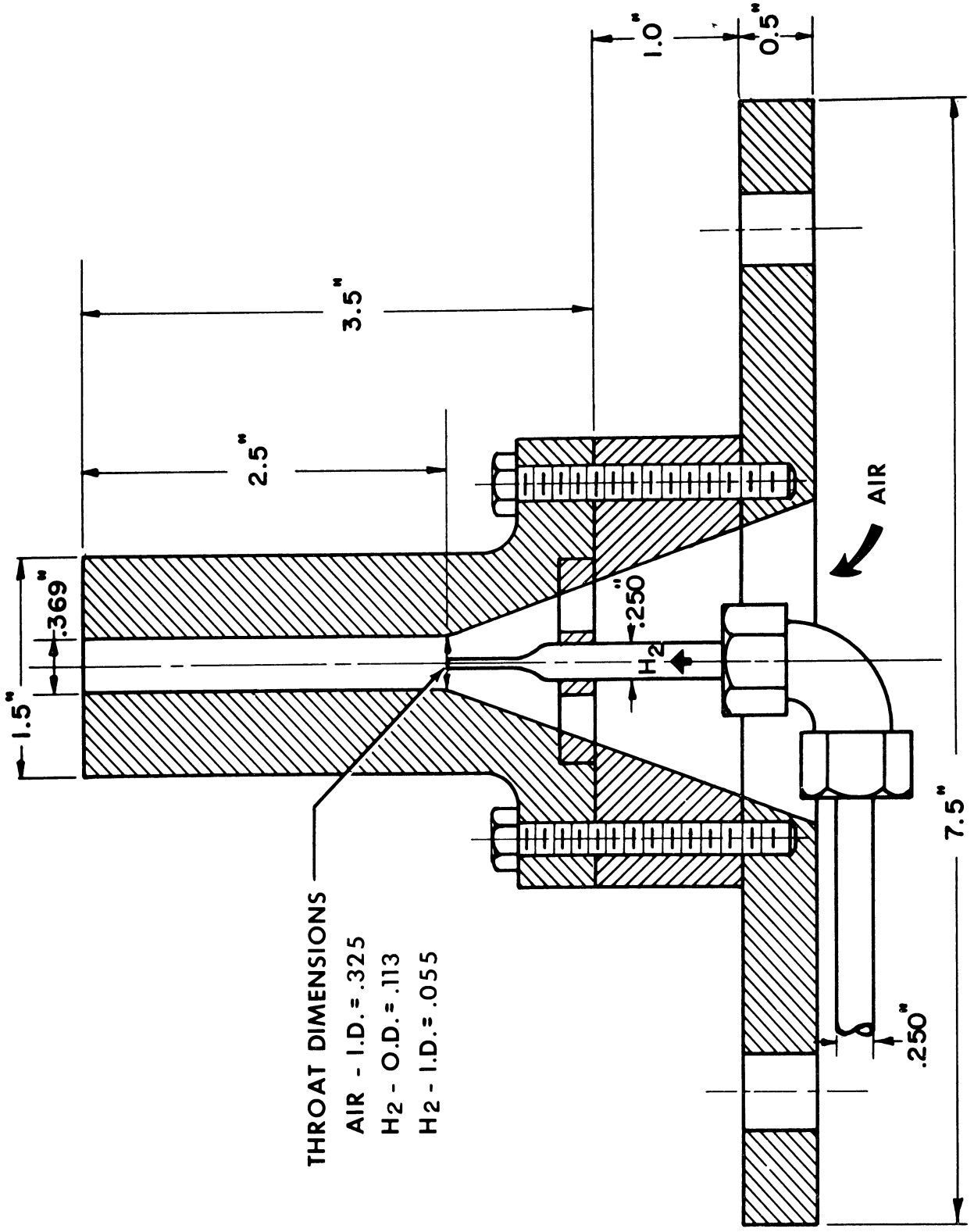

Figure 26. Supersonic Mixing Nozzle.

4.4 Instrumentation and Operating Procedure.

The instrumentation utilized can be divided into two broad classifications, that associated with measurements required for usual operation and that associated with particular experiments being run. It is intended to discuss only the former at this point and leave the other to the discussion of experimental results. The basic information obtained on experimental runs consists of the following:

Heat - up Cycle

a) flow rate of air

b) flow rate of propane

c) temperature in the burner

d) exit temperature of the heat exchanger

e) skin temperature of the heat exchanger

Blow - down Cycle

a) flow rate of air

b) flow rate of hydrogen

c) exit temperature of the heat exchanger

d) skin temperature of the heat exchanger

e) air stagnation pressure of the nozzle

f) air stagnation temperature of the nozzle

g) exit pressure of the nozzle

h) exit temperature of the nozzle

i) schlieren photograph of the jet

j) 16 mm movies of the combustion zone (when applicable)

The flow rate of air is determined from the stagnation pressure and temperature at the nozzle and the throat area, using isentropic flow relations. This method had been previously checked against a standard ASME sharp edged orifice and found to be in very close agreement. All pressures are read on standard bourdon type gages, unless otherwise indicated, which are mounted on the central control panel inside the laboratory.

Propane flow is determined by use of an ASME orifice with measurements of upstream pressure, pressure drop across the orifice, and upstream temperature. The flow rate of hydrogen is obtained through use of a venturi with a measurement of stagnation temperature and pressure as well as the pressure at the minium section. The temperature for the propane flow rate measurement is obtained by a fluid immersed bulb type thermocouple with the readout on a panel mounted gage. The hydrogen stagnation temperature is obtained by an iron constantan thermocouple. The pressure drops across orifices are measured on a U-tube manometer.

The temperature in the burner is obtained only for qualitative reasons in order to determine when the propane-air mixture has ignited. This temperature is measured by a bare wire platinum-platinum + 10% rhodium thermocouple which is imbedded in the ceramic lining. The output is fed into a multi-channel oscillograph. All temperatures, except for the propane stagnation temperature, are recorded in this way. The exit temperature of the heat exchanger is obtained in the same way as in the burner except that the thermocouple projects slightly into the stream. The skin temperature of the heat exchanger is taken at three axial locations by imbedding iron-

constantan thermocouples $\frac{1}{2}$ inch deep in the shell.

The stagnation temperature of the air entering the nozzle is obtained by use of a platinum-platinum + 10% rhodium thermocouple which projects into the stagnation chamber. No correction is made for radiation effects on this reading in that the walls are insulated and hence at a temperature close to the gas temperature. A qualitative measurement of gas temperature at the exit of the nozzle is obtained by means of a flush mounted platinum-platinum + 10% rhodium thermocouple.

The jet structure is recorded by schlieren photography using the system outlined in Figure 27. The light source is a 100 watt zirconium lamp situated one focal length from the collimating mirror. This mirror is located at one of its focal lengths from the center of the jet while the second mirror is at 2 of its focal lengths from the jet. The diameter of the first mirror is 6 inches and that of the second $7\frac{1}{4}$ inches. The f-numbers are 8 and 5.4 respectively. The knife edge, located one focal length from the second mirror, is a razor blade. The image is recorded on a 35 mm movie camera which is operated from within the laboratory.

In addition to schlieren photography, 16 mm movies are taken of the self-luminous combustion zone. This camera is also operated remotely.

A schematic of the basic instrumentation and flow control components utilized is shown in Figure 28. Photographs of one of the nozzles that have been used are shown in Figure 29. This nozzle differs somewhat from that shown in Figure 26 in that the hydrogen is introduced through the flange and one of the spokes directly to the needle. The hot air flows over the outside of these spokes. The two fittings shown at the end of the

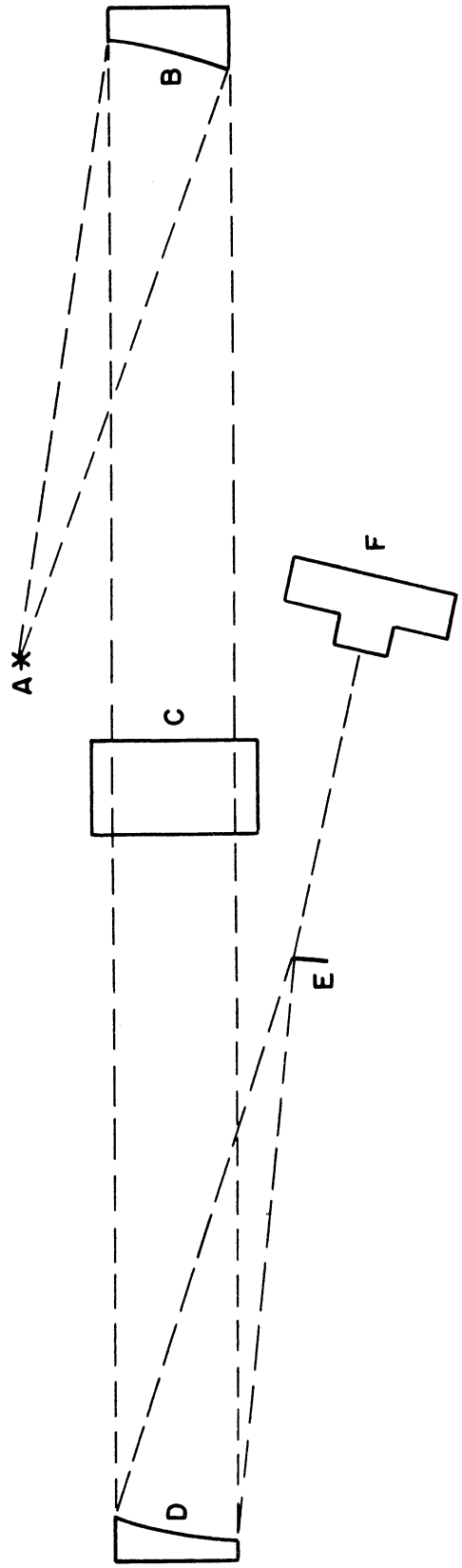

A - LIGHT SOURCE
B - PARABOLIC MIRROR, COLLIMATING
C - OPEN JET TEST SECTION
D - PARABOLIC MIRROR, FOCUSING
E - KNIFE EDGE
F - CAMERA

Figure 27. Schlieren Arrangement.

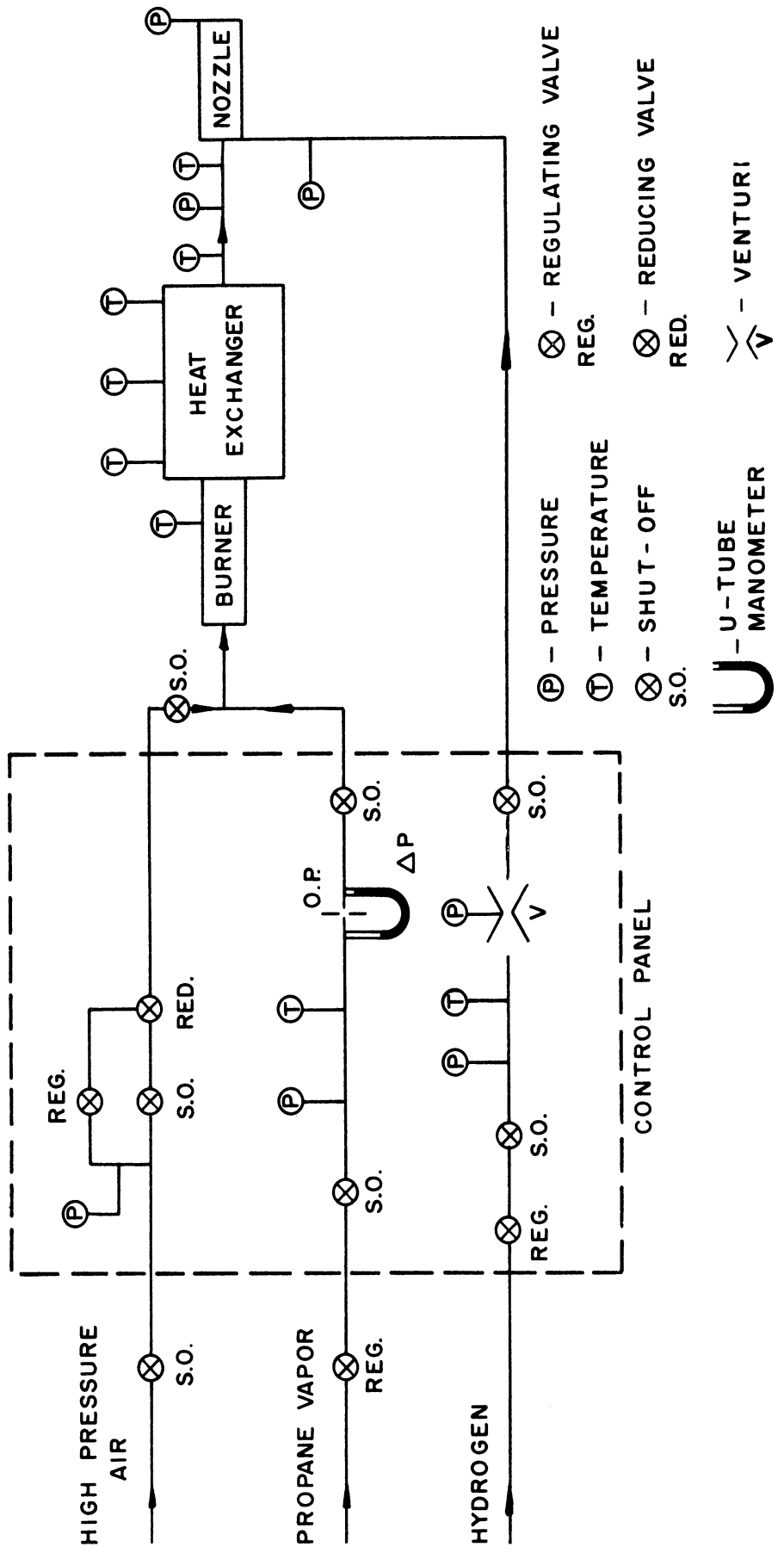

Figure 28. Basic Instrumentation and Flow Control Components.

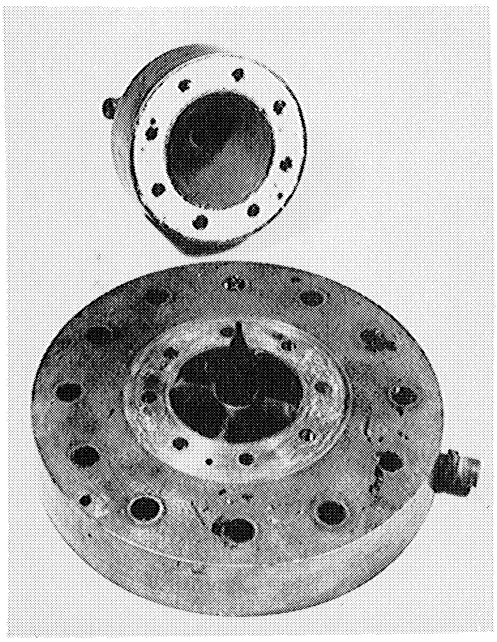

(a) Exploded View

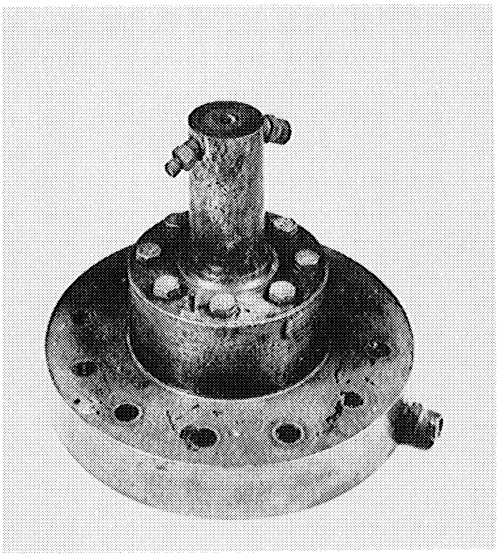

(b) Assembly View

Figure 29. Exploded and Assembly Views of Mixing Nozzle.

assembled nozzle are for the exit pressure and temperature. A photograph of the nozzle mounted on the insulated exhaust pipe of the heat exchanger is shown in Figure 30. Also shown are the 16 mm camera, the schlieren light source and collimating mirror, and the tungsten ribbon light source, two lenses, and the spectrometer for sodium D-line temperature determination.

The usual operating procedure is to warm up the heat exchanger with the nozzle removed so that the hot exhaust gases are not passing through the nozzle for the many hours (approximately 8) required. The propane-air mixture ratio is maintained somewhat lean in order to keep the flame temperature below the melting point of the alumina pebbles (approximately 3200°F). During this heat-up time the instrumentation is readied and some flow rate and temperature data recorded. Once the desired exit temperature of the heat exchanger is reached the flow is stopped and the nozzle mounted on the exhaust pipe. The hydrogen line and nozzle water cooling lines are connected and last minute adjustments made to the instrumentation associated with the recording of test data.

On blowdown the air flow is first established and allowed to stabilize. A short exposure on the schlieren camera is then taken and flow rate information recorded. The desired hydrogen flow is then established and the same information recorded. In addition a short exposure on the 16 mm is taken along with any other measurements required for the particular experiment being run.

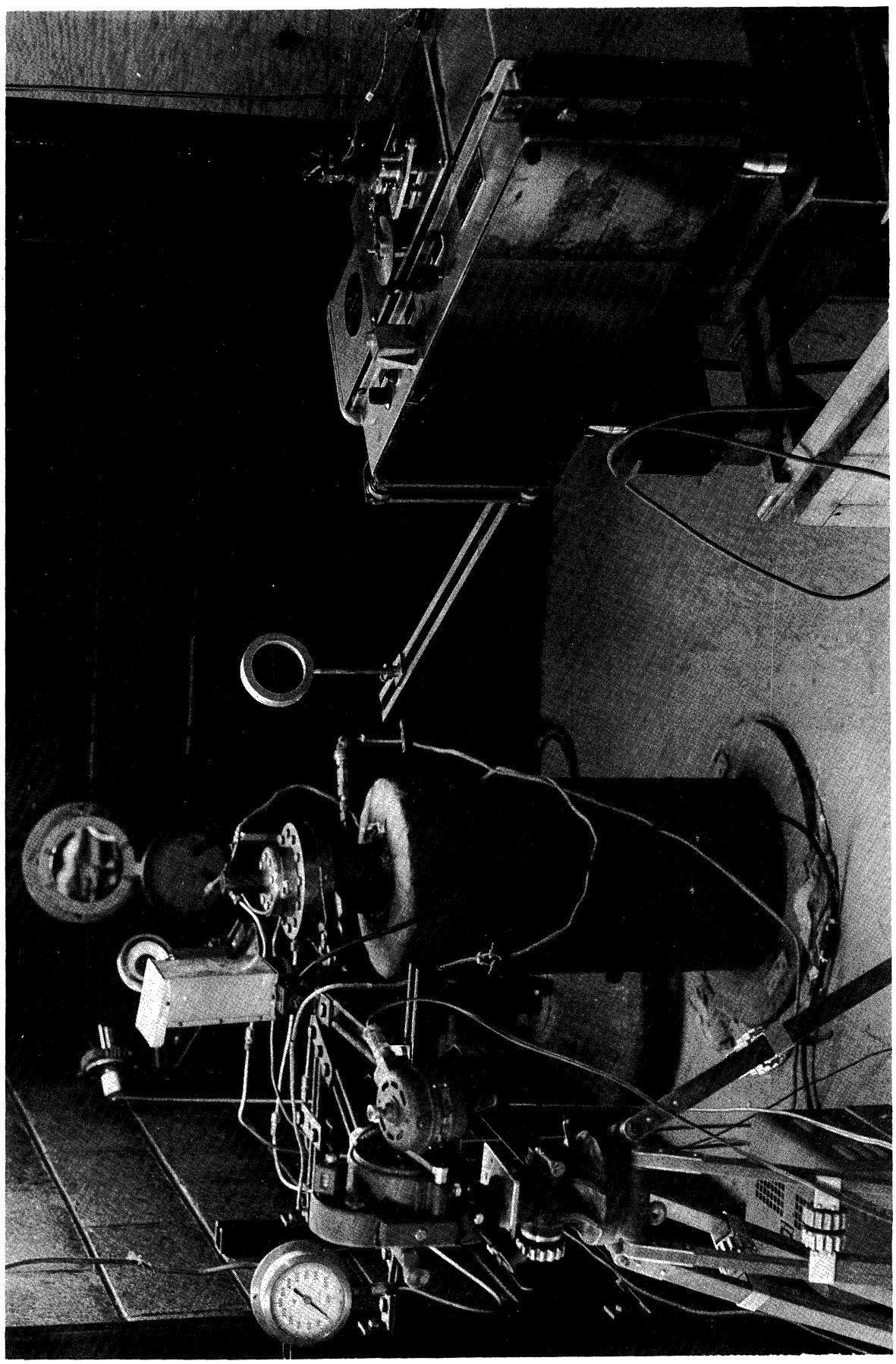

Figure 30. Photograph of Experimental Equipment.

V EXPERIMENTAL RESULTS

5.1 Temperature - Time Performance of the Heat Exchanger.

Measurements have been made on the delivery temperature of the heat exchanger versus time for both the heat-up cycle and the blow-down cycle. These histories are dependent, of course, on the rate of mass flow through the exchanger. Results obtained for three different flow rates on heat-up are shown in Figure 31, where G is the mass rate of flow of combustibles per second per square foot of heat exchanger cross sectional area. This area is approximately 0.85 square feet. It is readily apparent that the higher flow rates can materially shorten the time required to achieve a certain temperature.

Figure 32 represents the temperature-time history on blow-down for a typical air flow rate of about 0.54 pounds per second. The delay indicated in attaining maximum temperature is attributable to the cooling off of the exhaust stack of the heat exchanger between runs. As seen, there is a uniform delivery temperature for a period of many minutes. This testing time is of sufficient duration for practically all of the experiments envisioned. On long runs that have been made, in the order of 15 minutes, the outlet temperature has dropped by only about 100°F.

The maximum temperature attained so far has been 2100°F which is below that desired. This temperature could probably be exceeded by either heating at higher flow rates or by enrichening the mixture (perhaps even oxygen enrichment). Neither of these solutions have been tried to date. For one thing, there has been evidence of a hot spot at about the center

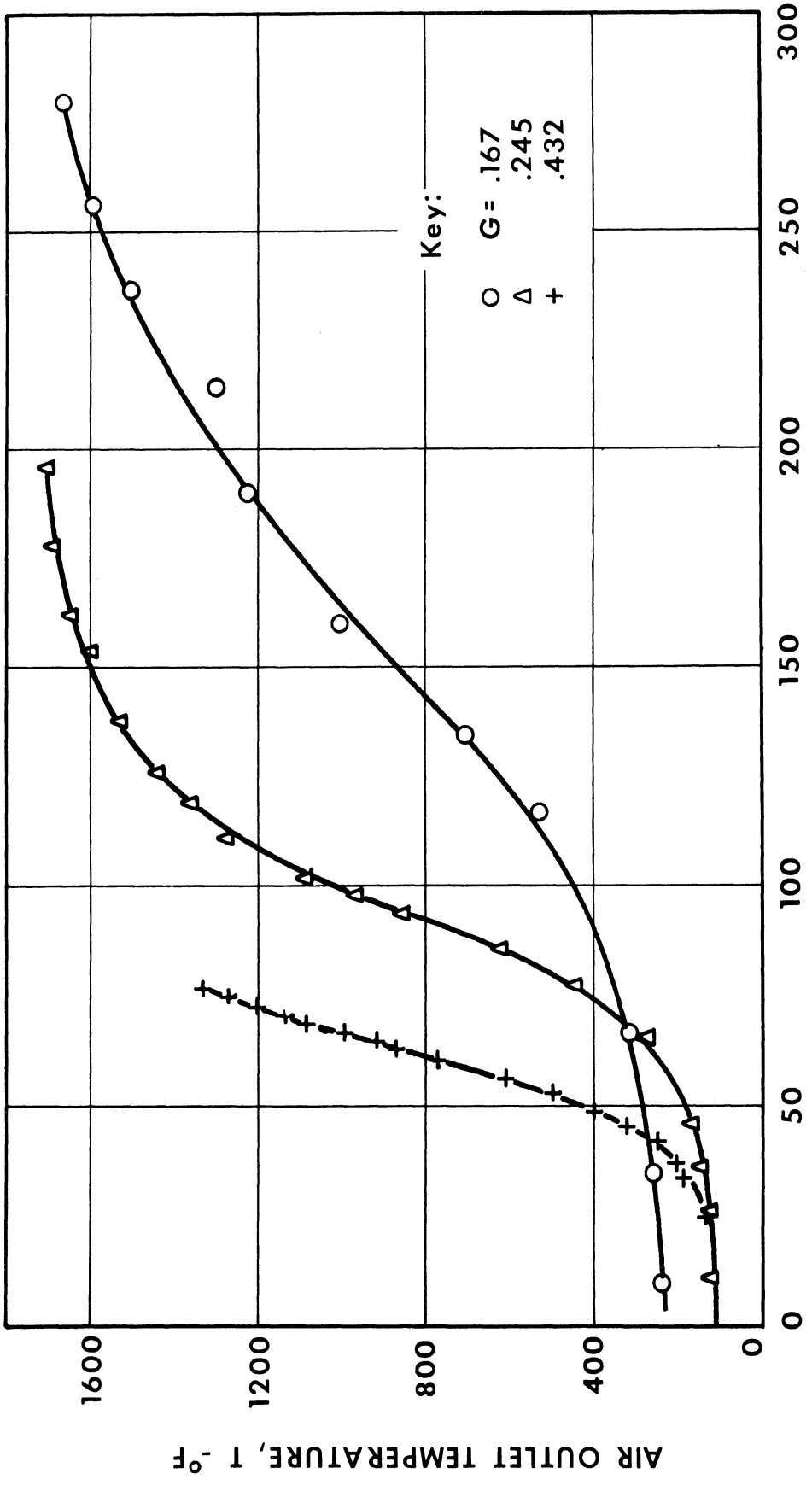

Figure 31. Experimental Temperature-Time Performance of the Air Heat Exchanger on Heat-up.

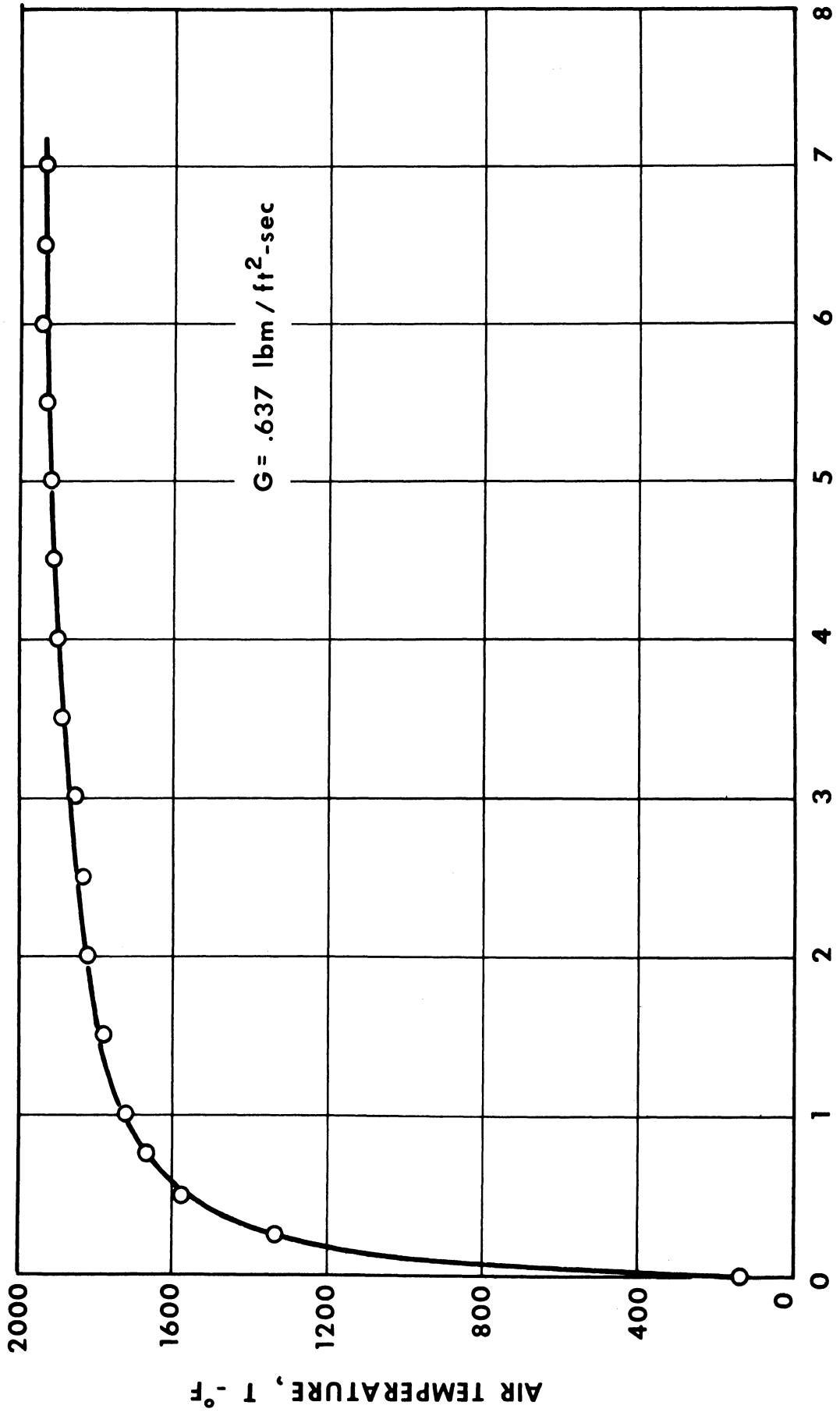

Figure 32. Experimental Temperature - Time Performance of the Air Heat Exchanger on Blow-down.

of the heat exchanger. This is indicated by a rapid bubbling of the cooling water at this point as well as a higher indicated skin temperature. Presumably there is a crack or cracks in the annular ceramic liner and it would be dangerous to push the exchanger much harder. In addition there is a limited increase allowable for the propane enrichment in view of melting point limitation of the pebbles. In view of these considerations, the heat exchanger is heated more gradually than is indicated in Figure 31 and the heat-up time usually required is about 8 hours.

5.2 Nozzle Performance.

The discussion of the mixing nozzle in section 4.3 pointed out the desireability of rapid expansion of the gases and the avoidance of strong shocks in the mixing zone so as not to realize premature combustion. These qualitative deductions have evidently been borne out by the experimental results obtained. That is, when operating at or near design conditions no difficulty is experienced with premature combustion. However, it has been noted that when the heat exchanger temperature drops it is necessary to increase the fuel-air ratio substantially to obtain ignition behind the shock. Under these conditions combustion inside the nozzle is often realized. This combustion has been detected by three separate and distinct ways. Firstly, when it occurs there is a very luminous inner cone at the exit of the nozzle. Secondly, the appearance of the cone is accompanied by an appreciable rise in nozzle exit temperature. Thirdly, the nozzle exit pressure is quite sensitive to energy release within the nozzle and the onset of premature combustion has led to much higher exit pressures. It might be added that when this occurs there is a

marked increase in the noise level.

Some typical experimental results are indicated in Table I for two different hydrogen needles and for runs with and without combustion inside the nozzle. The calculated values, according to the approach of section 4.3, do not agree too well with these results. This discrepancy is not surprising and may be attributed to the following effects:

1) incomplete mixing
2) appreciable viscous effects inside the hydrogen needles
3) boundary layer effects
4) uncertainty in Mach number of hydrogen at point of injection

5.3 Measurements in the Open Jet.

Inasmuch as the isentropic core of the open jet (discussed in section 3.3) represents the test section in these experiments, it is essential that the flow conditions into the shock wave be determined. This involves measurement of the free stream static or stagnation temperature, static or stagnation pressure, Mach number, and fuel-air ratio. The experimental technique used to effect these measurements is described below.

The stagnation pressure was measured by means of a total head probe made of 1/16 inch O.D. stainless steel tubing which was mounted on a sting located downstream. The pressures obtained are, of course, the stagnation pressure behind a normal shock at the local Mach number, this Mach number being unknown. A series of measured pressures along the centerline of the jet is shown in Figure 33. Measurements are shown for two cases one for air alone and the other for air plus hydrogen. The gases were not heated at all for these runs. In order to interpret these results in terms

TABLE I

SOME SUPERSONIC MIXING RESULTS

		$M_{a1} = 1$						$A_1/A_2 = 0.706$		
Run No.	Nozzle	A_{f_1}/A_1	A_{a_1}/A_1	P_{s_a} psia	P_{s_f} psia	T_{s_a} °R	$\dot{w}_f/\dot{w}_a$	P_2 psia	T_2 °R	Remarks
87	A2/H3	0.0162	0.936	514.3	514.3	2155	.0056	123.3	2010	
88	A2/H3	0.0162	0.936	514.3	464.3	2160	.00467	122.3	2020	
89	A2/H3	0.0162	0.936	514.3	414.3	2160	.00387	121.3	2020	
90	A2/H3	0.0162	0.936	514.3	364.3	2170	.0036	120.3	2030	
91	A2/H3	0.0162	0.936	514.3	314.3	2180	.0027	119.3	2040	
92	A2/H3	0.0162	0.936	514.3	264.3	2180	.00179	118.3	2040	
131	A2/H3	0.0162	0.936	500	364.3	1940	.00288	122.3	1820	
56	A2/H3	0.0162	0.936	514.3	514.3	2070	.00515	119.3	1933	
147	A2/H3	0.0162	0.936	434.3	524.3	1670	.00672	116.3	1570	
148	A2/H3	0.0162	0.936	439.3	564.3	1620	.00672	179.3	1515	Burning in nozzle
84	A2/H3	0.0162	0.936	524.3	524.3	2140	.0071	164.3	2005	Burning in nozzle
192	A2/H2	0.0252	0.878	464.3	314.3	1720	.00498	101.3	1600	
201	A2/H2	0.0252	0.878	529.3	314.3	2120	.00447	112.3	1960	

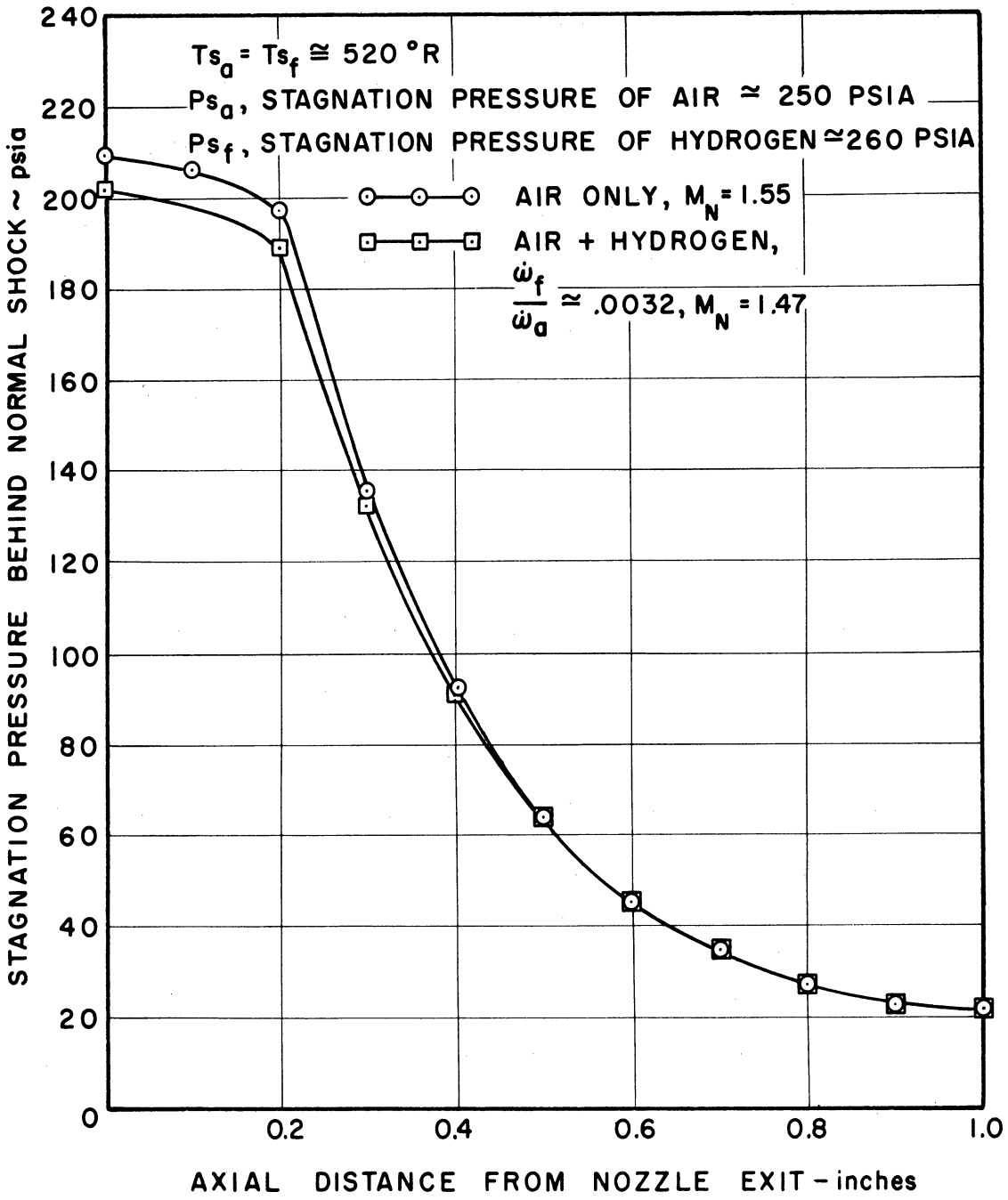

Figure 33. Pressure Measurements along the Centerline of the Open Jet.

of Mach number it is necessary to know the local stagnation pressure upstream of the shock. This information was obtained by measuring the total pressure behind a shock and the wall static pressure at the exit of the nozzle. The Mach number was then calculated from the Rayleigh pitot tube formula. Knowing the exit Mach number and static pressure, the isentropic relations yielded the upstream stagnation pressure. The Mach number distribution along the centerline of the jet was then readily determined through use of the normal shock relations, the measured downstream total pressure, and the assumption of constant stagnation pressure from the nozzle exit to the shock. Such results, deduced from the measured results of Figure 33, are plotted in Figure 34, where now the axial distance is non-dimensionalized by the nozzle exit diameter. Also included on the figure are similar experimental results for a heated air jet (T_{sa} = 1200°R). It can be seen that the main effect of the hydrogen flow is to lower the exit Mach number slightly. This difference between the "air only" curve and "air plus hydrogen" curve then remains roughly constant over the whole range. On the other hand, the heated air jet leads to a slightly higher Mach number at the nozzle exit but then to somewhat lower values at the higher Mach numbers in the open jet. This difference is in the wrong direction to be explained by water vapor condensation so it is believed to be attributable to transverse heat transfer. A theoretical curve, based on the theory of Adamson and Nicholls [31], is also shown in Figure 34. This curve should be compared to the unheated "air only" curve where the exit Mach number is 1.55. The agreement is considered to be quite good.

It should be pointed out that the Mach number distribution in

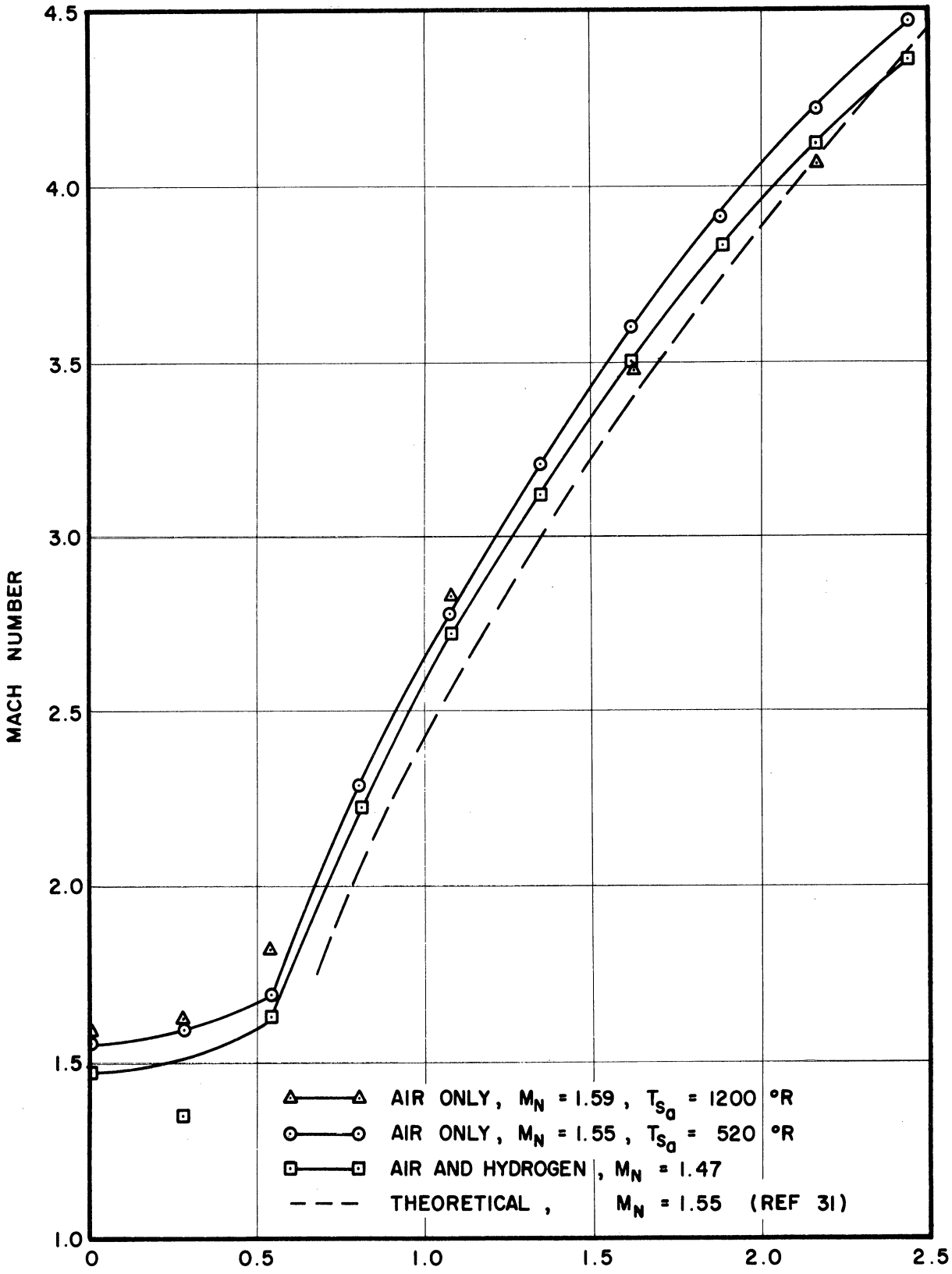

Figure 34. Mach Number Distribution along Centerline of Open Jet.

the open jet is independent of the pressure level provided the ratio of exit pressure to ambient pressure is sufficiently high. The pressure level enters only in determining the axial extent of the isentropic core flow, that is, the Mach disc location.

Total pressure measurements were also effected immediately down-stream of the Mach disc at different radial positions. These results are shown in Figure 35 for heated and unheated air and reveal that the flow is quite uniform over most of the Mach disc area.

A series of total pressure measurements behind the Mach disc for different disc locations (i.e., different total pressure levels) indicated that at higher Mach numbers the total pressure is a constant and equal to 1.46 atmospheres. This information along with the well known fact that the downstream Mach number behind strong normal shocks approaches an asymptotic value indicates a constant static pressure in this region. Similarly, for a given total temperature, the static temperature in this region will be a constant even though the normal shock may occur at different high Mach numbers. This characteristic is very favorable to many of the combustion experiments of interest here.

Measurements were also made on the distribution of hydrogen in the jet. The details of these measurements have been reported in Reference 35. Briefly, a sample of the jet was obtained by immersing a small probe in the jet at the desired location and allowing the sample to flow into a previously evacuated sample bottle. The sample was then processed chemically to ascertain the hydrogen-air ratio. Such samples were taken at a number of radial positions behind the disc. The results

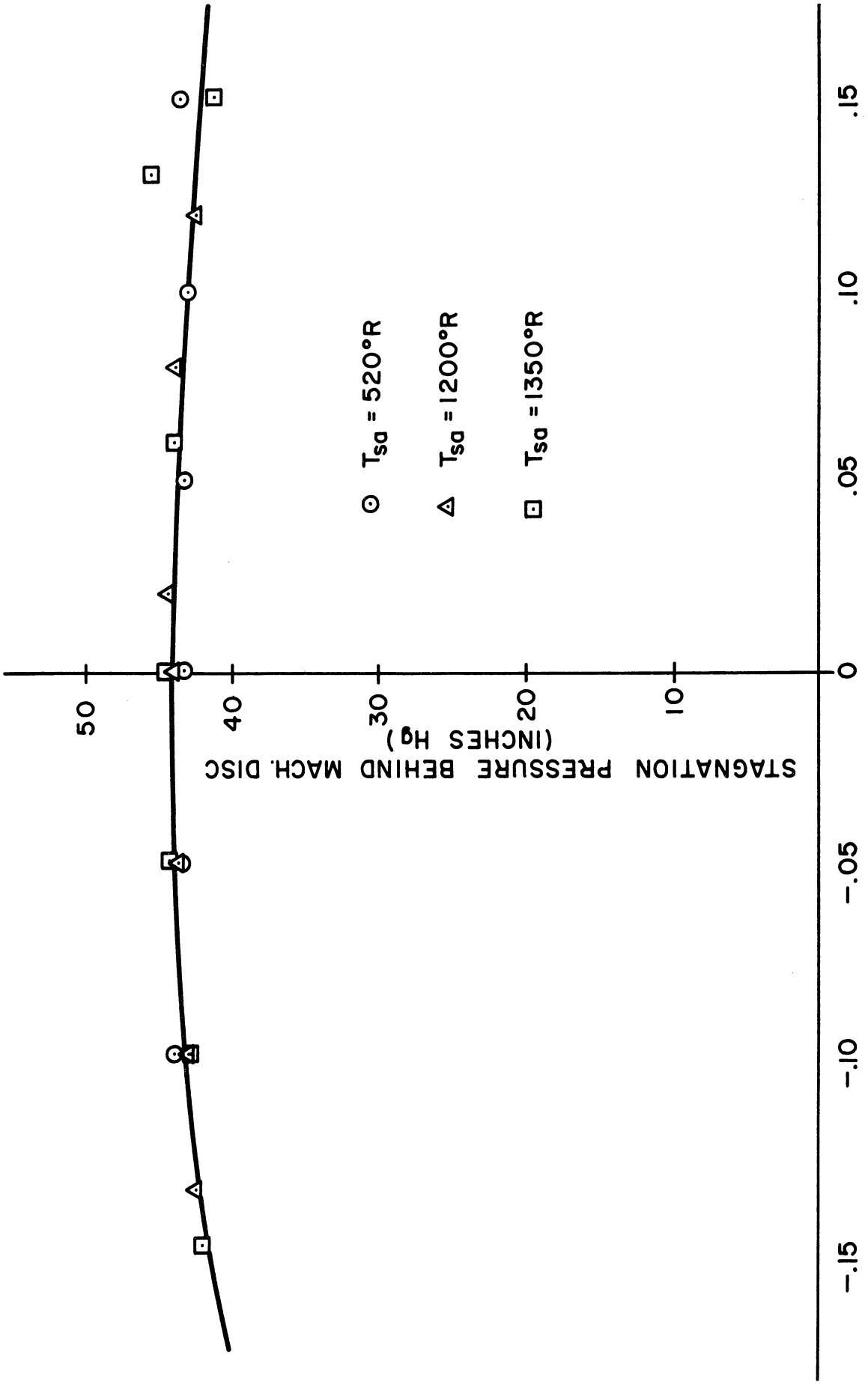

Figure 35. Stagnation Pressure Measurements behind Mach Disc.

are shown in Figure 36 and it can be seen that the concentration is uniform over most of the disc area. The centerline concentration is much richer than the overall average concentration because the hydrogen is originally introduced on the centerline and incomplete mixing is realized. Of course, the centerline concentration is the one of importance to these experiments. Other similar measurements were made at elevated temperatures (T_{sa} up to 1350°R) which indicated an even greater ratio of centerline fuel-air ratio to overall fuel-air ratio. Inasmuch as these measurements could not be effected at the highest temperatures of interest (combustion would destroy the probe), it has been necessary to use the results obtained. Thus the centerline fuel-air ratio for any given run is taken as 4.25 times the overall ratio. This value is based on the highest temperature runs made. There were indications from the other measurements that this value would not change much at higher temperatures.

5.4 Establishment of Stable Detonation Waves.

Using the experimental arrangement described, many experiments were conducted which led to very stable shock-wave -- combustion-zone configurations. In these cases, the desired air flow was established and hydrogen was then added until combustion was initiated behind the Mach disc. The resultant phenomenon was recorded by 35 mm schlieren photography as well as by 16 mm observation of the visible flame front. Data were taken during operation with air alone as well as during the combustion phase. It was found difficult to detect the combustion zone on the schlieren photographs, so that it was necessary to superimpose

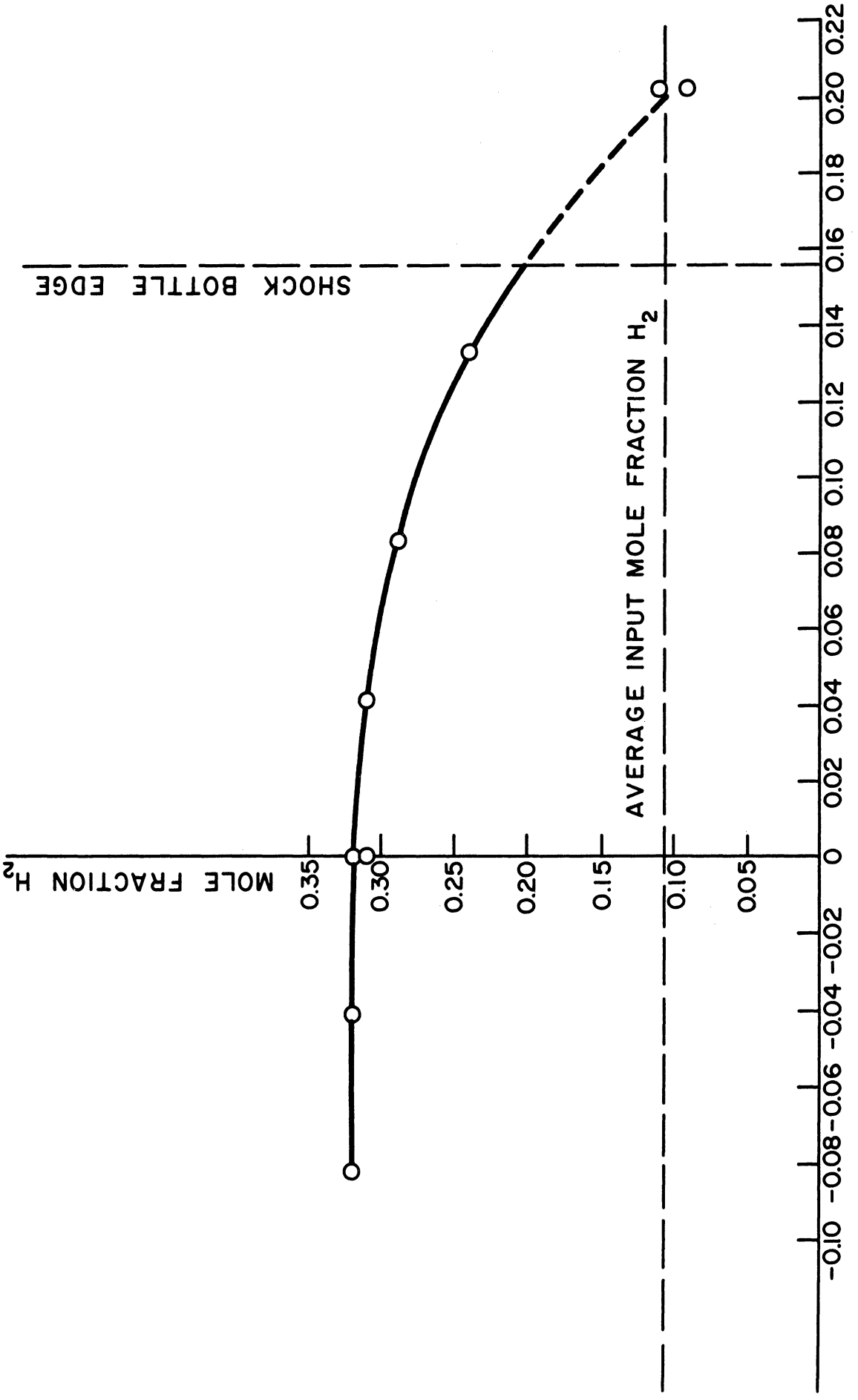

Figure 36. Radial Distribution of Hydrogen at Mach Disc.

the 16 mm results on the schlieren to determine relative positions of the combustion front and shock zone. A later technique consists of displaying the visible image directly on the 35 mm schlieren film so that relative positions are easily determined. A reference object of known dimensions, photographed by both cameras, allowed the determination of absolute distances. A typical pair of photographs, magnified to the same scale, appear as Figure 37. The flame shape and position is dotted in on the schlieren photograph. As is evident, there is a small distance between the position of the Mach disc and the initiation of combustion. This distance corresponds to a time of about 25 μ seconds for the conditions of the run shown, and represents a chemical ignition time delay. That is, it is the time between the instant of preparation of the gas for combustion by the shock wave and the time when appreciable chemical reaction takes place. The rather intense luminousity of the flame is attributed to the sodium added in the form of common salt. Otherwise the hydrogen-air flame emits very little light in the visible spectrum and is difficult to see. The occurrence of the ignition time delay along with a static pressure measurement at the exit of the nozzle gives almost conclusive proof that little or no combustion occurs within the nozzle. Another visible photograph of the same phenomenon is shown in Figure 38. Here the nozzle exit can be seen in more detail and the flame is better defined. In particular the initial portion of the flame is quite flat and distinct. This is typical of higher temperature runs.

Experiments have also been performed wherein a small flame was detected at the exit of the nozzle, as shown in Figure 39. In this case there appears to be no ignition-time-delay zone and combustion is

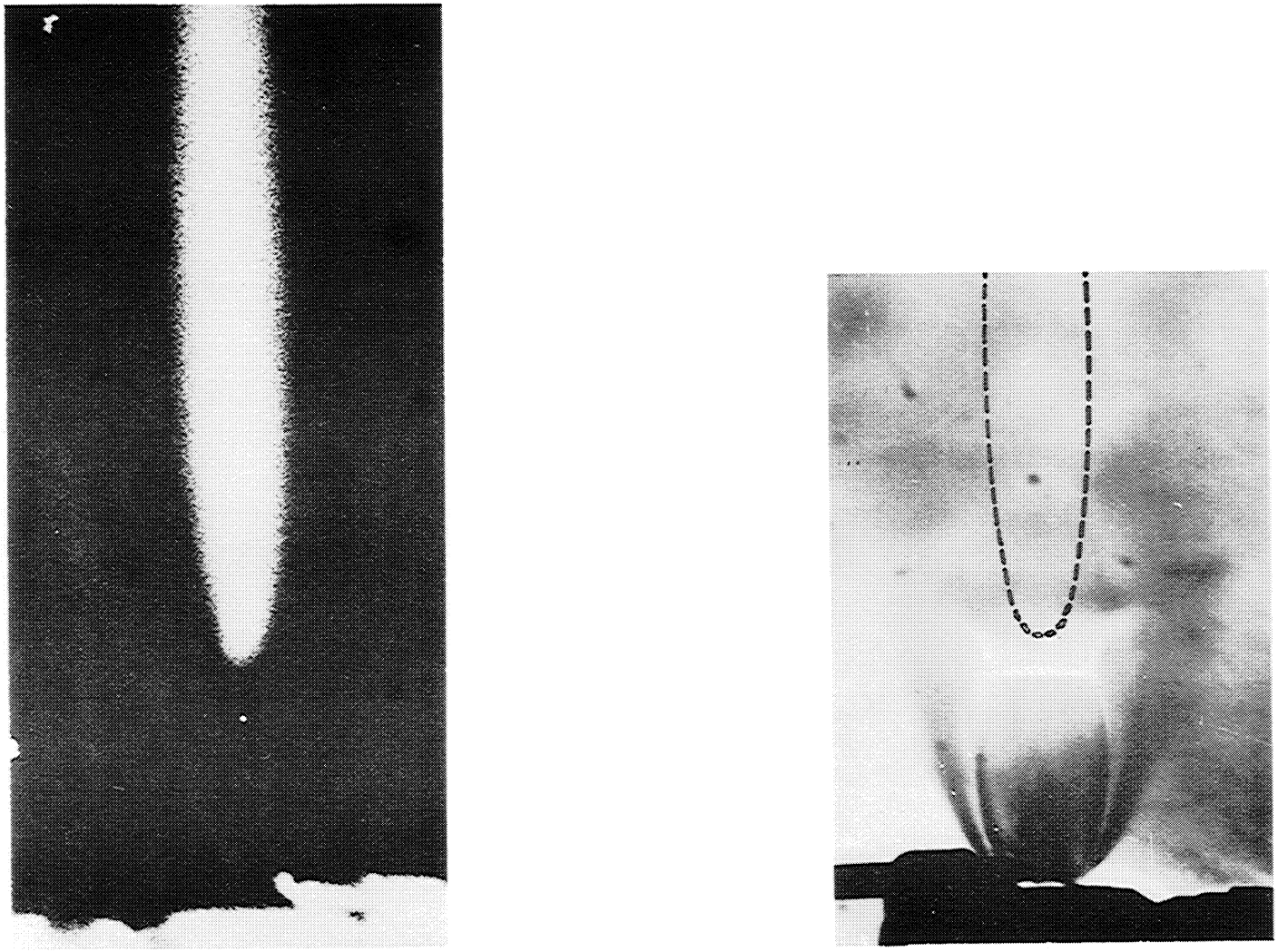

Figure 37. Visible and Schlieren Photographs of Jet During Combustion (no apparent burning at nozzle exit).

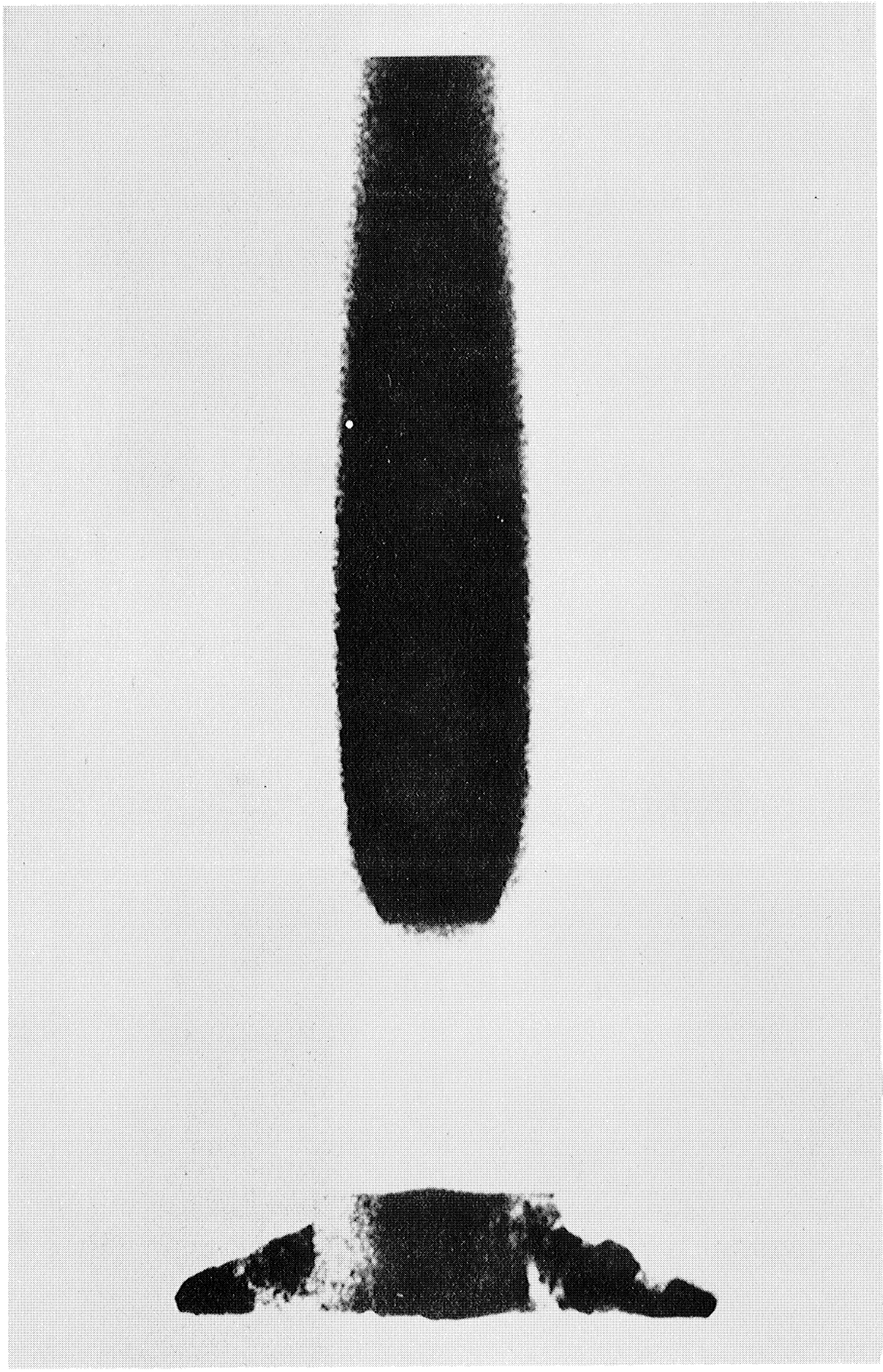

Figure 38. Visible Photograph of Flame.

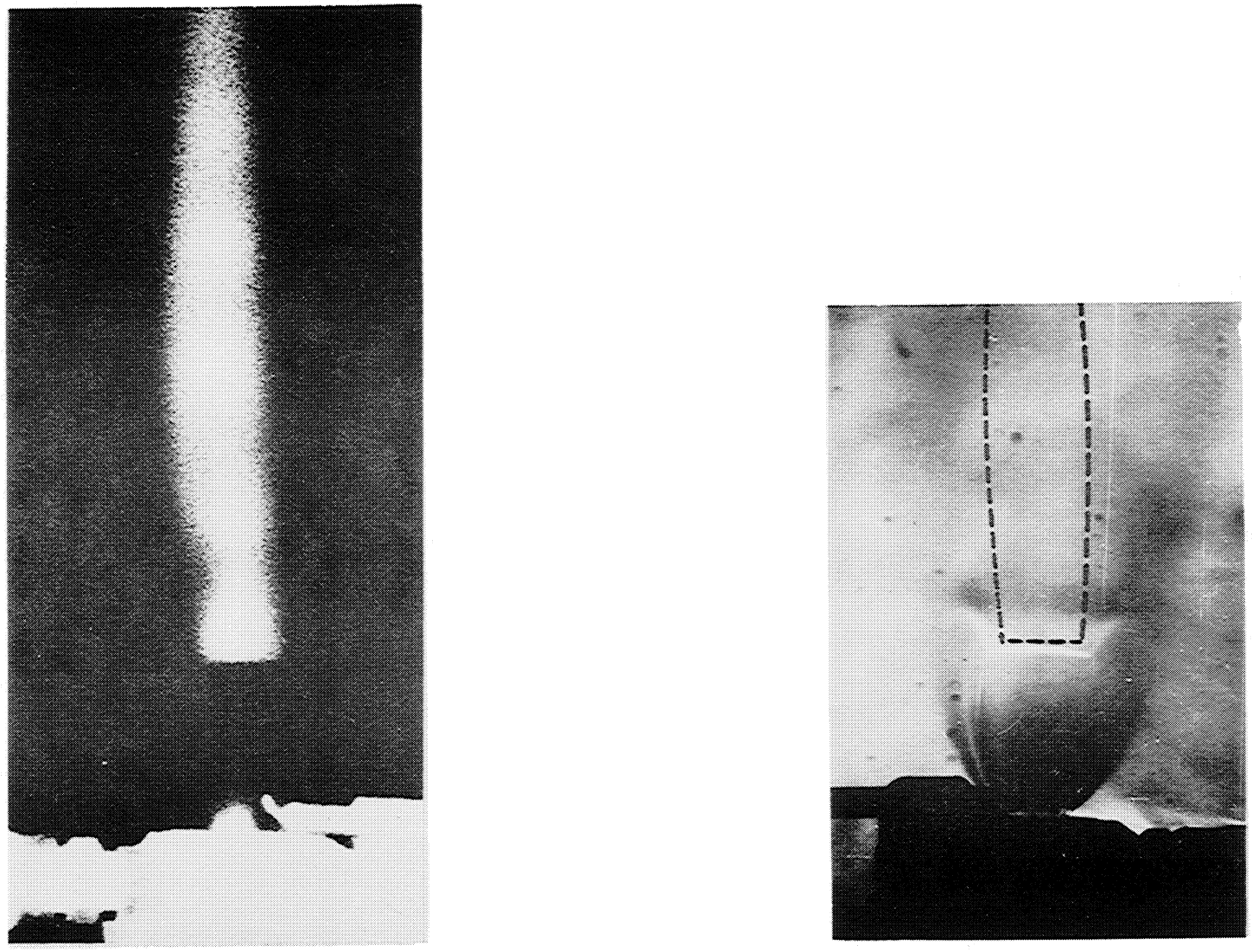

Figure 39. Visible and Schlieren Photographs of Jet During Combustion (flame cone at nozzle exit).

initiated right at the shock front. This is readily explainable since premature combustion within the nozzle serves to increase the stagnation temperature of the gases and thus the static temperature immediately downstream of the shock. The chemical kinetics, depending exponentially on temperature, are then sufficiently rapid to yield time delays shorter than can be resolved experimentally. Of course, this is no longer a true hydrogen-air detonation in that some hydrogen has been consumed. In experiments of this type, an appreciable increase in the nozzle exit pressure (i.e., 115 to 175 lb/sq. in.) was noted at the onset of combustion in the nozzle. Furthermore, a temperature increase was detected by a thermocouple immersed in the stream immediately outside the nozzle. Approximate calculations on the above experimentally observed conditions showed that the pressure increase can be explained by a relatively small heat addition. In other words, only a small portion of the input hydrogen actually burned in the nozzle. Combustion of the remaining hydrogen presumably occurred downstream of the Mach disc.

In many of the experiments of the type shown in Figure 37 there was no apparent interaction of the combustion with the shock. That is, the initiation of combustion did not change the shock position and hence not the shock Mach number. It did, however, modify slightly the size of the disc and the shape of the reflected shocks. It is doubtful that such waves can be classified as standing detonation waves. This distinction is discussed later.

In May, 1958, it is believed that the first demonstration of a stabilized gaseous detonation wave was realized. In this experiment the same procedure was followed as outlined above but the stagnation

temperature of the air was higher (2600°R). The air flow was first established and the jet was photographed by both cameras. Hydrogen was then added and combustion initiated. Examination of the data revealed that the original Mach number into the shock, that is, with air alone, was 6.1. This was determined from the previously measured Mach number distribution. However, with the onset of combustion, the shock wave was driven upstream to a lower Mach number of approximately 5.7. Also, the ignition time delay was the shortest observed to date (about 10μ seconds). Calculations reveal that the final wave corresponds very closely to the Chapman-Jouguet detonation wave. Accordingly, the author would consider this to be a stabilized detonation wave. Whether this can appropriately be called a Chapman-Jouguet detonation wave is somewhat open to question as will be discussed in section 7.1.

5.5 Ignition Delay Distances.

The experiments just described not only led to the establishment of stable detonation waves but also served to display a well defined ignition delay zone in a steady flow system. This latter benefit was admittedly unforeseen. The implication of this result is that the experimental technique developed has great potential as a tool in the study of chemical kinetics. Consequently considerable effort has been spent investigating, theoretically as well as experimentally, this aspect of the problem. The experimental measurements obtained are presented in this section and the reduction of the data in the following section. It was decided to separate this information because the method of data reduction employed can introduce some errors. The reason for this will become apparent in the next section.

A plot of some raw data showing ignition delay distance versus input (overall average) fuel-air ratio at about constant temperature is shown in Figure 40. The numbers by the individual points correspond to run numbers. The data for these runs and those to follow are tabulated in the next section as Table II. It should not be interpreted from this graph that increasing fuel-air ratio necessarily increases time delay. Ignition delay distance (or time) is strongly dependent upon temperature, the temperature of interest here being that behind the normal shock. With this experimental technique wherein the hydrogen is not heated, the temperature behind the shock is altered as different amounts of hydrogen are used even though the air stagnation temperature remains essentially constant. Furthermore, different fuel-air ratios yield different velocities behind the shock even for constant temperature due to the change in speed of sound of the gas. Consequently, the data of Figure 40 must be reduced before any conclusions can be drawn.

The above data, along with that of many other runs, are presented in Figure 41, where the delay distance is plotted versus reciprocal temperature on semi-log paper. The reason for this choice of presentation will become obvious after the results of the theoretical analysis. In general, each point shown corresponds to a different fuel-air ratio so that it is difficult to draw inferences at this time.

5.6 Reduction of Ignition Delay Data.

In order to interpret the ignition delay results in terms of physically meaningful variables and to be able to compare them with theory,

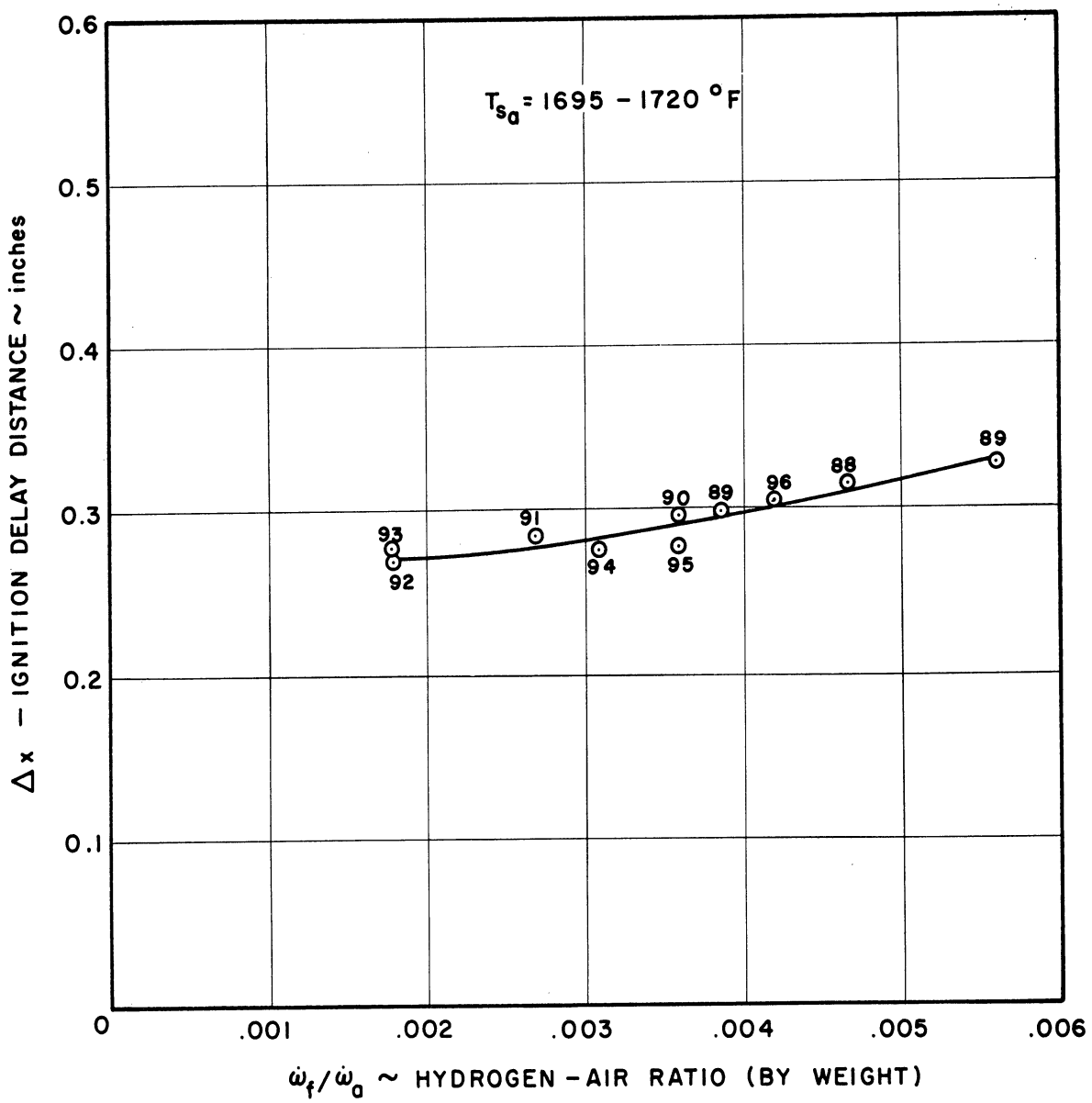

Figure 40. Ignition Delay Distance versus Input Fuel-Air Ratio.

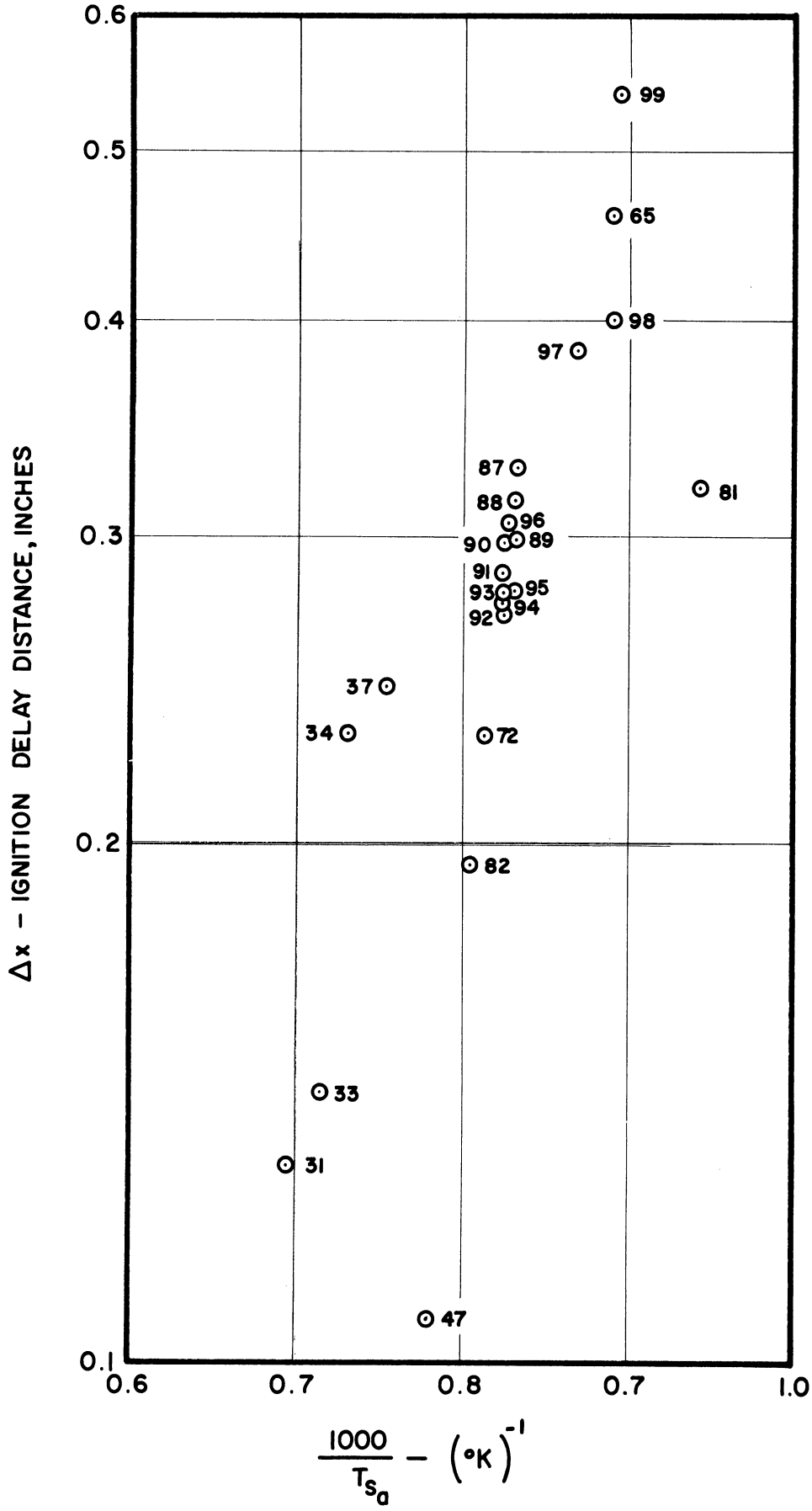

Figure 41. Ignition Delay Distance versus Air Stagnation Temperature.

the raw data must be reduced. The ignition time delay, which is of interest here, is dependent upon the static pressure, static temperature, and composition behind the shock wave. Thus it is essential that these quantities be determined from the measured values of air stagnation temperature (T_{sa}), overall input fuel-air ratio ($\frac{\dot{w}_f}{\dot{w}_a}$), and ignition delay distance (Δx). The ideal way of determining these required quantities would, of course, be to measure them under actual run conditions. To date this approach has not been feasible because of the high temperatures encountered in the flame. Water cooling of the sensing probe is required if the probe is to withstand these conditions. However, the scale of the experiment is too small to accommodate such a probe without altering the flow conditions. Hence it has been necessary to rely on a calibration procedure which, admittedly, is subject to some error. However, because of the high Mach numbers of interest here, there are a few simplifications that can be used to a great degree of accuracy. It was pointed out earlier that at these high Mach numbers the stagnation pressure behind the Mach disc is a constant at 1.46 atmospheres. This was found experimentally both in the presence of a flame and without the flame. Now the downstream Mach number is very close to the asymptotic value so that the downstream static pressure and temperature are constant percentages of the stagnation values. In view of this and the fact that the experimental temperature range covered is from about 1900-2600°R, the following values will be taken as constants immediately downstream of the shock;

a) ratio of specific heats = γ = 1.35

b) Mach number = M = 0.40

c) ratio of static to stagnation temperature = $\frac{T}{T_t}$ = 0.972

d) P = 0.9 x 1.46 = 1.31 atmospheres

The determination of the composition at the Mach disc was described in section 5.3 and the conclusion reached that to the best approximation this fuel-air ratio could be taken as 4.25 times the overall ratio. This factor has been used in reducing the data.

A critical step lies in the determination of T_t, the total temperature at the Mach disc, for T follows directly from it and this is the dominant variable. In general T_t differs from the measured T_{sa} as a result of heat transfer to the nozzle walls and heating of the hydrogen. The former heat loss will be taken to be negligible. Support for this conclusion is given by the results of some unshielded thermocouple measurements at the Mach disc location. While an accurate radiation correction for this thermocouple was not available, any reasonable correction to the probe reading indicated a very small value of $T_{sa} - T_t$ for the case of no hydrogen flow. Another reason for not reducing T_{sa} to account for losses in the nozzle is that the T_{sa} is already somewhat lower than the actual because of radiation effects.

The change in stagnation temperature as a result of the mixing of air and hydrogen is appreciable and cannot be neglected. As has been mentioned, this cannot be determined under actual run conditions so that a calibration procedure is utilized. The aim of this procedure is to establish the effective fuel-air ratio, $\left(\frac{\dot{w}_f}{\dot{w}_a}\right)_{eff}$, for the mixing as a function of the overall fuel-air ratio.

In general, $\left(\frac{\dot{w}_f}{\dot{w}_a}\right)_{eff}$ is a value between the overall ratio and the measured centerline ratio of 4.25 times the overall ratio. The difference arises from the transfer of heat from the hotter outer portions of the flow into the mixing zone. The manner in which $\left(\frac{\dot{w}_f}{\dot{w}_a}\right)_{eff}$ is determined in the calibration procedure and ultimately used in reducing raw data is described in the following.

In order to evaluate the magnitude of $T_{sa} - T_t$ as a result of mixing with hydrogen, a number of experiments were performed at a few different temperatures with and without hydrogen flow. The procedure was to measure T_{sa} and also the total temperature at the Mach disc by means of a semi-shielded thermocouple. Again, these measurements were restricted to temperatures below those leading to combustion. The particular chromel-alumel thermocouple used was selected because the radiation and aerodynamic recovery corrections had been determined by Glawe, Simmons, and Stickney [36] under conditions very similar to those encountered here.* The following equation, which corrects the measured temperature for radiation and recovery errors, is taken from this latter reference. Values for the constants for a number of probe designs are also given in the reference.

$$T_t = \left\{ T_w + \frac{K^*_{RAD}}{\sqrt{MP}} \left(\frac{T_w}{1000}\right)^{-0.18} \left[\left(\frac{T_w}{1000}\right)^4 - \left(\frac{T_d}{1000}\right)^4 \right] \right\} \left(\frac{1}{1-\Delta}\right) \qquad (5.1)$$

where:

T_w = indicated junction temperature, °R

T_d = equivalent duct temperature, °R

P = pressure, atmospheres

---

* This probe is available commercially from Aero. Research Instrument Co., Chicago, Illinois.

M = Mach number

K^*_{RAD} = radiation - correction coefficient

Δ = recovery correction factor = $\dfrac{T_t - T_g}{T_t}$

T_g = temperature of gas surrounding junction

For the experiments described here the equivalent duct temperature (temperature of the surrounding)is the ambient temperature. Therefore,

$$\left(\frac{T_d}{1000}\right)^4 << \left(\frac{T_w}{1000}\right)^4$$

so that,

$$T_t \simeq \left[T_w + \frac{K^*_{RAD}}{\sqrt{MP}}\left(\frac{T_w}{1000}\right)^{3.82}\right]\left(\frac{1}{1-\Delta}\right) \qquad (5.2)$$

The results of a series of measurements made at about a constant air stagnation temperature and different hydrogen flows are shown in Figure 42. From the data it is desired to evaluate T_t for each condition. Because of the presence of the shock wave and of hydrogen, which differs from the experimental calibration procedure of the reference, it was decided to obtain the value of K^*_{RAD} and Δ from the experimental data at zero hydrogen flow. That is, $T_{sa}=T_t$ and T_w were measured and substituted into Equation (5.2). This yielded $K^*_{RAD}=f(\Delta)$. The actual values for each were selected in light of this and the values reported in reference (36). The values selected are $K^*_{RAD}=9.5$ and $\Delta = 0.01$.

With the values of the constants now known, Equation (5.2) can be solved for T_t for any given hydrogen flow, using the values from Figure 42 for $T_w=T_{sa}-(T_{sa}-T_w)=1765-(T_{sa}-T_w)$. These results can be substituted into the energy equation (Equation 4.14, where $T_{s2}=T_t$) in order to evaluate the effective hydrogen -air ratio, $\left(\dfrac{\dot{w}_f}{\dot{w}_a}\right)_{eff}$, for the mixing process.

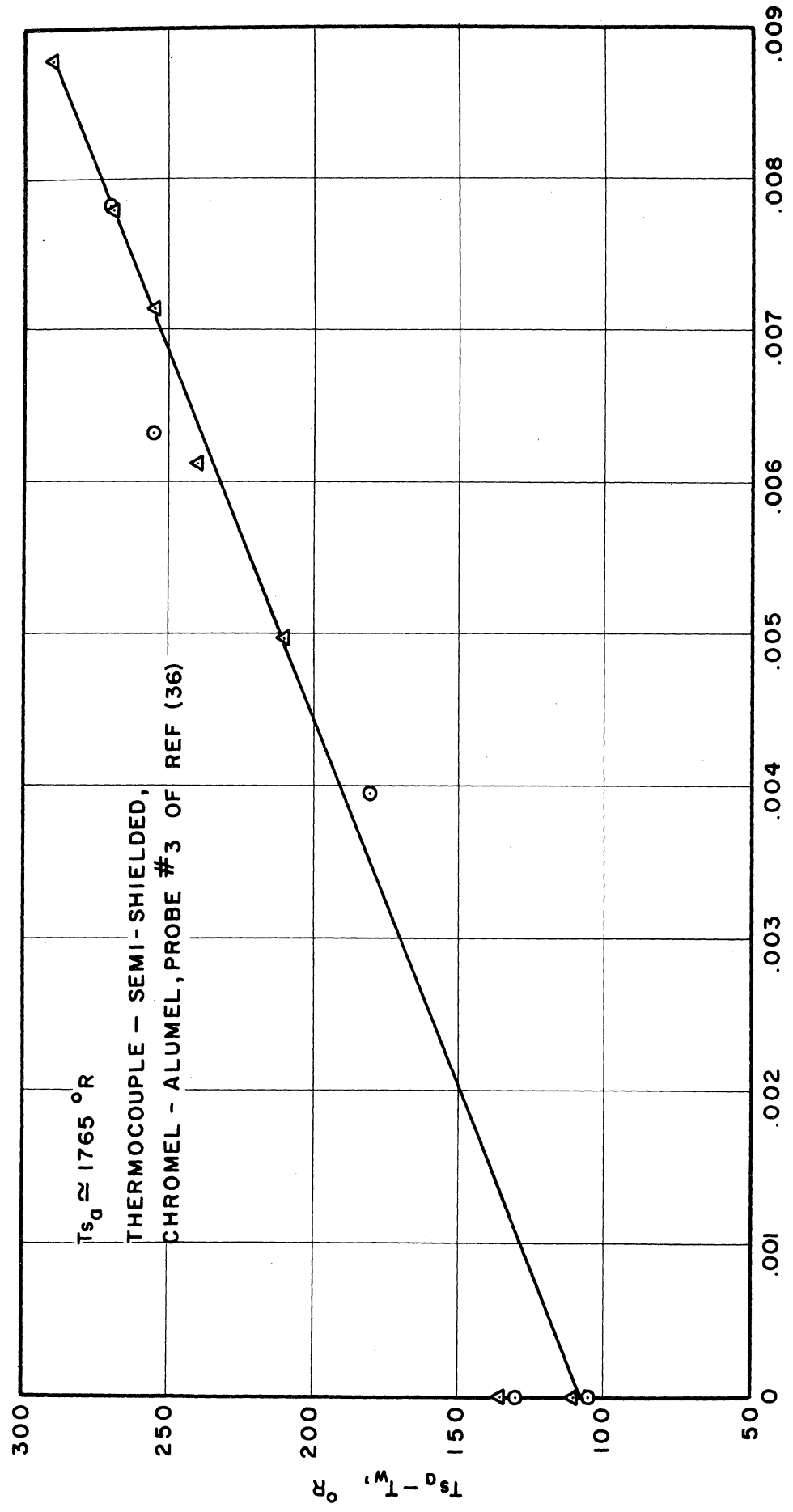

Figure 42. Measured Stagnation Temperature in Jet at Different Hydrogen Flows.

This results in a variation of $\left(\frac{\dot{w}_f}{\dot{w}_a}\right)_{eff}$ with $\left(\frac{\dot{w}_f}{\dot{w}_a}\right)$. Actually this functional dependence is probably temperature sensitive but in light of concentration measurements this effect would appear to be small.

The procedure just outlined served only to establish the effective fuel-air ratio versus overall ratio. The procedure followed for reducing actual ignition delay data is as follows. The measured value of $\left(\frac{\dot{w}_f}{\dot{w}_a}\right)$ for any particular run yields $\left(\frac{\dot{w}_f}{\dot{w}_a}\right)_{eff}$ directly from the calibration. This value along with the measured T_{sa} was substituted into the energy equation (4.14) and the equation solved for T_t. Once this is obtained T follows immediately as $M = 0.4$ is known. The molecular weight at shock location is determined by taking the fuel-air ratio as 4.25 times the overall fuel-air ratio as previously determined in the calibration runs. The calculations of the speed of sound, velocity, and ignition time delay then follow in a straightforward manner.

The results of many experimental runs with the data reduced in the manner described are shown in Table II. As can be noted, the delays are all in the microsecond range.

TABLE II

IGNITION DELAY RESULTS

Run #	T_{sa} °R	$\frac{\dot{w}_f}{\dot{w}_a}$	η_{H_2}	Δx in.	$\left(\frac{\dot{w}_f}{\dot{w}_a}\right)_{eff}$	T_t °R	T °R	m	a ft/sec	V ft/sec	τ μsec
87	2155	.0056	.0751	.328	.00875	1970.8	1915	20.4	2510	1004	27.2
88	2160	.00467	.063	.315	.00715	2006	1950	21.8	2450	980	26.8
89	2160	.00387	.053	.299	.0058	2032.8	1975	22.9	2403	961.2	25.95
90	2170	.0036	.049	.298	.0054	2050	1992	23.4	2390	956	26.0
91	2180	.0027	.038	.285	.00395	2090	2030	24.6	2355	942	25.22
92	2180	.00179	.025	.269	.0025	2121.9	2065	26.1	2305	922	24.3
93	2180	.00179	.025	.277	.0025	2121.9	2065	25.9	2313	925.2	24.95
94	2180	.0031	.043	.274	.0046	2076.3	2015	24.1	2370	948	24.1
95	2175	.0036	.049	.278	.0054	2054.8	1997	23.4	2395	958	24.15
96	2175	.0042	.0567	.304	.00635	2027	1968	22.5	2420	968	26.2
97	2070	.00515	.069	.384	.0080	1908.8	1855	21.1	2425	970	33.0
98	2020	.00424	.057	.400	.00645	1891.9	1838	22.4	2350	940	35.5
99	2010	.00348	.048	.540	.0052	1905.6	1852	23.5	2300	920	49.0
65	2020	.0056	.0745	.460	.00875	1851	1800	20.4	2435	974	39.4
72	2210	.00583	.0774	.230	.00915	2012.4	1955	20.1	2555	1022	18.75
81	1910	.00267	.037	.320	.0039	1837.6	1786	24.7	2200	880	30.3
82	2235	.0090	.114	.193	.01465	1935	1880	15.9	2820	1128	14.25
47	2305	.00709	.109	.106	.0113	2054	1995	16.5	2850	1140	7.75
31	2590	.0039	.0537	.130	.00588	2427.5	2360	22.8	2635	1054	10.27
33	2515	.00474	.0638	.143	.0073	2324.4	2260	21.7	2640	1056	11.27
34	2460	.00619	.0817	.231	.00977	2220	2158	19.6	2715	1086	17.71
37	2385	.00461	.0621	.246	.0071	2211	2150	21.9	2565	1026	19.97

VI THEORETICAL ANALYSIS OF THE IGNITION TIME DELAY

6.1 Presentation of the Problem.

It was pointed out in the last section that the experimental results have shown the existence of a delay period separating the shock wave and visible combustion zone. This delay period occurs even though the temperature behind the shock is well above the ignition temperature. To the best of the author's knowledge, these experiments represent the first, and to date, only, demonstration of a chemical ignition time delay in a steady flow detonating system. In view of these results, it appeared essential and opportune to consider this facet theoretically and attempt to corroborate the experimental observations. Such knowledge is of great value to the understanding of the structure of a detonation wave and further it is essential to the identification of the phenomenon observed. In addition, it is well to assess the value of this experimental technique for possible application to the determination of fundamental chemical kinetic constants.

Many investigators have considered the problem of ignition time delays for a number of fuel-oxidant combinations. Until recently, however, these studies have been restricted to relatively low temperatures and hence long delays. Furthermore, the experimental techniques have led to many inconsistencies and complications. For example, it has been found that in the case of experiments conducted in vessels, the ignition delay time depends not only on pressure, temperature, and composition, but also on vessel size and the nature of the vessel wall or wall coating. Another technique often used is that of injecting the fuel into a preheated oxidant stream and then

noting the time or distance traversed to the onset of combustion. This technique is only accurate, of course, if the mixing time is negligible compared to the delay time. In 1956 Brokaw [37] observed that; "results obtained by different methods are not entirely in accord; in particular, for hydrogen-air mixtures delays differ by as much as a hundredfold at a given temperature." Brokaw discusses thermal ignition in this reference and summarizes most of the data available to that time. Subsequent to this, Drell and Belles [38] surveyed the combustion properties of hydrogen and briefly summarized the ignition delay results. More recently shock tube results have become available which cover a much higher temperature range and which allowed the more accurate determination of kinetic constants. These latter results are more applicable here and will be referenced and discussed at appropriate times in the ensuing text.

The problem to be considered is demonstrated in Figure 43, which is a magnified combination schlieren and visible, photograph of a typical shock wave-combustion zone configuration for hydrogen-air. The ignition time delay zone, that zone between the shock and combustion, is clearly distinguishable. Included in the figure is a schematic outlining the major aspects of interest here. As indicated, a mixture of hydrogen and air is processed by a normal shock at a relatively high Mach number. Behind the shock the flow is subsonic so that the temperature is not far from the stagnation temperature. This temperature, for the cases of interest here, is above the "ignition" temperature for the prevailing conditions of pressure and mixture ratio. Now it is known -cf: Semenov, [39] and Lewis and von Elbe [15] -that under these conditions an induction period must exist before any explosion

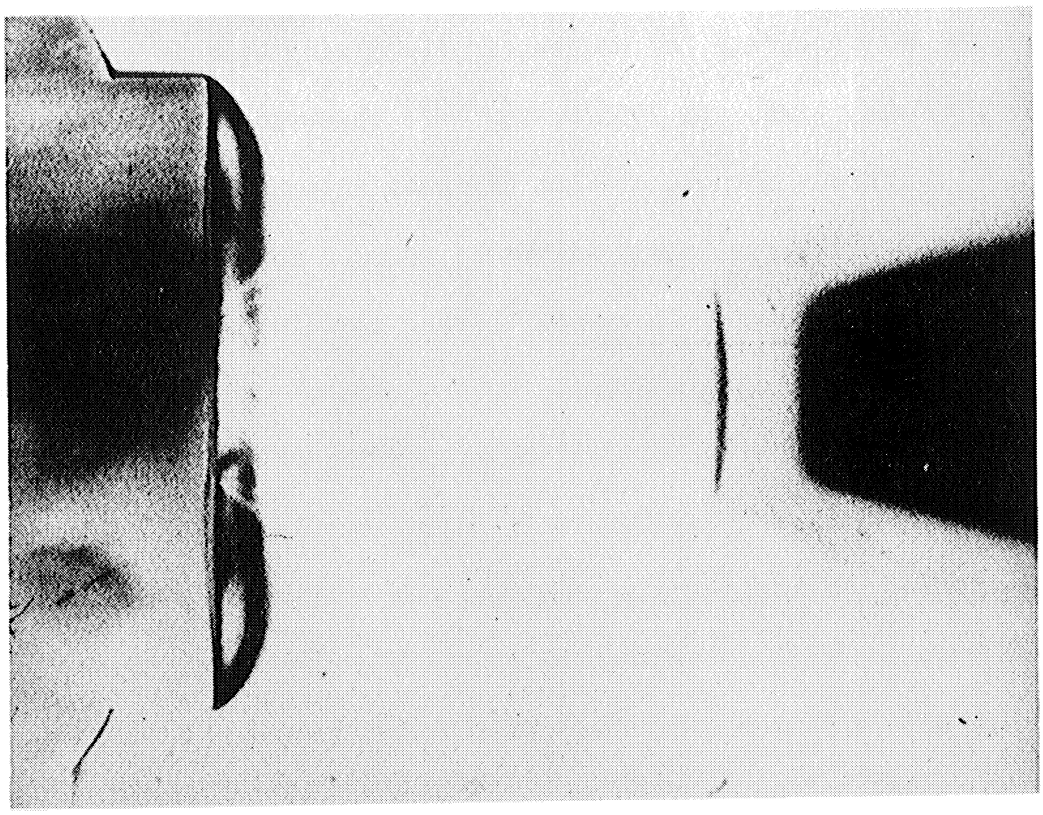

(a) Photograph of a Jet.

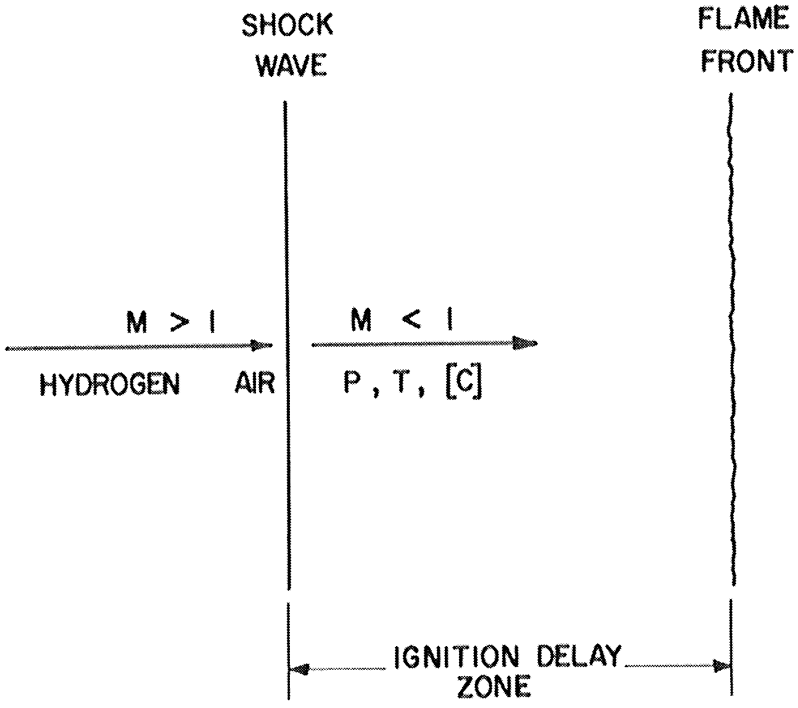

(b) Schematic of Ignition Delay Zone

Figure 43. Ignition Delay Zone.

(very rapid and luminous chemical reactions) can materialize. This induction period arises from the finite time required for the collision and dissociation of molecules which lead to the formation of radicals, these radicals being the participants in the eventual rapid reactions. The method of attack will thus center around the prediction of the rate of growth of radicals and the concentration required to effectively initiate the flame front.

The problem will now be generalized to the extent of including reactions of the type:

$$\chi H_2 + y O_2 + z B \longrightarrow \text{Products}$$

where B is some unspecified inert gas. Hence various hydrogen-oxygen concentrations as well as diluent concentrations will be considered. Now let,

$N = \chi + y + z$ = number of moles of reactants.

$[C]_o$ = number of moles per cc, initially.

$\frac{\chi}{N}$ = number of moles of H_2 per total moles of reactants, initially.

$\frac{y}{N}$ = number of moles of O_2 per total moles of reactants, initially.

$[C]$ = number of moles per cc, at any time.

It will be assumed that no chemical reaction occurs across the shock wave and further that the gases are immediately equilibrated in the

rotational and translational degrees of freedom. Realizing that shock waves are only a few mean free paths in thickness, that only a very few molecular collisions are required to equilibrate the rotational and translational degree, and that chemical reaction times are much greater than these times, it would appear that these assumptions are perfectly justifiable. Supporting arguments for these conclusions are given by Bethe and Teller [40], Wood [41], and many others. In addition to these assumptions, it will also be assumed that the vibrational mode is frozen; that is, not excited. Many more collisions are required to equilibrate this mode than the two previously mentioned. Hence, under certain conditions it is conceivable that the relaxation time could be less than or of the same order as the ignition time delay. In this case the subsequent results obtained will be subject to some error. On the other hand if this relaxation time is long, the assumption is justified. This effect will be much more pronounced at high temperatures and is, to a lesser degree, dependent on the species concentrations. For the temperatures considered in this study it is believed that the assumption of vibrationally cold flow is entirely warranted. More will be said on this point later.

In view of the above, the prevailing conditions at time zero ($t = 0$), which corresponds to a point immediately downstream of the shock, can be written;

$$[H]_0 = [O]_0 = [OH]_0 = [H_2O]_0 = 0$$

$$[H_2]_0 = \frac{\varkappa}{N}[C]_0$$

$$[O_2]_0 = \frac{\gamma}{N}[C]_0 \qquad (6.1)$$

Throughout the induction zone it is safe to assume no change in the number of moles per cc (i.e. $[C]$= constant) inasmuch as the total number of moles of radicals and H_2O formed is relatively small. In fact it will be brought out later that $[H_2]$ and $[O_2]$ remain almost constant. For the same reason (changes only on the microscopic level), the thermodynamic coordinates and hydrodynamic variables remain fixed so that it is possible to divorce the chemical kinetics from the fluid mechanics. This, of course, greatly simplifies the problem.

6.2 Pertinent Reactions and Rates of Reaction.

Some of the most important reactions characterizing the combustion of $H_2 - O_2$ mixtures have been postulated by various authors - cf. Semenov [39] and Lewis and von Elbe [15]. There has not been complete agreement on all of these reactions. Recently, Duff [42] considered 9 reactions and calculated, by iterative techniques, the reaction profile behind a shock wave moving through a $2H_2 + O_2 + X_e$ mixture such that the pressure and temperature immediately downstream of the shock were 1.150 atmospheres and 1737°K respectively. For this purpose he utilized the best known values of the rate constants, Inasmuch as Duff's reaction scheme appears to be the most comprehensive and recent and is in the temperature range of interest here, his proposed reactions will be considered in this work. The aim will be to reduce the reaction scheme to a form that can be handled analytically so that functional information can be gained.

The reactions to be considered are given in Table III.

TABLE III

PERTINENT REACTIONS

No.	Reaction
I	$H_2O + M \xrightarrow{k_1} OH + M + H$
II	$H_2 + M \xrightarrow{k_2} 2H + M$
III	$O_2 + M \xrightarrow{k_3} 2O + M$
IV	$OH + M \xrightarrow{k_4} O + H + M$
V	$O_2 + H_2 \xrightarrow{k_5} 2\,OH$
VI	$O_2 + H \xrightarrow{k_6} OH + O$
VII	$H_2 + O \xrightarrow{k_7} OH + H$
VIII	$H_2 + OH \xrightarrow{k_8} H_2O + H$
IX	$2\,OH \xrightarrow{k_9} H_2O + O$

(M = some third body)

The reactions have been written as proceeding only in the forward direction. This is legitimate for the induction period in that the gas immediately behind the shock is far removed from equilibrium and hence the reverse reaction rates will be negligible (i.e.: the equilibrium constant $\rightarrow \infty$). Of course in the later stages as the reaction nears equilibrium the reverse rates will have to be taken into account. Fortunately, for the problem at hand, this added complexity will not arise.

The reaction rate constant, k_i (the subscript i referring to the particular reaction in Table III), is given by:

$$k_i = A_i T^{m_i} \exp\left(-\frac{E_i}{RT}\right) \qquad (6.2)$$

The values of A_i, m_i, and E_i, as given by Duff, are tabulated in Table IV.

TABLE IV

VALUES FOR THE REACTION RATE CONSTANT

Reaction No.	E (cal/mole)	m	A $\left(\frac{\text{moles}}{\text{cc}}\right)^{-1}\text{sec}^{-1}$
I	(a) 1.1473×10^5	-1.5	10^{21}
	(b) 1.1473×10^5	-1.5	10^{23}
II	1.0324×10^5	-1.5	10^{21}
III	1.1796×10^5	-1.5	10^{21}
IV	1.01×10^5	-1.5	10^{21}
V	7×10^4	0	10^{14}
VI	(a) 2.0×10^4	0	10^{14}
	(b) 1.8×10^4	0	4×10^{14}
VII	6×10^3	0	3×10^{14}
VIII	2.5×10^3	0	3×10^{14}
IX	2.5×10^3	0	3×10^{14}

Taking the third body concentration, M, to be the total concentration, C, the rate expression for each of the reactive species may be written as;

$$\frac{d[H]}{dt} = [H_2O][C]k_1 + 2[H_2][C]k_2 + [OH][C]k_4 - [O_2][H]k_6 + [H_2][O]k_7 + [H_2][OH]k_8 \qquad (6.3)$$

$$\frac{d[O]}{dt} = 2[O_2][C]k_3 + [OH][C]k_4 + [O_2][H]k_6 - [H_2][O]k_7 + [OH]^2k_9 \qquad (6.4)$$

$$\frac{d[OH]}{dt} = [H_2O][C]k_1 - [OH][C]k_4 + 2[O_2][H_2]k_5 + [O_2][H]k_6 + [H_2][O]k_7 - [H_2][OH]k_8 - 2[OH]^2 k_9 \qquad (6.5)$$

$$\frac{d[H_2O]}{dt} = -[H_2O][C]k_1 + [H_2][OH]k_8 + [OH]^2 k_9 \qquad (6.6)$$

$$\frac{d[O_2]}{dt} = -[O_2][C]k_3 - [O_2][H_2]k_5 - [O_2][H]k_6 \qquad (6.7)$$

$$\frac{d[H_2]}{dt} = -[H_2][C]k_2 - [O_2][H_2]k_5 - [H_2][O]k_7 - [H_2][OH]k_8 \qquad (6.8)$$

It is convenient to non-dimensionalize the Equations (6.3) through (6.8) by dividing through by $[C]$. We then denote the dimensionless concentrations (the mole fractions) as,

$$\eta_H = \frac{[H]}{[C]} \quad , \quad \eta_O = \frac{[O]}{[C]} \quad , \text{ etc.}$$

The rate equations then become;

$$\frac{d\eta_H}{dt} = \eta_{H_2O}[C]k_1 + 2\eta_{H_2}[C]k_2 + \eta_{OH}[C]k_4 - \eta_{O_2}\eta_H[C]k_6 + \eta_{H_2}\eta_O[C]k_7 + \eta_{H_2}\eta_{OH}[C]k_8 \qquad (6.9)$$

$$\frac{d\eta_O}{dt} = 2\eta_{O_2}[C]k_3 + \eta_{OH}[C]k_4 + \eta_{O_2}\eta_H[C]k_6 - \eta_{H_2}\eta_O[C]k_7 + \eta_{OH}^2[C]k_9 \qquad (6.10)$$

$$\frac{d\eta_{OH}}{dt} = \eta_{H_2O}[C]k_1 - \eta_{OH}[C]k_4 + 2\eta_{O_2}\eta_{H_2}[C]k_5 + \eta_{O_2}\eta_H[C]k_6$$

$$+ \eta_{H_2}\eta_O[C]k_7 - \eta_{H_2}\eta_{OH}[C]k_8 - 2\eta_{OH}^2[C]k_9 \quad (6.11)$$

$$\frac{d\eta_{H_2O}}{dt} = -\eta_{H_2O}[C]k_1 + \eta_{H_2}\eta_{OH}[C]k_8 + \eta_{OH}^2[C]k_9 \quad (6.12)$$

$$\frac{d\eta_{O_2}}{dt} = -\eta_{O_2}[C]k_3 - \eta_{O_2}\eta_{H_2}[C]k_5 - \eta_{O_2}\eta_H[C]k_6 \quad (6.13)$$

$$\frac{d\eta_{H_2}}{dt} = -\eta_{H_2}[C]k_2 - \eta_{O_2}\eta_{H_2}[C]k_5 - \eta_{H_2}\eta_O[C]k_7$$

$$- \eta_{H_2}\eta_{OH}[C]k_8 \quad (6.14)$$

In addition to these rate expressions we can write the equations expressing conservation of hydrogen atoms and oxygen atoms. Confining our attention to a mass of fixed identity which moves away from the shock (Lagrangian System), these relations are,

$$\eta_H + \eta_{OH} + 2\eta_{H_2O} + 2\eta_{H_2} = 2(\eta_{H_2})_0 \quad (6.15)$$

and

$$\eta_O + \eta_{OH} + \eta_{H_2O} + 2\eta_{O_2} = 2(\eta_{O_2})_0 \quad (6.16)$$

where $(\eta_{H_2})_0$ and $(\eta_{O_2})_0$ are the initial mole fractions of H_2 and O_2. Actually, because of the very small amounts of radicals generated in the induction zone, Equations (6.15) and(6.16) add no information and reduce to the very good approximations,

$n_{H_2} = (n_{H_2})_0 =$ constant $\qquad$ $n_{O_2} = (n_{O_2})_0 =$ constant

These simplifications will be used in the analysis to follow and will be justified later.

Now it is possible to simplify the rate expressions somewhat by looking at the order of magnitude of the individual terms. For this purpose the temperature range, $1000°K \leq T \leq 2000°K$, will be considered. The values for the rate constants at a few different temperatures in this range are given in Table V where the reaction rate numbers and constants are taken from Table IV. For instance, k_{1a} refers to reaction number I with the (b) values for E and A.

TABLE V

REACTION RATE CONSTANT AT DIFFERENT TEMPERATURES

$k_i \left(\frac{\text{moles}}{\text{cc}}\right)^{-1} \text{sec}^{-1}$	T°K 1000°K	1500°K	2000°K
k_{1a}	2.51×10^{-9}	3.24×10^{-1}	3.31×10^{3}
k_{1b}	2.51×10^{-7}	3.24×10	3.31×10^{5}
k_2	7.97×10^{-7}	1.61×10	5.62×10^{4}
k_3	5.02×10^{-10}	1.05×10^{-1}	1.41×10^{3}
k_4	2.50×10^{-6}	3.24×10	1.00×10^{5}
k_5	5.02×10^{-2}	6.30×10^{3}	2.24×10^{6}
k_{6a}	4.26×10^{9}	1.02×10^{11}	6.53×10^{11}
k_{6b}	4.68×10^{10}	9.52×10^{11}	4.32×10^{12}
k_7	1.47×10^{13}	4.00×10^{13}	6.63×10^{13}
k_8	8.53×10^{13}	1.30×10^{14}	1.60×10^{14}
k_9	8.53×10^{13}	1.30×10^{14}	1.60×10^{14}

In comparing the importance of individual terms of the rate equations we note that η_{O_2} and η_{H_2} are of order unity, written as $O(\eta_{O_2}) = 1$ and $O(\eta_{H_2}) = 1$. The total concentration, $[C]$, is common to all terms so that it doesn't enter. Also the concentrations of all radicals are much less than that of H_2 or O_2. That is,

$$\eta_H << 1 \qquad \eta_{H_2O} << 1 \qquad \eta_{OH} << 1 \qquad \eta_O << 1$$

Consider, then, the first two terms for the rate of formation of hydrogen atoms, Equation (6.9). From Table V, $k_1 \simeq k_2$, but $\eta_{H_2O} << \eta_{H_2}$ so that,

$$\eta_{H_2O}[C]k_1 << 2\eta_{H_2}[C]k_2$$

Similarly,

$$\eta_{OH}[C]k_4 << 2\eta_{H_2}[C]k_2$$

In the case of the k_6 term, $k_6 >> k_2$ but $\eta_H << \eta_{H_2}$ so that no conclusions can be drawn as to relative magnitude at this point. The same is true for the k_7 and k_8 terms. Actually in order to drop the terms above from the rate expression it should be required that they be small compared to the summation of the remaining terms. In this case there is no difficulty and the inequality shown is sufficient to justify dropping the terms.

In the same way small terms may be dropped from the other rate expressions. In particular it may be noted that

$$\eta_{OH}^2[C]k_9 << \eta_{H_2}\eta_{OH}[C]k_5$$

because $k_5 = k_9$ and $\eta_{OH} << \eta_{H_2}$. In the equation for $\frac{d\eta_O}{dt}$ (Equation 6.10) the k_8 term doesn't appear so the k_9 term will be retained. The resultant simplified equations become:

$$\frac{d\eta_H}{dt} = 2\eta_{H_2}[C]k_2 - \eta_{O_2}\eta_H[C]k_6 + \eta_{H_2}\eta_O[C]k_7 + \eta_{H_2}\eta_{OH}[C]k_8 \quad (6.17)$$

$$\frac{d\eta_O}{dt} = 2\eta_{O_2}[C]k_3 + \eta_{O_2}\eta_H[C]k_6 - \eta_{H_2}\eta_O[C]k_7 + \eta_{OH}^2[C]k_9 \quad (6.18)$$

$$\frac{d\eta_{OH}}{dt} = 2\eta_{O_2}\eta_{H_2}[C]k_5 + \eta_{O_2}\eta_H[C]k_6 + \eta_{H_2}\eta_O[C]k_7 - \eta_{H_2}\eta_{OH}[C]k_8 \quad (6.19)$$

$$\frac{d\eta_{H_2O}}{dt} = -\eta_{H_2O}[C]k_1 + \eta_{H_2}\eta_{OH}[C]k_8 \quad (6.20)$$

$$\frac{d\eta_{O_2}}{dt} = -\eta_{O_2}\eta_{H_2}[C]k_5 - \eta_{O_2}\eta_H[C]k_6 \quad (6.21)$$

$$\frac{d\eta_{H_2}}{dt} = -\eta_{O_2}\eta_{H_2}[C]k_5 - \eta_{H_2}\eta_O[C]k_7 - \eta_{H_2}\eta_{OH}[C]k_8 \quad (6.22)$$

These equations are valid throughout the entire induction zone but at different times different terms predominate. Utilizing these equations it is now proposed to examine the rate of increase of radical concentrations in the early stages of the induction zone as well as in the later stages. The resultant expressions will then be "connected" and an arbitrary definition invoked which will yield an analytical expression for the ignition delay time.

6.3 Initial Rate of Growth of Radical Concentrations.

A Maclaurin series expansion can be written for $\eta_H = \eta_H(t)$ about the point immediately behind the shock wave ($t = 0$). This expansion is;

$$\eta_H(t) = \eta_H(0) + t\,\dot{\eta}_H(0) + \frac{t^2}{2!}\ddot{\eta}_H(0) + \cdots \quad (6.23)$$

where,

$$\dot{\eta}_H = \frac{d\eta_H}{dt} \quad ; \quad \ddot{\eta}_H = \frac{d^2\eta_H}{dt^2} \quad ; \quad \text{etc}$$

For the sake of simplicity, the following definitions are made:

$$a = [C]k_1 \qquad f = \eta_{O_2}[C]k_6$$

$$b = 2\eta_{H_2}[C]k_2 \qquad g = \eta_{H_2}[C]k_7$$

$$c = 2\eta_{O_2}[C]k_3 \qquad h = \eta_{H_2}[C]k_8$$

$$\varepsilon = 2\eta_{O_2}\eta_{H_2}[C]k_5 \qquad i = [C]k_9$$

The rate equations for the radicals then become:

$$\dot{\eta}_H = b - f\eta_H + g\eta_O + h\eta_{OH} \tag{6.24}$$

$$\dot{\eta}_O = c + f\eta_H - g\eta_O + i\eta_{OH}^2 \tag{6.25}$$

$$\dot{\eta}_{OH} = \varepsilon + f\eta_H + g\eta_O - h\eta_{OH} \tag{6.26}$$

$$\dot{\eta}_{H_2O} = -a\eta_{H_2O} + h\eta_{OH} \tag{6.27}$$

The initial conditions, as given in Equation (6.1), are:

$$\eta_H(0) = \eta_O(0) = \eta_{OH}(0) = \eta_{H_2O}(0) = 0$$

The other constants required in Equation (6.23) may be obtained from these conditions and Equations (6.24) - (6.26). They are:

$$\dot{\eta}_H(0) = b \qquad \dot{\eta}_O(0) = c \qquad \dot{\eta}_{OH}(0) = \varepsilon$$

$$\ddot{\eta}_H(0) = -fb + gc + h\varepsilon$$

$$\ddot{\eta}_O(0) = fb - gc$$

$$\ddot{\eta}_{OH}(0) = fb + gc - h\varepsilon \tag{6.28}$$

$$\dddot{\eta}_H(0) = -f(-fb+gc+h\varepsilon) + g(fb-gc) + h(fb+gc-h\varepsilon)$$
$$\dddot{\eta}_O(0) = f(-fb+gc+h\varepsilon) - g(fb-gc) + 2i\varepsilon^2$$
$$\dddot{\eta}_{OH}(0) = f(-fb+gc+h\varepsilon) + g(fb-gc) - h(fb+gc-h\varepsilon)$$

Substitution into (6.23) yields;

$$\eta_H(t) = bt + (-fb+gc+h\varepsilon)\frac{t^2}{2!}$$
$$+\left[-f(-fb+gc+h\varepsilon) + g(fb-gc) + h(fb+gc-h\varepsilon)\right]\frac{t^3}{3!}$$
$$+\left\{\begin{array}{l} -f\left[-f(-fb+gc+h\varepsilon)+g(fb-gc)+h(fb+gc-h\varepsilon)\right] \\ +g\left[f(-fb+gc+h\varepsilon)-g(fb-gc)+2i\varepsilon^2\right] \\ +h\left[f(-fb+gc+h\varepsilon)+g(fb-gc)-h(fb+gc-h\varepsilon)\right] \end{array}\right\}\frac{t^4}{4!}$$
$$+ \cdots +$$

We now consider the order of magnitude of each of the terms of each coefficient. For example,

$$\mathcal{O}\{fb\} = \mathcal{O}\{\eta_{O_2}[c]k_6 \cdot 2\eta_{H_2}[c]k_2\} = \mathcal{O}\{[c]^2 k_2 k_6\} = \{10^4[c]^2 ; 10^{17}[c]^2\}$$

where the first figure refers to a temperature of 1000°K and the second to 2000°K. Similarly,

$$\mathcal{O}\{gc\} = \mathcal{O}\{\eta_{H_2}[c]k_7 \cdot 2\eta_{O_2}[c]k_3\} = \{10^3[c]^2 ; 10^{17}[c]^2\}$$

$$\mathcal{O}\{h\varepsilon\} = \mathcal{O}\{\eta_{H_2}[c]k_8 \cdot 2\eta_{O_2}\eta_{H_2}[c]k_5\} = \{10^{12}[c]^2 ; 10^{20}[c]^2\}$$

Thus,

$$h\varepsilon \gg fb$$
$$h\varepsilon \gg gc$$

A similar analysis for the coefficient of t^3 yields,

$$k^2\varepsilon \gg gfb$$

$$k^2\varepsilon \gg fk\varepsilon$$

$$k^2\varepsilon \gg g^2c$$

For the coefficient of t^4;

$$k^3\varepsilon \gg gi\varepsilon^2$$

$$k^3\varepsilon \gg f^2k\varepsilon$$

$$k^3\varepsilon \gg fg^2b$$

$$k^3\varepsilon \gg g^3c$$

$$k^3\varepsilon \gg fk^2\varepsilon$$

$$k^3\varepsilon \gg fgk\varepsilon$$

Neglecting the small terms, we then have,

$$\eta_H(t) = bt + k\varepsilon\frac{t^2}{2!} - k^2\varepsilon\frac{t^3}{3!} + k^3\varepsilon\frac{t^4}{4!} - \cdots$$

or,

$$\eta_H(t) = bt + \frac{\varepsilon}{k}\left[\frac{(kt)^2}{2!} - \frac{(kt)^3}{3!} + \frac{(kt)^4}{4!} - \cdots\right]$$

This can be written,

$$\eta_H(t) = (b+\varepsilon)t + \frac{\varepsilon}{k}\left[\exp(-kt) - 1\right] \qquad (6.29)$$

provided,

$$\frac{(kt)^5 4!}{(kt)^4 5!} \ll 1$$

That is, if $kt \ll 5$

This is quite a conservative requirement so that actually the relation (6.29) can be expected to hold for greater times than given by this inequality. In identical fashion it can be shown that;

$$\eta_0(t) = ct - gc\frac{t^2}{2!} + fh\varepsilon\frac{t^3}{3!} - fh\varepsilon(g+h)\frac{t^4}{4!} + \cdots \quad (6.30)$$

and

$$\eta_{OH}(t) = \frac{\varepsilon}{h}\left[1 - \exp(-ht)\right] \quad (6.31)$$

or

$$\eta_{OH}(t) = (b+\varepsilon)t - \eta_H \quad (6.32)$$

Also,

$$\eta_{H_2O}(t) = \frac{\varepsilon}{h}\left[ht - 1 + \exp(-ht)\right] \quad (6.33)$$

or

$$\eta_{H_2O}(t) = \eta_H - bt \quad (6.34)$$

We can now obtain a simpler expression for $\eta_0(t)$ by noting that the η_{OH}^2 term in Equation (6.25) for $\dot{\eta}_0$ offers no contribution at small t. Neglecting this term and adding Equations (6.24) and (6.25) yields,

$$\dot{\eta}_0 + \dot{\eta}_H = b + c + h\eta_{OH}$$

Integrating,

$$\eta_0 = (b+c)t + h\int_0^t \eta_{OH}(\xi)\,d\xi - \eta_H$$

Introducing Equations (6.29) and (6.31) this reduces to,

$$\eta_0 = ct \quad (6.35)$$

Writing out the expression for $\eta_H(t)$ we have,

$$\eta_H(t) = \left\{2\eta_{H_2}[C]k_2 + 2\eta_{H_2}\eta_{O_2}[C]k_5\right\}t + \frac{2\eta_{H_2}\eta_{O_2}[C]k_5}{\eta_{H_2}[C]k_6}\left[\exp\left(-\eta_{H_2}[C]k_6 t\right) - 1\right] \quad (6.36)$$

The form of this equation suggests the introduction of a characteristic time of the reaction, t_c, based on the initial hydrogen concentration and fastest reaction rate.

That is,

$$t_c \equiv \frac{1}{\eta_{H_2}[c]k_8} \tag{6.37}$$

This time will obviously be very much shorter than the ignition delay time. Also define a dimensionless time, $t' = \frac{t}{t_c} = \eta_{H_2}[c]k_8 t$. Equation (6.36) then becomes;

$$\eta_H(t') = 2\left(\frac{k_2}{k_8} + \eta_{O_2}\frac{k_5}{k_8}\right)t' + 2\eta_{O_2}\frac{k_5}{k_8}\left(e^{-t'} - 1\right) \tag{6.38}$$

The dimensionless forms of Equations (6.31), (6.33), and (6.35) are;

$$\eta_{OH}(t') = 2\eta_{O_2}\frac{k_5}{k_8}\left[1 - e^{-t'}\right] \tag{6.39}$$

$$\eta_{H_2O}(t') = 2\eta_{O_2}\frac{k_5}{k_8}\left[t' - 1 + e^{-t'}\right] \tag{6.40}$$

$$\eta_O(t') = 2\frac{\eta_{O_2}}{\eta_{H_2}}\cdot\frac{k_3}{k_8}t' \tag{6.41}$$

The inequality, $kt \ll 5$ now becomes,

$$t' \ll 5$$

so that the expansions used are at least good for times satisfying this inequality.

Equations (6.38), (6.39), (6.40), and (6.41) are plotted in Figure 44 for a temperature of 1500°K and for a stoichiometric mixture of hydrogen-oxygen. That is, for the reaction $2H_2 + O_2$ so that $\eta_{H_2} = 2/3$ and $\eta_{O_2} = 1/3$. These results point out some interesting facets of the early stages of the induction period. The formation of hydrogen atoms

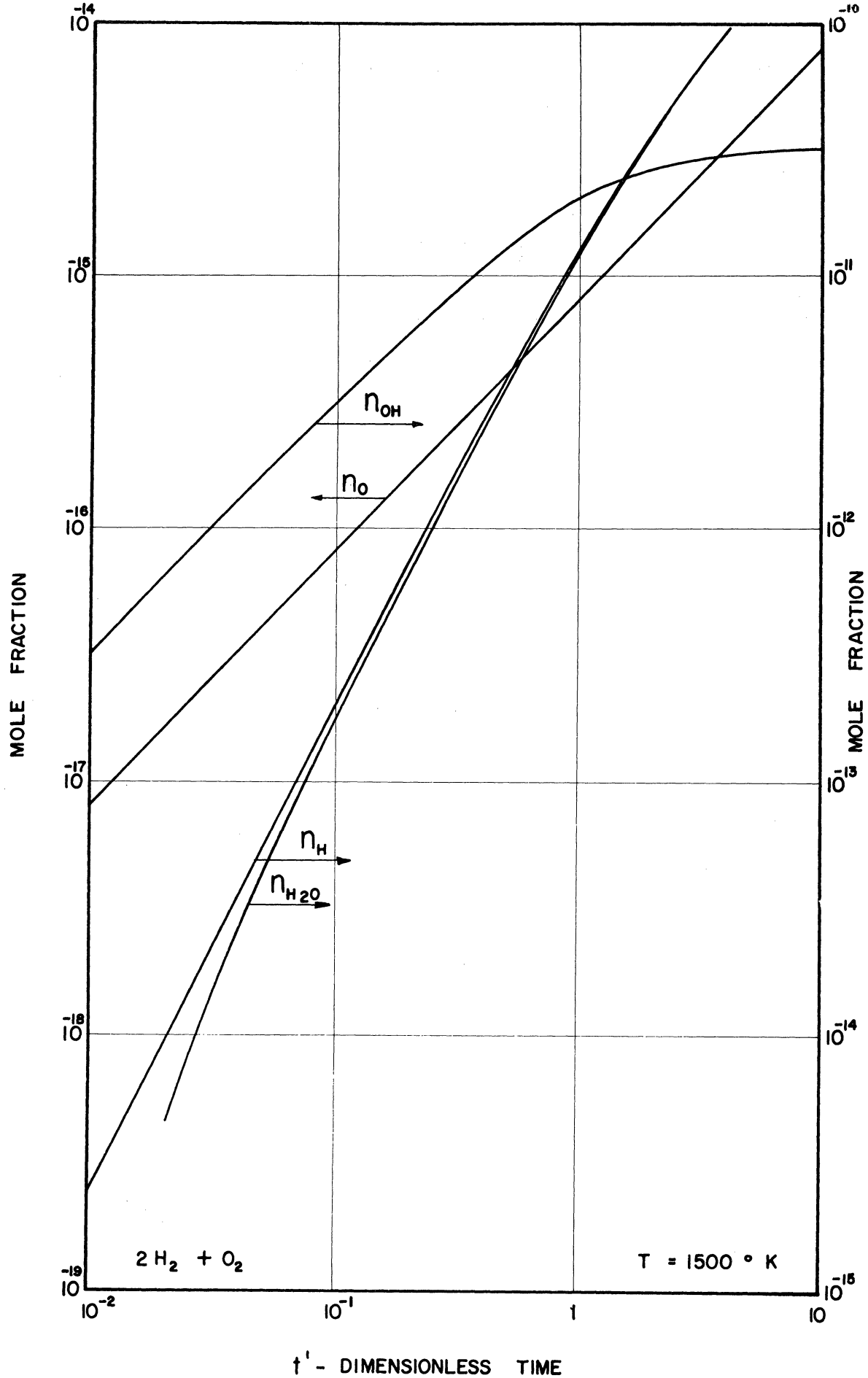

Figure 44. Radical Concentrations in the Early Stages of the Induction Period.

initially depends only on the dissociation of hydrogen but almost instantly the collisions of H_2 and O_2 molecules produce an appreciable OH concentration. The OH reacts extremely rapidly with H_2 $(H_2 + OH \rightarrow H_2O + H)$ so that it soon dominates as the main reaction producing H. Now the reaction, $H_2 + O_2 \rightarrow 2OH$, proceeds much more rapidly than does the dissociation of H_2 so that initially the OH concentration exceeds that of H. However, the reaction mentioned above soon depletes this excess of OH and, as can be seen in the figure, η_H overtakes η_{OH} at about the characteristic time. η_{OH} tends to approach a constant value.

It can also be noted that η_{H_2O} rapidly approaches η_H. This arises from the fact that the kt term in Equation (6.34) rapidly pales into insignificance compared to η_H. In other words the dominating reaction soon becomes that of $H_2 + OH \rightarrow H_2O + H$ which produces H_2O at the same rate as H. It can be further seen that η_O increases very slowly compared to η_H. This arises from the fact that as fast as O is produced by the $H + O_2 \rightarrow OH + O$ reaction, it is consumed almost equally as fast by the $H_2 + O \rightarrow OH + H$ reaction. Thus the only effective production of O in the early stages is due to the dissociation of oxygen, a process which is relatively leisurely at the temperatures considered here.

The time rates of change of η_H and η_{OH} can be readily obtained from Equations (6.29) and (6.31) and are;

$$\dot{\eta}_H(t') = \frac{b}{k} + \frac{\varepsilon}{k}\left(1 - e^{-t'}\right)$$

or,

$$k\dot{\eta}_H(t') = 2\eta_{H_2}[c]k_2 + 2\eta_{H_2}\eta_{O_2}[c]k_5\left(1 - e^{-t'}\right) \qquad (6.42)$$

and,

$$\dot{n}_{OH}(t') = \frac{\varepsilon}{h} e^{-t'}$$

or,

$$h\dot{n}_{OH}(t') = 2 n_{H_2} n_{O_2} [c] k_5 e^{-t'} \tag{6.43}$$

These equations are plotted in Figure 45 for the same conditions as before. It is seen that $\dot{n}_H$ approaches an asymptotic value of $\left(\frac{b+\varepsilon}{h}\right)$ while $\dot{n}_{OH}$ tends toward zero. Also, $\dot{n}_{OH}$ falls below $\dot{n}_H$ at about the characteristic time.

While all of the above numerical results apply only to a stoichiometric hydrogen-oxygen mixture, the general trends are indicative of those for any hydrogen-oxygen inert mixture provided n_{H_2} and n_{O_2} do not differ by orders of magnitude from the values used.

6.4 Rate of Increase of Radicals in the Later Stages of the Induction Zone.

The rate equations which hold throughout the induction zone are given by Equations (6.17) - (6.22). However, in the later stages of the induction zone, these equations can be further simplified. During the initiation period, small but all important concentrations of H, OH and O were generated. These concentrations serve to establish the action of the chain,

$$\begin{aligned} O_2 + H &\xrightarrow{k_6} OH + O \\ H_2 + O &\xrightarrow{k_7} OH + H \\ H_2 + OH &\xrightarrow{k_8} H_2O + H \end{aligned} \tag{6.44}$$

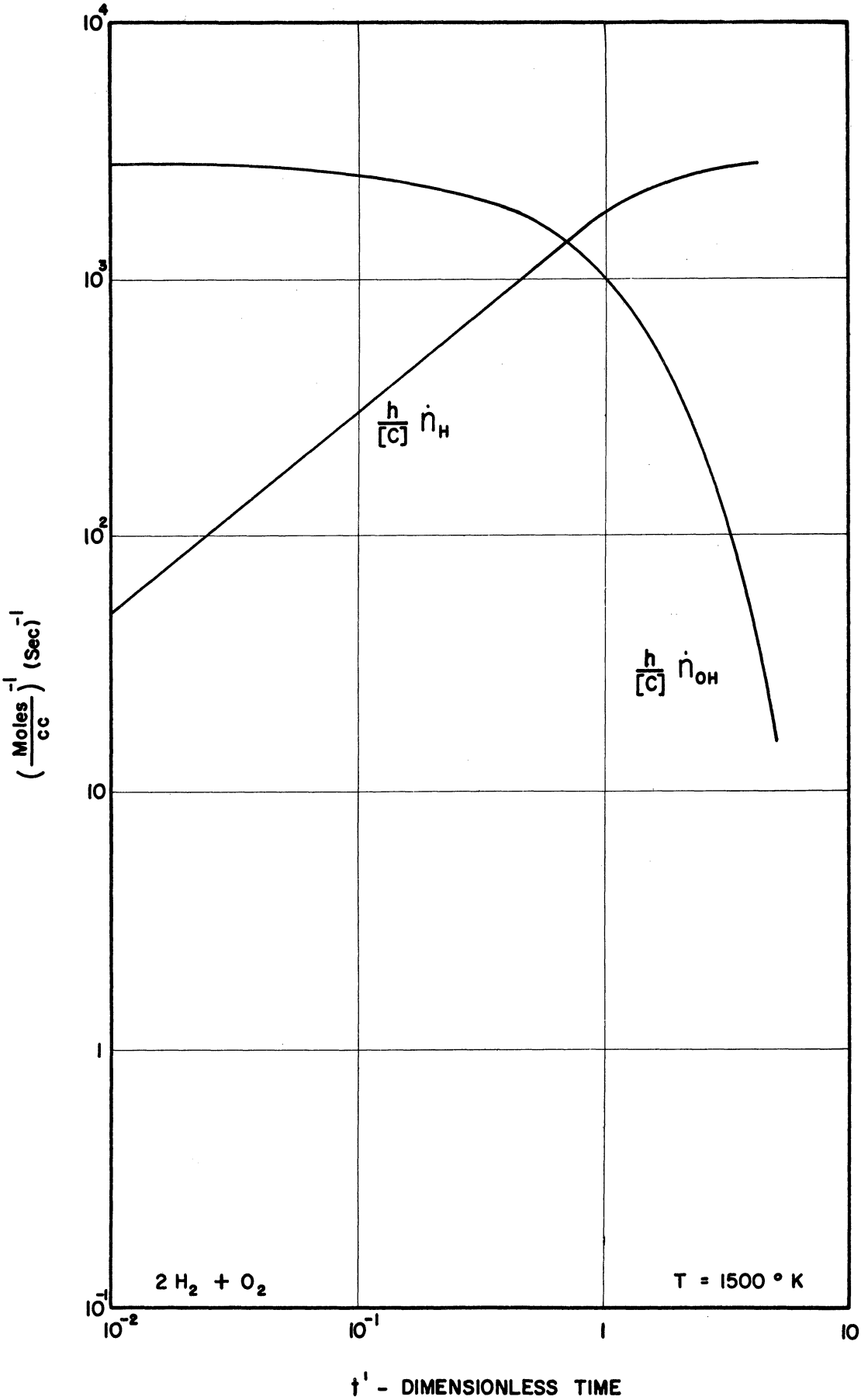

Figure 45. Rate of Growth of Radical Concentrations in the Early Stages of the Induction Period.

inasmuch as values of the rate constants k_6, k_7, and k_8 are very high (refer to Table V). The reaction, $2OH \xrightarrow{k_9} H_2O + O$ does not play a major role even though $k_7 = k_9$. This arises from the fact that the relatively large population of hydrogen molecules, as compared to the radical, allows reaction VIII to dominate in utilizing OH. The reactions VI and VII are the chain branching reactions while VIII is a chain propagating step. Noting that $k_8 > k_7$, and $k_8 > k_6$, it is reasonable to expect that the OH concentration will be at essentially steady state due to the action of the chain. Then the stoichiometry of the chain is,

$$3H_2 + O_2 \rightarrow 2H_2O + 2H \tag{6.45}$$

which predicts that H_2O will be formed at the same rate as is H. This is in agreement with the behavior at extremely small times as was seen earlier (Equation 6.34).

The importance of this chain is also indicated by looking at the order of magnitude of the terms in the rate expressions. That is, if we concern ourselves with value of $n_H \gg \frac{k_2}{k_6}$, $n_O \gg \frac{k_2}{k_7}$, and $n_{OH} \gg \frac{k_2}{k_8}$, then the dissociation term in the equation for $\dot{n}_H$ (Equation 6.17) becomes negligible. Similarly, we can neglect the dissociation terms in the other rate equations as well as the term, $2 n_{O_2} n_{H_2} [C] k_5$, if equivalent order conditions are satisfied. Finally, we retain only those terms of the terms of the rate equations which are of the order of $\dot{n}_H$.

The resultant equations are then;

$$\dot{n}_H = - n_{O_2} n_H [C] k_6 + n_{H_2} n_O [C] k_7 + n_{H_2} n_{OH} [C] k_8 \tag{6.46}$$

$$\dot{n}_O = n_{O_2} n_H [C] k_6 - n_{H_2} n_O [C] k_7 \tag{6.47}$$

$$\dot{n}_{OH} = n_{O_2} n_H [C] k_6 + n_{H_2} n_O [C] k_7 - n_{H_2} n_{OH} [C] k_8 \tag{6.48}$$

$$\dot{n}_{H_2O} = n_{H_2} n_{OH} [C] k_8 \tag{6.49}$$

$$\dot{n}_{O_2} = - n_{O_2} n_H [C] k_6 \tag{6.50}$$

$$\dot{n}_{H_2} = - n_{H_2} n_O [C] k_7 - n_{H_2} n_{OH} [C] k_8 \tag{6.51}$$

As is seen, the only remaining terms are those resulting from the action of the chain.

Applying the condition previously found that $\dot{n}_{H_2O} = \dot{n}_H$ yields,

$$n_{O_2} n_H [C] k_6 = n_{H_2} n_O [C] k_7 \tag{6.52}$$

This indicates that $\dot{n}_O = 0$; that is to say,

$$\dot{n}_O << \dot{n}_H$$

Also,

$$\dot{n}_{OH} = 2 n_{O_2} n_H [C] k_6 - n_{H_2} n_{OH} [C] k_8 \tag{6.53}$$

It was argued qualitatively above that there could be no rapid buildup of OH because it serves as the chain carrier. Furthermore, it was noted in the last section that the ratio, $\dot{n}_H / \dot{n}_{OH}$, rose to unity at extremely short times and continued to increase beyond that time. Consequently, we have;

$$\dot{n}_{OH} << \dot{n}_H$$

so that,

$$\dot{n}_{OH} = 0 = 2 n_{O_2} n_H [C] k_6 - n_{H_2} n_{OH} [C] k_8$$

or

$$n_{H_2} n_{OH} [C] k_8 = 2 n_{O_2} n_H [C] k_6 \tag{6.54}$$

In view of (6.52) and (6.54), Equation (6.46) becomes,

$$\dot{n}_H = 2 n_{O_2} n_H [C] k_6 \tag{6.55}$$

Integrating, $(n_{O_2} = \text{const.})$,

$$n_H(t) = K e^{2 n_{O_2} [C] k_6 t} \tag{6.56}$$

where K is the constant of integration. This constant is evaluated in the next section. Referring back to Equation (6.54) we see that,

$$n_{OH}(t) = 2 \frac{n_{O_2}}{n_{H_2}} \frac{k_6}{k_8} n_H = 2 \frac{n_{O_2}}{n_{H_2}} \frac{k_6}{k_8} K e^{2 n_{O_2} [C] k_6 t} \tag{6.57}$$

Thus we see that both n_H and n_{OH} increase exponentially in the later stages of the induction zone. This does not negate the condition $\dot{n}_{OH} = 0$ which merely implied that $\dot{n}_{OH} \ll \dot{n}_H$. In order to verify this inequality we differentiate (6.56) and (6.57) and take the ratio of the results. That is,

$$\frac{\dot{n}_{OH}}{\dot{n}_H} = 2 \frac{n_{O_2}}{n_{H_2}} \frac{k_6}{k_8} \simeq \frac{k_6}{k_8} \simeq 10^{-3}$$

which substantiates the arguments presented.

6.5 Complete Description of the Generation of Hydrogen Atoms.

The results of the last two sections may now be utilized to effect the integration of the rate equations throughout the entire induction period. Attention will be placed primarily on the rate of growth of the hydrogen atom concentration. Now in the very early stages of the induction period it was found that,

$$n_{H_2 O} = n_H - k t \tag{6.34}$$

It was pointed out that the "bt" term soon became insignificant and then, for all purposes, $n_{H_2O} = n_H$. Further, it was shown that this was also true in the later stages of the induction period. In other words the relation (6.34) is valid <u>throughout</u> the induction zone and represents the needed link that allows integration of the rate equation for the hydrogen atoms.

Differentiating (6.34) yields,

$$\dot{n}_{H_2O} = \dot{n}_H - b \tag{6.58}$$

Substituting Equations (6.24) and (6.27) into this relation (neglecting the first term in the $\dot{n}_{H_2O}$ expression as it was found to be small), we find,

$$\dot{n}_{H_2O} = k\, n_{OH} = \dot{n}_H - b = -f\, n_H + g\, n_O + k\, n_{OH} \tag{6.59}$$

This gives,

$$f\, n_H = g\, n_O \tag{6.60}$$

Previously this was found to be true only in the later stages but now we find that it holds for all t. For the temperature range of interest here and $n_{O_2}/n_{H_2} \simeq 1$ this infers that $n_O << n_H$.

Equation (6.24) now reduces to,

$$\dot{n}_H = b + k\, n_{OH} \tag{6.61}$$

and (6.26) is,

$$\dot{n}_{OH} = \varepsilon + 2f\, n_H - k\, n_{OH} \tag{6.62}$$

Differentiating (6.61) and combining the results with (6.62) leads to the following linear second order differential equation;

$$\ddot{n}_H + k\, \dot{n}_H - 2fk\, n_H = (\varepsilon + b)k \tag{6.63}$$

The solution is.

$$n_H = C_1 \exp\left(-\frac{k}{2} + \frac{k}{2}\sqrt{1 + \frac{8f}{k}}\right)t \tag{6.64}$$

$$+ C_2 \exp\left(-\frac{k}{2} - \frac{k}{2}\sqrt{1 + \frac{8f}{k}}\right)t \; - \frac{\varepsilon + b}{2f}$$

The constants may be determined by requiring the initial conditions to be satisfied. That is,

$$\text{at} \quad t=0, \quad \eta_H = 0 \quad ; \quad \text{at} \quad t=0, \quad \dot{\eta}_H = b$$

The resultant expression is,

$$\eta_H = \frac{\varepsilon+b}{4f}\left[\left(1+\frac{\rho f}{k}\right)^{-1/2}+1\right]\exp\left[-\frac{k}{2}+\frac{k}{2}\left(1+\frac{\rho f}{k}\right)^{1/2}\right]t$$
$$+\left\{\frac{\varepsilon+b}{2f}-\frac{\varepsilon+b}{4f}\left[\left(1+\frac{\rho f}{k}\right)^{-1/2}+1\right]\right\}\exp\left[-\frac{k}{2}-\frac{k}{2}\left(1+\frac{\rho f}{k}\right)^{1/2}\right]t$$
$$-\frac{\varepsilon+b}{2f} \qquad (6.65)$$

This expression is valid throughout the induction zone. The only limitations on Equation (6.65) arise from the inequalities used in deriving the expression, $\eta_{H_2 0} = \eta_H - bt$ and the steady state approximation on η_{OH}. These inequalities will be valid as long as η_{O_2} and η_{H_2} do not differ by orders of magnitude. One other assumption implicitly used was that η_{O_2} and η_{H_2} were constant throughout the induction period. This leads to negligible differences except for the very last portion of the delay zone. The resultant effect on the ignition time delay is very small as will be brought out later.

Equation (6.65) can be considerably simplified when we note that $\varepsilon >> b$ and $\frac{\rho f}{k} << 1$. Consequently,

$$\eta_H \cong \frac{\varepsilon}{2f} e^{2ft} + \frac{\varepsilon}{k} e^{-kt} - \frac{\varepsilon}{2f} \qquad (6.66)$$

This equation is not valid near $t = 0$ but becomes a good approximation for $t' \geq 10$. It is very adequate for predicting the ignition time delay. Further simplification may be effected by examining the ratio, R;

$$R = \frac{\frac{\varepsilon}{2f}\left(e^{2ft}-1\right)}{\frac{\varepsilon}{k}e^{-kt}} = \frac{k}{2f}e^{t'}\left(e^{\frac{2f}{k}t'}-1\right)$$

$$= \frac{k}{2f} e^{t'} \left[\frac{2f}{k} t' + \frac{\left(\frac{2f}{k} t'\right)^2}{2!} + \cdots \right]$$

$$= e^{t'} \left(t' + \cdots \right)$$

Hence,

$$R >> 1 \quad \text{if} \quad t' >> 1$$

Equation (6.66) can now be written,

$$n_H = \frac{\varepsilon}{2f} \left(e^{2ft} - 1 \right) \qquad t' \geq 10 \qquad (6.67)$$

Thus we see that after $t' \geq 10$ the only appreciable production of H arises from the action of the chain. At this point one cannot justify dropping the constant, $-\frac{\varepsilon}{2f}$, although it will turn out that it has negligible effect on delay time.

6.6 Ignition Time Delay.

It is now necessary to define a time, τ, which is characteristic of the ignition delay. Once a sufficient number of hydrogen atoms have been produced (late in the induction period), the various reactions occur rapidly and exothermally to the degree that the temperature begins to increase. This increases the reaction rate exponentially so that the temperature soon increases exponentially. Thus the "flame" is established shortly thereafter. It would appear logical then to define τ as the time required for n_H to attain some suitably high value, λ. The expression for ignition time delay can then be written directly for Equation (6.67). That is, from Equation (6.67)

$$\tau = \frac{1}{2f} \ln \left(\frac{2f}{\varepsilon} \lambda + 1 \right) \qquad (6.68)$$

In order to evaluate λ precisely, one would have to consider the rate equations and hydrodynamics simultaneously with the heats of reaction taken into account. In the case at hand, however, this complexity is not necessary for the reasons described above. Many equally valid criteria may be proposed for ascertaining λ, all of which lead to essentially the same value of τ. However it would appear consistent to arrive at a criteria based on the rate controlling reaction, $H + O_2 \xrightarrow{k_6} OH + O$.

For the late stages we had,

$$\dot{\eta}_H = 2\eta_{O_2}\eta_H[C]k_6 \tag{6.55}$$

Now in the very late stages of the induction zone η_{O_2} begins to drop off in accordance with Equation (6.50) which is,

$$\dot{\eta}_{O_2} = -\eta_{O_2}\eta_H[C]k_6 = -\tfrac{1}{2}\dot{\eta}_H \tag{6.69}$$

Integrating,

$$\eta_{O_2} - (\eta_{O_2})_0 = -\tfrac{1}{2}\eta_H \tag{6.70}$$

Differentiating (6.55),

$$\ddot{\eta}_H = 2\eta_{O_2}\dot{\eta}_H[C]k_6 + 2\dot{\eta}_{O_2}\eta_H[C]k_6 \tag{6.71}$$

Substituting (6.69) and (6.70) into (6.71) yields,

$$\ddot{\eta}_H = 2(\eta_{O_2})_0\dot{\eta}_H[C]k_6 - 2\eta_H\dot{\eta}_H[C]k_6 \tag{6.72}$$

Let us now arbitrarily say that λ will be that value of η_H corresponding to the inflection point in the η_H versus t curve. That is, where $\ddot{\eta}_H = 0$. From (6.72) we than obtain,

$$(\eta_H)_\tau = \lambda = (\eta_{O_2})_0 \tag{6.73}$$

This λ then defines a time characteristic of the ignition delay in a manner independent of the particular initial concentrations employed. As

seen, the actual value of λ is based on an initial concentration. Comparison of this criteria with the numerical results of Duff [42] reveal very good agreement with the prediction of time delay although the value of $(\eta_H)_\tau$ is somewhat beyond the extent of the η_H versus t curve.

Substituting for λ in (6.68) we have,

$$\tau = \frac{1}{2f} \ln\left(\frac{2f}{\varepsilon}\eta_{O_2} + 1\right)$$

where the subscript on η_{O_2} has been dropped but it is to be understood that it represents the initial mole fraction. Now $\frac{2f}{\varepsilon}\eta_{O_2} \gg 1$ so that,

$$\tau = \frac{1}{2f} \ln\left(\frac{2f}{\varepsilon}\eta_{O_2}\right) \tag{6.74}$$

or finally,

$$\tau = \frac{1}{2\eta_{O_2}[C]k_6} \ln\left(\frac{\eta_{O_2}}{\eta_{H_2}} \cdot \frac{k_6}{k_5}\right) \tag{6.75}$$

The log term in (6.75) has only slight influence on τ. Thus we see that the ignition time delay is dependent almost solely on the action of the chain! That is, the time required for the initiation processes to start the chain is negligible.

We can rewrite the equation, noting that $[C] = \frac{P}{RT}$, as

$$\tau = \frac{RT}{2\eta_{O_2}PA_6} e^{E_6/RT} \ln\left(\frac{\eta_{O_2}}{\eta_{H_2}} \cdot \frac{k_6}{k_5}\right) \tag{6.76}$$

The following conclusions can be drawn:

a) $\ln\tau$ is approximately proportional to reciprocal temperature wherein the slope is indicative of the activation energy of the $H + O_2$ reaction.

b) τ is inversely proportional to pressure.

c) τ is approximately inversely proportional to the initial mole fraction of oxygen.

d) τ is weakly sensitive to η_{O_2}/η_{H_2}.

e) τ is independent of the particular inert gas, being dependent only on the mole fraction of inert present.

Equation (6.76) is plotted in Figure 46 for both a stoichiometric hydrogen-oxygen and stoichiometric hydrogen-air mixture at one atmosphere. The values of k_6 were taken as those corresponding to k_{6b} in Table IV. A curve is also included for the hydrogen-oxygen mixture with $k_6 = k_{6a}$. As can be seen, the hydrogen-oxygen mixtures involve shorter time delays for the same value of the rate constant. This is due entirely to the difference in η_{O_2}. The curve for a rate constant k_{6a} gives longer delays because $k_{6a} < k_{6b}$. Also the slope is different corresponding to the difference in activation energy.

The assumption was made throughout most of the analysis that η_{O_2} could be taken as a constant. This can be justified through use of Equations (6.55) and (6.70) and the ignition delay criteria. This refinement leads to very little change in the predicted time delay. Similar statements can be made and proven for the constancy of η_{H_2}.

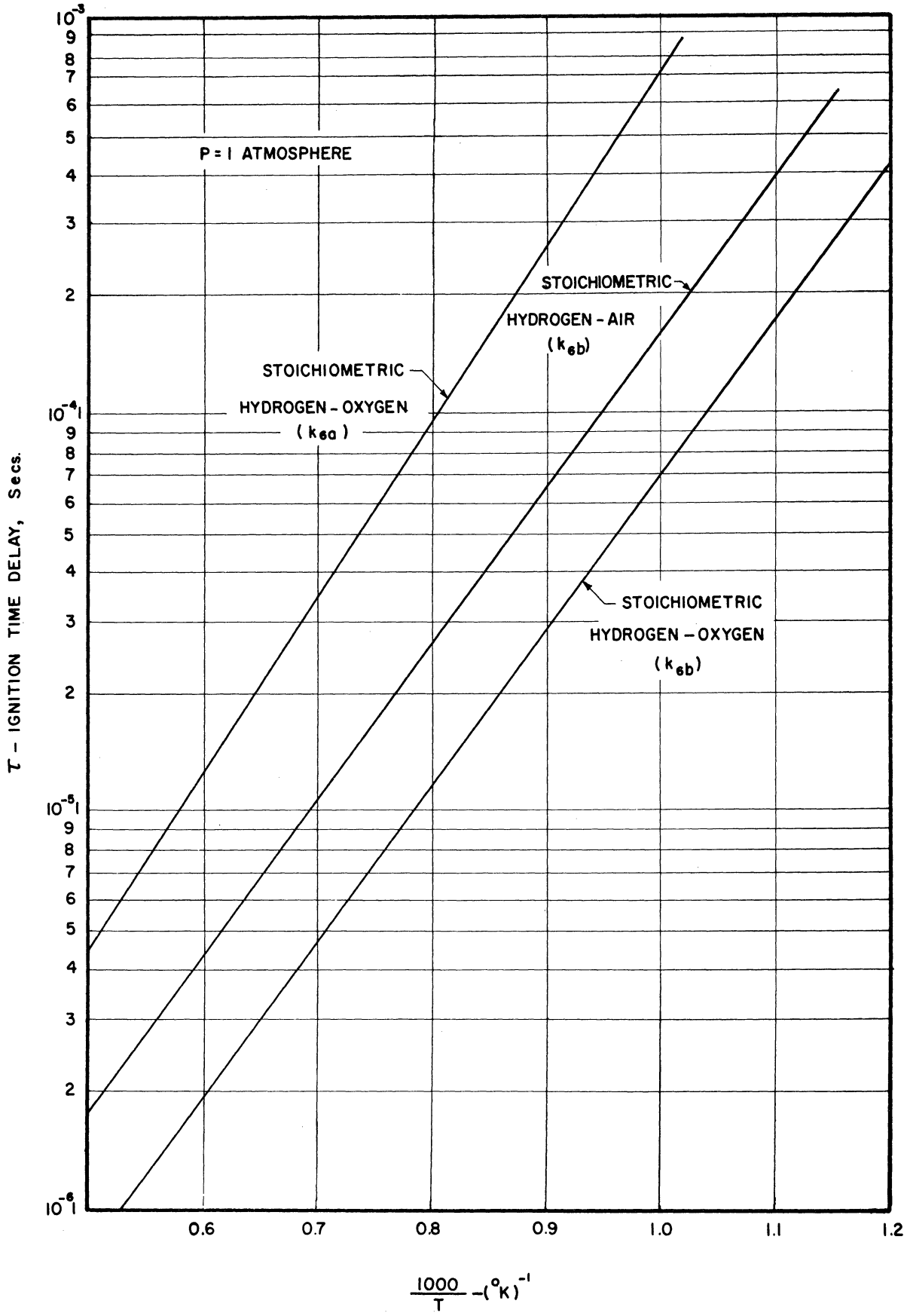

Figure 46. Ignition Time Delay for Hydrogen-Oxygen and Hydrogen-Air Mixtures at Different Temperature.

VII DISCUSSION OF RESULTS

7.1 Identification of the Shock-Combustion Configuration.

The experimental results described earlier showed that the stabilized shock wave-combustion zone configurations observed could be divided into three broad classifications. First there were those cases where combustion occurred within the nozzle and no ignition time delay was observed. These cases do not represent a "clean" experiment. That is, there is some partial combustion upstream of the shock so that the gas composition is no longer pure hydrogen-air. Also, there would undoubtedly be further combustion downstream of the shock. With the details of the combustion unknown it would appear hopeless, at least at this point, to be able to identify the wave as a type of detonation. Consequently no further attention will be given to this mode.

The second type experienced was a stable shock wave-combustion zone phenomenon wherein the initiation of combustion, after establishment of the shock, revealed no interaction with the shock. In these cases there has always been a very distinct separation between shock and combustion. The third type is identical to the second except that the initiation of combustion was observed to drive the shock upstream to a new lower Mach number. As indicated earlier this type was only observed at higher operating temperatures.

The question then naturally arises as to whether any of the above can rightfully be considered stable gaseous detonation waves and if they can, how should they be classified? At this point it is well to recall that detonation waves are classified as strong, weak, or Chapman-Jouguet on the basis of a one-dimensional constant area model. In

accordance with this model it is possible to predict for a given strength wave the Mach number at which a wave should propagate for some temperature and pressure, as well as the corresponding pressure and temperature ratios across the wave. In particular one then knows the stagnation temperature for the wave. Then if the standing detonation wave is to be classified as to strength it must satisfy all of the ratios across the wave as would exist for a moving wave of the same strength and it must be amenable to one-dimensional treatment. Let us consider, then, the case of a C-J detonation wave moving at a Mach number, M_{C-J}, into a free stream at temperature, T_1. Then the stagnation temperature , T_s can be given by:

$$\frac{T_s}{T_1} = 1 + \frac{\gamma-1}{2} M_{C-J}^2$$

But for C-J detonation, $M_{C-J}^2 = C/T_1$, where C is a constant. Therefore,

$$T_s = \frac{C}{M_{C-J}^2} + \left(\frac{\gamma-1}{2}\right) C \qquad (7.1)$$

and it can be seen that a lower stagnation temperature is predicted for high Mach number C-J detonation (low static temperatures) than is required at low Mach numbers (high static temperature). A plot of this equation is shown in Figure 47 for both a stoichiometric and a lean mixture of hydrogen-air. The value of C is determined from the known experimental or computed value of M_{C-J} at $T_1 = 520°R$ (refer to Figure 4). Similar curves could be drawn for F = const > 1 (strong detonation) and these curves would lie above the C-J curve shown for any given fuel-air ratio. Now it is very interesting that the experimental data obtained wherein there was no evidence of interaction between the shock and combustion corresponds to

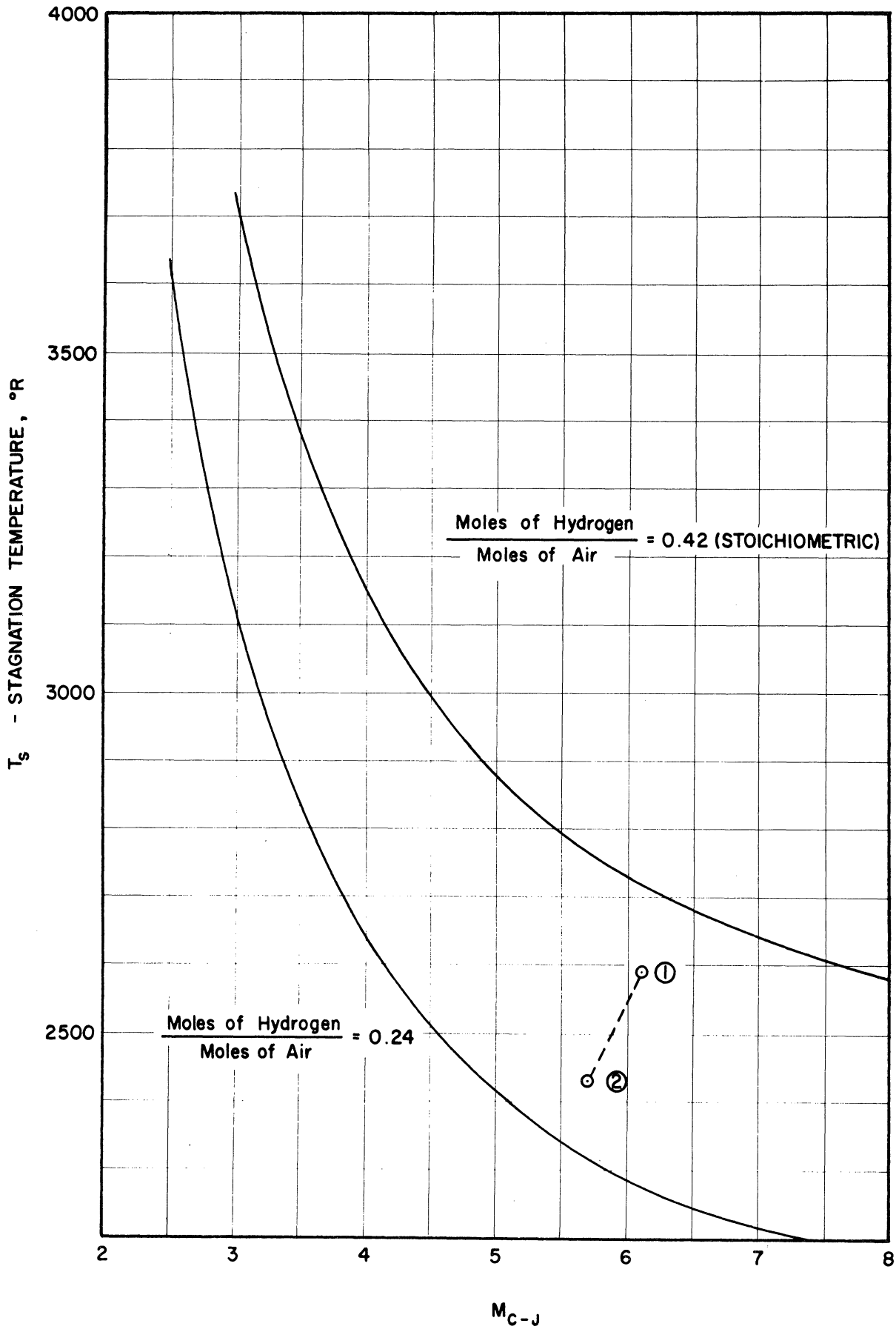

Figure 47. Stagnation Temperature for Chapman-Jouguet-Detonation.

operating conditions below the appropriate fuel-air ratio curve of Figure 47. In contrast, the experimental run described earlier where there was an observed interaction corresponded to an operating condition above the appropriate curve. On one run the Mach number into the shock, prior to any hydrogen addition, was 6.1 and the stagnation temperature of the air about 2590°R. This corresponds to point (1) in the figure. With the establishment of stable combustion at a mixture ratio of 0.24 moles of hydrogen per mole of air, the wave moved upstream to a Mach number of 5.7 (point 2); the stagnation temperature dropping to about 2430°R because of the mixing loss. As can be seen, this final point lies reasonably close to the C-J curve when we consider the possible experimental errors. It is concluded that such waves are actually stabilized detonation waves and probably of the C-J type although the possibility of a strong detonation cannot be ruled out.

Some reservations must be made as far as strength is concerned because of the non-constancy of the stream tube area. This arises from the slope of the slip lines at the Mach reflection. The usual effect of this is to cause an acceleration of the subsonic flow downstream of the shock, although with combustion superimposed it is difficult to say just what the details of the flow are. The effect will be minimized when the characteristic length of the reaction zone is small compared to a characteristic length of the flow field; the logical choice for this latter length being the diameter of the Mach disc. Consequently the situation becomes more favorable at higher temperatures in that the reaction length decreases exponentially with temperature.

To date, it is uncertain whether or not strong detonation waves have been stabilized in this experimental facility. The difficulty lies in the limited accuracy of the experimental measurements and an incomplete knowledge of the combustion region. It is felt that the existence of strong waves is not precluded on the grounds of stability but is only a question of proper boundary conditions. Gross [43, 44] has reported on the attainment of stable strong detonations in the test section of a supersonic combustion tunnel. His combustion process is generated by a Mach disc which is established in the center of the stream by the reflection of shocks from two wedges which are located on opposite walls. A diffuser is located downstream so that the test section is effectively isolated from atmospheric pressure. This is not the case with the open jet. Again it is difficult to classify these waves, not only because of the reasons mentioned above but also because of the very non-uniform fuel-air ratio across the Mach disc in Gross' case. Consequently there is a considerable difference in heat release along neighboring streamlines and each portion of the wave is at a different Mach number because of the difference in molecular weight. With these great changes across the disc one wonders if it is still valid to talk about one-dimensional constant area comparisons. Apparently there are still many questions unanswered in this regard.

7.2 Comparison of the Ignition Time Delay Analysis with Experimental Results and Other Analyses.

Until relatively recently no ignition time delay measurements for hydrogen-oxygen mixtures in the 1000°K - 2000°K temperature range had

been made because of the extremely short times involved. With the advent of the shock tube and short response time instrumentation, a new tool became available capable of providing results in the range mentioned. Steinberg and Kaskan [45] utilized the shock tube to study the time delay of a stoichiometric mixture of hydrogen and oxygen at the low end of this temperature range. Their technique consisted of reflecting a shock wave from the closed end of the tube and then noting the time to the first indication of combustion as detected by a photocell. By virtue of this technique different temperatures were obtained at different pressure levels behind the shock even though the initial charge pressure was maintained a constant. Consequently the concentration (moles/cc) behind the shock varied for every different temperature. Steinberg obtained results for two initial pressure levels but because of considerable scatter reported the results as one best-fit equation holding for all of the runs. Their "average" equation is plotted in Figure 48 *. In order to compare theory with these results it was necessary to take the average concentration at each temperature corresponding to the two pressure levels. The theoretical curve calculated from Equation (6.75) is included in Figure 48 for comparison where $k_6 = k_{6b}$. Because of the averaging procedure necessitated, it is difficult to draw conclusions as to the reasons for the comparatively small discrepancy between experiment and theory. It might be noted that the slope of the theoretical curve is almost parallel to the experimental curve. This is some evidence for the validity of the activation energy 1.8×10^4 cal/mole. Another fact worth noting is that the experimental curve exceeds the theoretical curve by a constant ratio of about 2. More attention will be

---

* Steinberg and Kaskan's equation (1), page 668 of the Fifth Symposium, obviously contains an error in the value of the constant. Instead of this being 3.4×10^{-4}, it should be approximately 2.35×10^{-4} in order to be consistent with his curve of Fig. 3. The latter value has been used plotting his data.

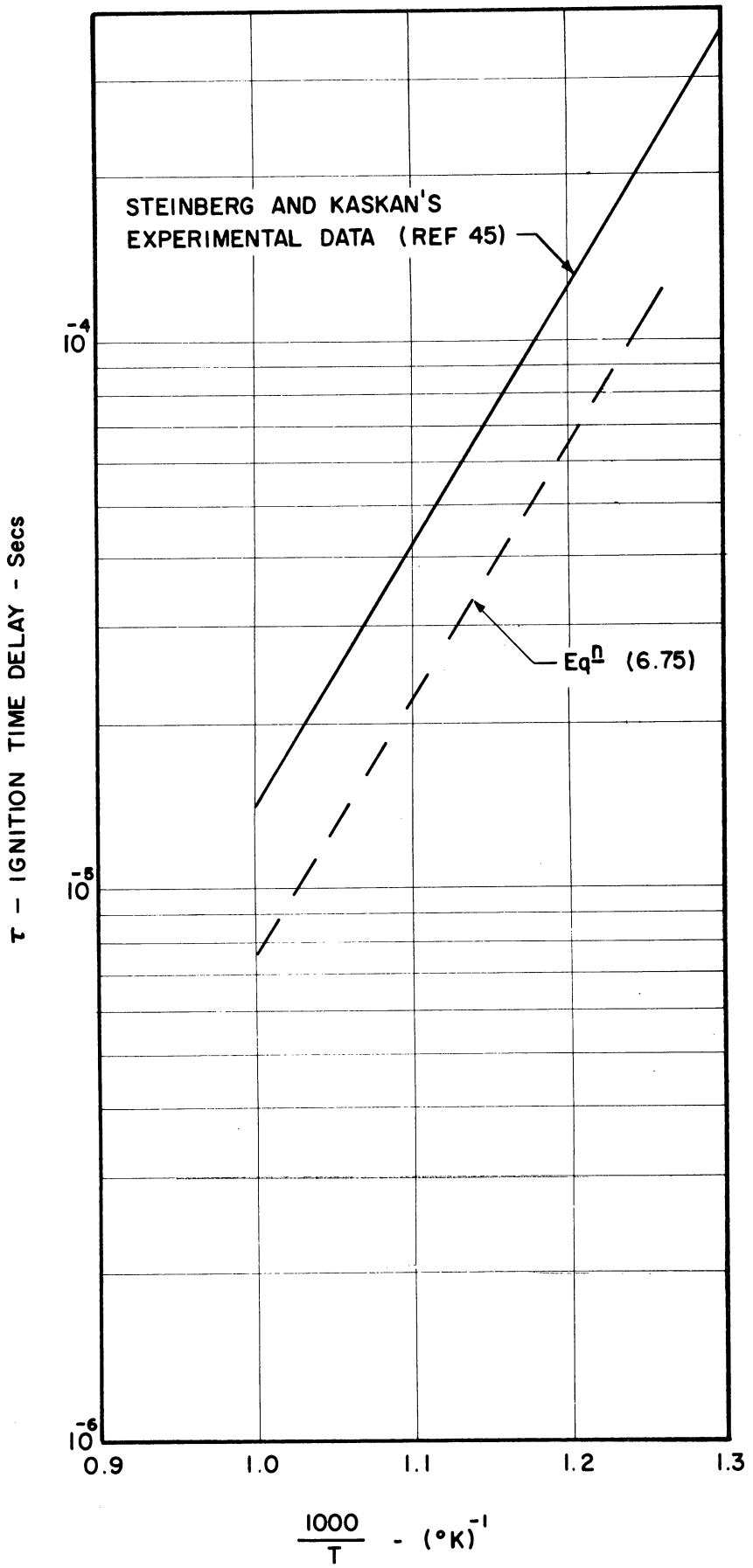

Figure 48. Comparison of Theory with the Experimental Data of Reference 45.

given to this later after the discussion of other results. The results also indicate that the theoretical analysis retains its accuracy to temperatures as low as T = 770°K whereas some of the simplifications used in the theoretical analysis began to break down around 1000°K.

Duff's work [42] has been cited earlier and was drawn upon heavily as a guide in the present study. His detailed calculations for a $2H_2 + O_2 + Xe$ mixture at a temperature of 1737°K and a pressure of 1.15 atmospheres led to a value of about 2.1 μ secs for the delay time, taking this at the inflection point of the temperature curve. The theoretical calculation by use of Equation (6.75) predicts a lag of 1.8 μ secs. This agreement is considered quite good.

Many experiments have been run in connection with the present work wherein ignition time delays in the temperature range of interest were measured in a steady flow system. These results were tabulated in Table II. Inasmuch as each of these runs are at varying fuel-air ratio and since the predominant effect of fuel-air ratio arises from the initial oxygen concentration, it is well to consider $\eta_{O_2}[C]\tau = [O_2]\tau$ vs. $1/T$. In this way the differences in fuel-air ratio from run to run can be almost entirely masked and hence better comparison with theory obtained. The resultant values of $[O_2]\tau$ for the experimental runs of Table II are listed in Table VI. These results are plotted in Figure 49 along with a plot of Equation (6.75) where $k_6 = k_{6_f}$. The experimental values are all seen to be smaller than the theoretical prediction. A number of effects can contribute to this difference. Experimentally, errors are incurred in the measurement of temperature, delay distances, and fuel-air ratio. Further

TABLE VI

EXPERIMENTAL IGNITION DELAY RESULTS, HYDROGEN-AIR

Run No.	η_{H_2}	η_{O_2}	T °R	τ secs.	$[O_2]\tau$ $\frac{\text{moles}}{\text{cc}}$ - secs.	$\frac{1000}{T}$ $(°K)^{-1}$
31	.228	.162	2360	10.27×10^{-6}	2.025×10^{-11}	.763
33	.271	.153	2260	11.27×10^{-6}	2.19×10^{-11}	.796
34	.347	.137	2158	17.71×10^{-6}	3.235×10^{-11}	.834
37	.264	.155	2150	19.97×10^{-6}	4.13×10^{-11}	.8375
47	.463	.113	1995	7.75×10^{-6}	1.261×10^{-11}	.902
65	.316	.144	1800	39.4×10^{-6}	9.07×10^{-11}	1.0
72	.329	.141	1955	18.75×10^{-6}	3.885×10^{-11}	.921
81	.157	.177	1786	30.3×10^{-6}	8.65×10^{-11}	1.01
82	.485	.108	1880	14.25×10^{-6}	2.35×10^{-11}	.957
87	.319	.143	1915	27.2×10^{-6}	5.84×10^{-11}	.94
88	.267	.154	1950	26.8×10^{-6}	6.08×10^{-11}	.923
89	.225	.163	1975	25.95×10^{-6}	6.16×10^{-11}	.911
91	.161	.176	2030	25.22×10^{-6}	6.28×10^{-11}	.898
93	.106	.188	2065	24.95×10^{-6}	6.53×10^{-11}	.872
94	.183	.172	2015	24.1×10^{-6}	5.91×10^{-11}	.894
97	.293	.149	1855	33.0×10^{-6}	7.62×10^{-11}	.97
98	.242	.159	1838	35.5×10^{-6}	8.84×10^{-11}	.978
99	.204	.167	1852	49.0×10^{-6}	1.269×10^{-10}	.972

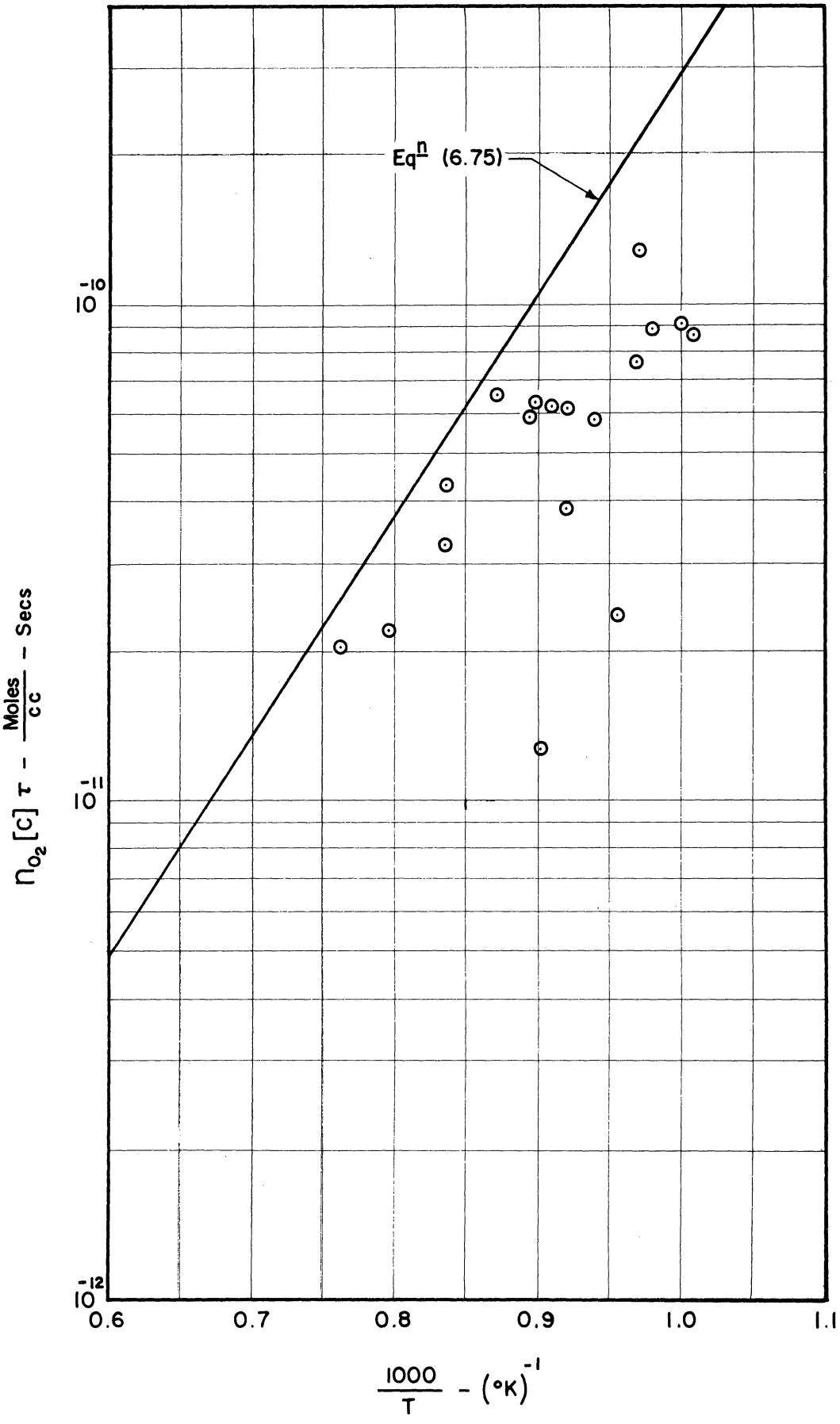

Figure 49. Comparison of Theoretical and Experimental Time Delays; Hydrogen-Air.

errors undoubtedly arise in the method of reducing the data. One hint as to a source of some discrepancy might be gained from the two worst points, runs 47 and 82. These two runs represent the two richest mixtures and thus suggest that the method of correcting the total temperature for mixing losses is subject to appreciable error at mixture ratios far removed from the calibration mixture ratio. No consistent error in this regard has been found however. It should be noted that an error in the temperature of 30°K can have a relatively appreciable effect on the data. For instance, with an error of $\pm$ 30°K in the neighborhood of 1110°K ($\frac{1000}{T} = 0.9$) we would have, $0.878 \leq \frac{1000}{T} \leq 0.926$.

Probably the greatest source of scatter in the data arises from the complicated flow field downstream of the shock as described earlier. If one considers only the 5 highest temperature runs, the agreement with theory is seen to be very good and there is a minimum of scatter. It is felt, then, that in those cases where the flame front is not too far from the shock (higher temperature operation) the assumption of a one dimensional constant area stream tube will be quite valid. This goes back to what was pointed out earlier, that is that the reaction length must be small compared to the Mach disc diameter. Additional evidence for this belief is furnished from run numbers 91, 89, 88, and 87. These runs were made on the same day and represent increasing mole fractions of hydrogen in the order given. Reference to Table II shows that the delay distances increase in that order and reference to Figure 49 shows that the agreement with theory gets progressively worse.

The theoretical curve of Figure 49 could be displaced to give

better agreement by merely using a higher value of the rate constant and/or a lower value of λ. With the exact values of activation energy and frequency factor unknown this would be warranted if there were less scatter and uncertainty in the experimental points. In fact the prediction of these values would be one of the aims of experiments of this type. At the present time, however, more accurate measurements are required. Preferably this means that temperatures, pressures, and composition measurements should be effected under actual run conditions in order to forego the use of calibration procedures which do not cover the entire range of operation. To effect such measurements water cooled probes would undoubtedly be required which are too large for the present small scale experiments. All in all it is felt that the agreement of experiment with theory as reported here is very satisfactory and that it has been proven that this experimental technique, with some refinements, has great application to the study of chemical kinetics.

Other results on induction times in the hydrogen-oxygen reaction have been reported by Schott and Kinsey [46]. They diluted the gas appreciably with argon so as to lengthen the induction period. The experiments were conducted in a shock tube using both the incident and reflected shock technique. The shock wave was detected by a schlieren system and the end of the induction zone by the absorption of OH radiation. Their tests ranged from $0.0043 \leq \eta_{O_2} \leq 0.02$ and $0.5 \leq \eta_{H_2}/\eta_{O_2} \leq 5.5$. The resultant data are given by their equation,

$$\log\left\{[O_2]\tau\left(\frac{\text{moles}}{\text{liter}}\text{-sec}\right)\right\} = -10.647 + (3966 \pm 625)\frac{1}{T}$$

This equation is plotted in Figure 50 along with the theoretical prediction of this paper ($k_6 = k_{6B}$). In order to calculate the theoretical curve the values, η_{O_2} = .0049 and $\eta_{H_2}/\eta_{O_2} = 2$, were used inasmuch as points obtained at these ratios by Schott and Kinsey seemed to lie close to their fitted curve. The agreement between experiment and theory is good with the only appreciable difference being in the slopes. This could, of course, be resolved by use of a different value of the rate constant in the theoretical prediction. The value used corresponded to k_{6b} wherein the activation energy, E_{6b} , was 18 k cal/mole. Thus the experimental results would indicate a lower value of E_6 . Schott and Kinsey measured the slope of the curve and arrived at $E_6 = 18.1 \pm 2.9$ $k$cal/mole. Actually, in view of Equation (6.75), the slope corresponds only <u>approximately</u> to the rate controlling activation energy. It is tempting to ascertain the values of A_6 and E_6 which will give perfect agreement between experiment and theory. For this purpose we will match the curves between $\frac{1000}{T} = 0.7$ (where there is perfect agreement) and $\frac{1000}{T} = 1.0$. It is well to stay away from the higher temperatures because the theoretical curve is no longer a true straight line and also the effects of the dissociation of hydrogen begin to enter. The solution for A_6 and E_6 is obtained by assuming $k_6 = k_{6b}$ at $\frac{1000}{T} = 0.7$ and then solving Equation (6.75) for k_6 at 1000°K, setting $\eta_{O_2}[C]\tau$ equal to the experimental value of 2.09×10^{-10}. This results in the following values; $A_6 = 1.78 \times 10^{14}$ and $E_6 = 15.7$ $k$cal/mole. This would appear to be quite low for the activation energy although it is interesting that it is so close to the value of 16 $k$cal/mole, the amount by which reaction VI is endothermic.

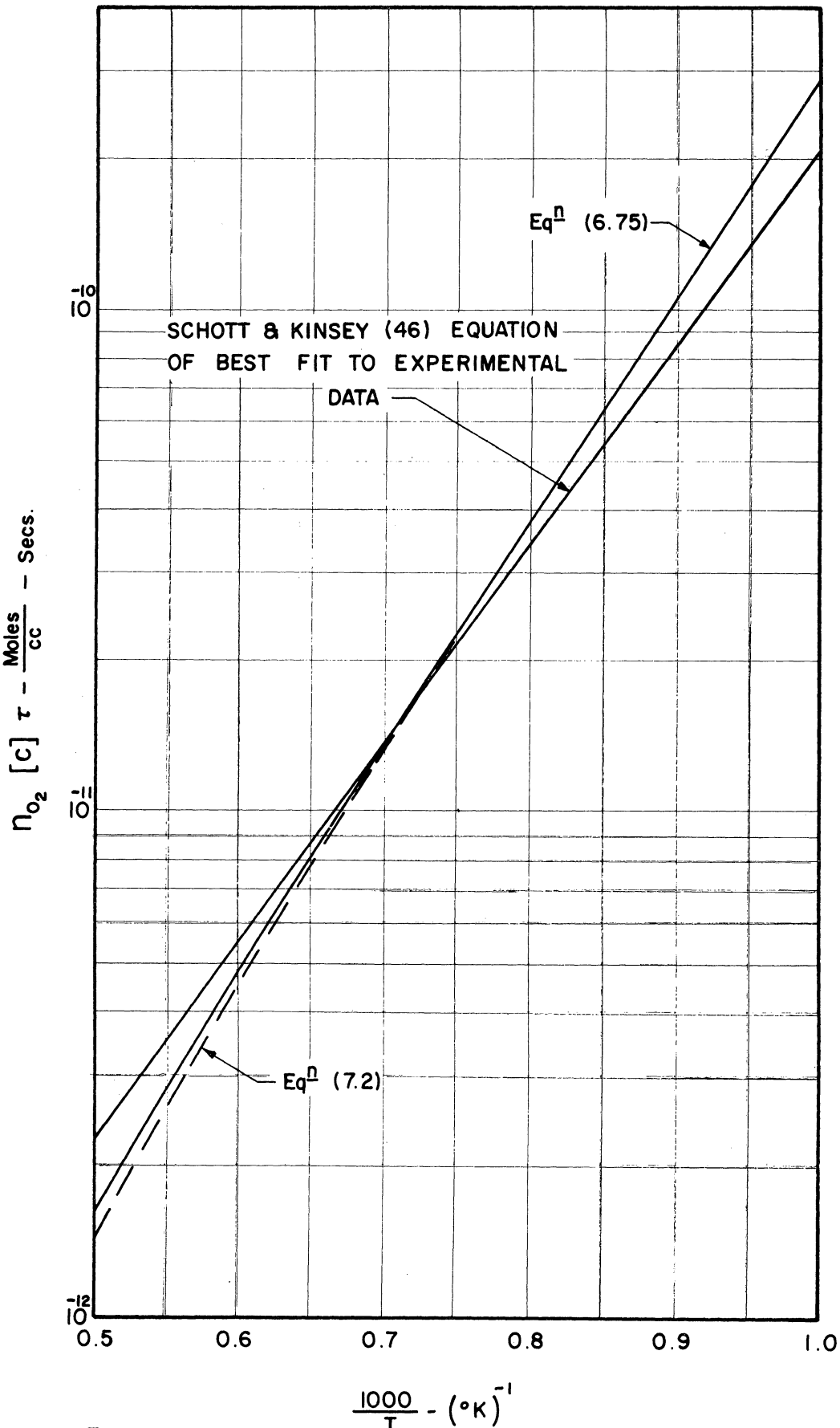

Figure 50. Comparison of the Theoretical Delay Time with the Results of Reference (46).

If these values are used to compare theory with the experimental results obtained in this research study (Figure 49), somewhat better agreement is realized although the evidence is too meager to draw conclusions at this time. These low values would be contradicted by the results of Steinberg (Figure 48) wherein an activation energy closer to 18 $k$cal/mole was indicated.

The very low values of η_{O_2} and η_{H_2} used by Schott and Kinsey begin to upset some of the order of magnitude conclusions utilized in arriving at Equation (6.75). Referring back to Equation (6.65), we see that the simplifications $\mathcal{E} >> b$ and $h >> 4f$ led to the simpler final form as given in Equation (6.74).

Reexamining these inequalities, we have;

$$\frac{h}{4f} = \frac{\eta_{H_2}[C]k_8}{4\eta_{O_2}[C]k_6}$$

Thus as long as $\eta_{H_2}/\eta_{O_2} = O(1)$ the inequality $h >> 4f$ is still valid. However, the ratio of $\mathcal{E}/b$, which is the relative importance of the two initiation processes for the production of H, becomes,

$$\frac{\mathcal{E}}{b} = \frac{2\eta_{O_2}\eta_{H_2}[C]k_5}{2\eta_{H_2}[C]k_2} = \eta_{O_2}\frac{k_5}{k_2}$$

Values for this ratio at a few different temperatures are listed in Table VII.

TABLE VII

RELATIVE IMPORTANCE OF INITIATION PROCESSES IN THE PRODUCTION OF HYDROGEN ATOMS

T - °K	$\frac{\epsilon}{b}$	$\frac{\epsilon}{b}$ ($\eta_{O2} = 0.02$)
800	$5.66 \times 10^6 \ \eta_{O_2}$	1.13×10^5
1000	$6.3 \times 10^4 \ \eta_{O_2}$	1.26×10^3
1500	$3.91 \times 10^2 \ \eta_{O_2}$	7.82
2000	$4.0 \times 10 \ \eta_{O_2}$	0.8

Thus we see that at the higher temperatures the dissociation of hydrogen cannot be neglected in the case of highly diluted gases. It is believed that this will have some bearing on the interpretation of the results of Schott and Kinsey. The equation for ignition time delay may be refined to allow for these cases. That is:

$$\eta_H = \left(\frac{\epsilon + b}{2f}\right) e^{2ft}$$

so that,

$$\tau = \frac{1}{2f} \ln\left(\frac{2f}{\epsilon + b} \cdot \lambda\right)$$

or,

$$\tau = \frac{2.303}{2\eta_{O_2}[C]k_6} \log\left[\frac{\frac{\eta_{O_2}^2}{\eta_{H_2}} \cdot \frac{k_6}{k_2}}{\eta_{O_2}\frac{k_5}{k_2} + 1}\right] \qquad (7.2)$$

This equation is plotted as the dashed line in Figure 50 with $k_6 = k_{6'}$ and for the same conditions as before.

Schott and Kinsey mentioned an experimental trend toward higher

$\eta_{O_2}[c]\tau$ with increasing η_{O_2} at a fixed temperature. The answer would appear to be given by Equation (7.2) . When hydrogen dissociation is unimportant this product should depend on η_{O_2}/η_{H_2} as is seen in Equation (6.75).

The same authors interpreted their data in terms of a theoretical analysis based on the branching chain mechanism. Thus they were led to the form,

$$\frac{[H]_\tau}{[H]_*} = e^{2\eta_{O_2}[c]k_6\tau}$$

where $[H]_*$ is the concentration of H at some insignificantly small time where the exponential variation is still valid. They equated the rate of initiation of H to the rate of chain branching in order to determine $[H]_*$. They defined the induction time as the time for the OH concentration to reach the threshold of detectability experimentally.

VIII CONCLUSIONS

The major results, and conclusions that may be inferred from these results, arising from this research investigation of stabilized detonation waves may be summarized as follows:

1) Hydrogen-air detonation waves have been sucessfully stabilized in the open jet of an underexpanded supersonic nozzle. It is believed that these waves are of the Chapman-Jouguet type although the possibility of strong detonations cannot be ruled out. The existence of these waves offers the attractive possibility of application to hypersonic ramjets.

2) It has been found possible to inject hydrogen into a hot supersonic air stream without combustion even though the stagnation enthalpy was well above that required for combustion. This is of experimental interest in that it affords a way of studying combustion processes in high speed streams without the requirement of an external ignition source.

3) Over most of the experimental range covered, the flame front was separated from the shock front by a distance which is due to ignition delay time. So far as is known, this is the first case of a well defined ignition delay zone in a steady flow system. Thus the experimental technique utilized represents a promising new tool for the study of chemical kinetics.

4) The experimental realization of the ignition delay zone inspired a theoretical treatment of the pertinent chemical kinetics in

order to substantiate the results obtained. This analysis led to a complete time dependent description of the radical concentration growths between the shock and flame front. The imposition of a requirement on the hydrogen atom concentration required to effectively initiate combustion allowed determination of an ignition time delay criteria. Thus a closed form solution was realized for the ignition time delay. Agreement between this analysis and experiment is good. The analysis serves to shed light on the dominant processes and to avoid errors in deducing the activation energy of the rate controlling reaction from experimental results.

BIBLIOGRAPHY

1. Roy, M. M. Comptes Rendus de l'Academic des Sciences. Paris: Feb. 1, 1946.

2. Dunlap, R., Brehm, R. L., and Nicholls, J. A. "A Preliminary Study of the Application of Steady-State Detonative Combustion to a Re-Action Engine." Jet Propulsion, 28, No. 7, (July, 1958), 451-456.

3. Gross, R. A., and Sargent, W. H. "A Detonation Wave Hypersonic Ramjet." Fairchild Engine Division, Fairchild Engine and Airplane Corporation. Paper presented at Second Symposium on Advanced Propulsion Concepts, Oct., 1959.

4. Morrison, R. B. "A Shock Tube Investigation of Detonative Combustion." Univ. of Michigan Rep. UMM-97, Jan., 1952.

5. Nicholls, J. A., Morrison, R. B., Reid, F. A., and Ong, R. "Detonative Combustion." Univ. of Michigan Final Report Project M898, Aug., 1953.

6. Berthelot, M. "Sur la Vitesse de Propagation des Phenomenes Explosifs dans les gas." Comptes Rendus, de l'Academic des Sciences, Paris, 18-22.

7. Mallard, E. and LeChatelier, H. "Sur la Vitesse de Propagation de L'inflammation dans les Melanges Explosifs." Comptes Rendus, de l'Academic des Sciences, Paris, (July 18, 1881), 145-148.

8. Chapman, "On the Rate of Explosion in Gases." Phil. Mag., 47, (1899), 90.

9. Jouguet, "Sur la Propagation des Reaction Chimiques dans les Gas." J. MATHEMATIQUE, 6, No. 1,(1905), 347; 6, No. 2, (1906), 6.

10. Adamson, T. C., Jr., and Morrison, R. B. "On the Classification of Normal Detonation Waves." Jet Propulsion, 25, (1958), 400.

11. Eisen, C. L., Gross, R. A., and Rivlin, R. J. "Theoretical Calculations in Gaseous Detonations." Fairchild Engine Division, Deer Park, N.Y., AFOSR TN 58-326; ASTIA AD 154230, March 15, 1958.

12. Hoelzer, C. A. and Stobaugh, W. K. "Influence of Initial Pressure on Detonation Parameters in Combustible Gases." ASTIA AD 26709, WADC, March, 1954.

13. Gealer, R. L. "The Influence of High Pressure on the Properties of H_2-O_2 Detonation Waves." Univ. of Michigan, Ph.D. Thesis, June, 1958.

14. Rutkowski, J., and Nicholls, J. A. "Considerations for the Attainment of a Standing Detonation Wave." Proc. Gas Dynamics Symposium on Aerothermochemistry, Northwestern Univ., Aug., 1955.

15. Lewis, R. L., and von Elbe, G. Combustion, Flames and Explosions of Gases. New York: Academic Press Inc., (1951), 579-627.

16. Cannon, C. D., and Jewell, L. D. "Preliminary Study of the Effect of Initial Temperature on Detonation Parameters." ASTIA AD 26804, WADC, March, 1954.

17. Moyle, M. P. "The Effect of Temperature on the Detonation Characteristics of H_2-O_2 Mixtures." Univ. of Michigan, Ph.D. Thesis, Dec., 1956.

18. Bone, W. A., Fraser, R. P., and Wheeler, W. H. Phil. Trans. Roy. Soc. London: A 235, (1936), 29.

19. Nicholls, J. A., Morrison, R. B., and Cullen, R. E. "Measurements on Gaseous Detonation Waves." Second ONR Symposium on Detonation, Washington, D. C., Feb. 9, 10, 11, 1955.

20. Gordon, W. E., Mooradian, A. T. and Harpes, S. A. "Limit and Spin Effects in Hydrogen-Oxygen Detonations." Seventh Symposium on Combustion, London, Buttersworth Sci. Pub., 487-494.

21. Hirschfelder, J. O., and Curtiss, C. F. "Theory of Detonations. I. Irreversible Unimolecular Reaction." The J. Chem. Phy., 28, (1958), 1130.

22. Linder, B., Curtiss, C. F., and Hirschfelder, J. O. "Theory of Detonations. II. Reversible Unimolecular Reaction." The J. Chem. Phy., 28, (1958), 1147.

23. Curtiss, C. F., Hirschfelder, J. O., and Barnett, M. P. "Theory of Detonations. III. Ignition Temperature Approximation." The J. Chem. Phy., 30, (1959), 470.

24. Samaras, D. G. "Gas Dynamic Treatment of Exothermic and Endothermic Discontinuities." Canadian Journal of Research, 26, Section A, No. 1, Jan., 1948.

25. Siestrunck, R., Fabri, J., and Le Grives, E. "Some Properties of Stationary Detonation Waves." Fourth Symposium on Combustion, William and Wilkins Co., Baltimore, 1953.

26. Chinitz, W., Bohrer, L. C., and Foreman, K. M. "Properties of Oblique Detonation Waves." AFOSR TN 59-462, ASTIA No. AD 215 267, April 15, 1959.

27. Prandtl, L. Über die stationaren Wellen in einem Gasstrahle, Physik Z., 5, (1904), 599-601; also, Neue Untersuchungen über die strömende Bewegung der Gase und Dämpfe, Phsik Z., 8, (1907), 23-32.

28. Owen, P. L., and Thornhill, C. K. The Flow in an Axially-Symmetric Supersonic Jet from a Nearly Sonic Orifice into a Vacuum. Brit.: A.R.C. Technical Report, R. and M 2616, 1952.

29. Love, Eugene S., and Grigsby, C. E. Some Studies of Axisymmetric Free Jets Exhausting from Sonic and Supersonic Nozzles into Still Air and into Supersonic Streams. NACA, RML54L31, 1955.

30. Wilcox, D. E., Weir, A., Nicholls, J. A., and Dunlap, R. "Location of Mach Discs and Diamonds in Supersonic Air Jets." J. Aero. Sci., 24, (1957), 150.

31. Adamson, T. C., Jr., and Nicholls, J. A. "On the Structure of Jets from Highly Underexpanded Nozzles Into Still Air." J. Aero/Space Sci., 26, (1959), 16.

32. Dabora, E. K. "Regenerative Heat Exchanger with Heat-Loss Consideration." Univ. of Michigan Eng. Res. Inst. Report 2284-14-T, Ann Arbor, Aug., 1957. Also issued as AFOSR TN 57-613, and ASME Paper No. 58-SA-29.

33. Dabora, E. K., Moyle, M. P., Phillips, R., Nicholls, J. A., and Jackson, P. L. "Description and Experimental Results of Two Regenerative Heat Exchangers." Univ. of Michigan Eng. Res. Inst. Report 2284-18-T, Ann Arbor, Feb., 1958.

34. Wilder, J. R., Jr., and Hindersinn, K. "Spreading of Supersonic Jets in Supersonic Streams." Aero. Eng. Rev., Oct., 1953.

35. Nicholls, J. A., Dabora, E. K., and Gealer, R. L. "Studies in Connection with Stabilized Detonation Waves." Seventh Symposium on Combustion, London, Buttersworth, Sci. Pub., 144-150.

36. Glawe, G. E., Simmons, F. S., and Stickney, T. M. "Radiation and Recovery Corrections and Time Constants of Several Chromel-Alumel Thermocouple Probes in High Temperature High Velocity Gas Streams." NACA TN 3766, October, 1956.

37. Brokaw, R. S. "Thermal Ignition, with Particular Reference to High Temperatures." Selected Combustion Problems, II, Butterworths Sci. Pub., London, England, 1956.

38. Drell, I. L., and Belles, F. E. "Survey of Hydrogen Combustion Properties." NACA RM E57D24, 1957.

39. Semenov, N. N. "Some Problems in Chemical Kinetics and Reactivity." II, Princeton University Press, 1958.

40. Bethe, H. A., and Teller, E. "Deviations from Thermal Equilibrium in Shock Waves." Rep. No. X-117, Ballistic Res. Lab., Aberdeen Proving Ground, 1945.

41. Wood, G. P. "Calculations of the Rate of Thermal Dissociation of Air Behind Normal Shock Waves at Mach Numbers of 10, 12, and 14." NACA TN 3634, April, 1956.

42. Duff, R. E. "Calculation of Reaction Profiles Behind Steady-State Shock Waves. I. Application to Detonation Waves." The J. Chem. Phy., 28, (1958), 1193.

43. Gross, R. A. "Research on Supersonic Combustion." ARS Journal, 29, (1959), 63.

44. Gross, R. A., and Oppenheim, A. K. "Recent Advances in Gaseous Detonation." ARS Journal, 29, (1959), 173.

45. Steinberg, M., and Kaskan, W. E. "The Ignition of Combustible Mixtures by Shock Waves." Fifth Symposium on Combustion, Reinhold Publishing Corporation, 1955.

46. Schott, G. L., and Kinsey, J. L. "Kinetic Studies of Hydroxyl Radicals in Shock Waves. II. Induction Times in the Hydrogen-Oxygen Reaction." The J. Chem. Phys., 29, (1958), 1177.